Report No. 03-69-07

Final Report

60-GHz INTEGRATED RF HEAD

By W. S. Jones and G. R. Pierson

January 1969

Prepared under Contract No. NAS 12-555 by
Texas Instruments Incorporated
P.O. Box 5012
Dallas, Texas 75222

National Aeronautics and Space Administration
Electronics Research Center
Cambridge, Massachusetts

Report No. 03-69-07

Final Report

60-GHz INTEGRATED RF HEAD

By W. S. Jones and G. R. Pierson

January 1969

Prepared under Contract No. NAS 12-555 by
Texas Instruments Incorporated
P.O. Box 5012
Dallas, Texas 75222

National Aeronautics and Space Administration
Electronics Research Center
Cambridge, Massachusetts

ABSTRACT

The initial purpose of this contract was to develop the technology to fabricate a monolithic, integrated 60.8-GHz receiver. The detailed requirements are as follows: 1) Develop a 60.8-GHz solid state microminiature source, having a maximum dc input of 2 W. 2) Integrate the above source as local oscillator with a balanced mixer to achieve a 14-dB double-sideband noise figure, with 20 dB of isolation from local oscillator to RF and a maximum input VSWR of 1.4. 3) Develop an IF preamplifier in microstrip form using chip transistors, to have a center frequency of 60 MHz with 100 MHz untuned bandwidth, a noise figure of 1.5 dB, a 50-ohm output impedance and a gain of 20 to 30 dB. The entire receiver was to operate for a period of one year and to be able to withstand radiation equivalent to an altitude of 2000 nautical miles above the earth's atmosphere.

Investigation of the electrical characteristics of the GaAs substrate has been carried out, and discrete active devices such as Gunn diodes and Schottky barrier diodes have been fabricated. Measurements of these devices, incorporated into oscillators and mixers, gave the following results:

- A monolithic single-ended mixer tested as a detector had a minimum detectable signal (M.D.S.) of −54 dBm/Hz at 87 GHz
- A balanced mixer had a M.D.S. of −125.5 dBm/Hz at 69 GHz
- A monolithic Gunn oscillator gave an output of 1.5 mW at 28 GHz.

These results show that this approach is feasible, but additional development work is necessary before practical monolithic integrated receivers are a reality.

Technology was also developed to fabricate an alternative receiver in hybrid form on quartz substrate. An investigation of the electrical characteristics of quartz substrate and quartz microstripline circuits has been made which shows it to be suitable as a substrate for microstripline circuitry. A mixer and quadrupler have been constructed, and a conversion loss of 20 dB has been measured for the quadrupler, multiplying from 12.5 to 50 GHz.

A waveguide approach to the receiver was instigated, and two methods for obtaining the local oscillator power at 60 GHz were considered, i.e., directly, using an avalanche diode, or a Gunn diode in the LSA mode, or using a waveguide quadrupler from 15 to 60 GHz.

After feasibility studies, it was decided that the direct generation of 60 GHz using avalanche diodes was the most promising approach. Output power of greater than 5 mW was obtained at 60.8 GHz and greater than 20 mW at 57 GHz. The efficiency of the latter device was 1%.

A receiver was set up at 60.8 GHz using a single-ended mixer having a conversion loss of approximately 9 dB. A double-sideband noise figure of 13 to 14 dB was measured. This does not include the coupler attenuation of 6 dB in the measurement set up. A balanced mixer will give an overall noise figure of 13 to 14 dB, using the local oscillator power presently available.

A low-noise IF preamplifier having a noise figure of 1.5 dB, and pass band from 10 to 110 MHz (±1 dB) has been fabricated. Although the requirements of very low noise figure and wide bandwidth generally conflict, this preamplifier meets or exceeds the requirements of this contract.

The major technological achievements of this contract have been: a) fabrication of operating prototype monolithic active devices on semi-insulating GaAs substrate at millimeter-wave frequencies, b) attaining sufficient power at 60 GHz, using a silicon avalanche diode oscillator, to drive a balanced mixer, and c) fabricating an extremely low-noise wide-bandwidth integrated circuit preamplifier.

TABLE OF CONTENTS

SECTION	TITLE	PAGE
I.	INTRODUCTION	1
II.	MONOLITHIC INTEGRATED CIRCUIT APPROACH	5
	A. Material Technology	5
	B. Fabrication of Gunn Diode Oscillator	5
	C. Fabrication of Schottky Barrier Diodes	7
	D. Circuit Design and Evaluation	9
	1. Dielectric Constant of GaAs	9
	2. Theoretical RF Power Loss of Striplines on GaAs	14
	a. Dielectric Loss	14
	b. Conductor Loss	15
	3. Transitions	16
	a. Antenna-Coaxial Transducer	16
	b. Antenna Feedthrough Transducer	18
	c. Ridged Waveguide Transducer	19
	4. Striplines and Passive Stripline Circuit Elements	19
	a. Striplines	23
	b. Microstripline Resonant Cavities	27
	c. Microstripline Rejection Filter	28
	5. Gunn Diode Circuits	31
	6. Mixer Circuits	37
	7. Complete Receiver	40
III.	HYBRID CIRCUIT APPROACH	45
	A. Substrates	45
	B. Quartz Microstriplines	46
	C. Balanced Mixer	49
	D. Local Oscillator Source	55
	1. Multiplier	55
	2. Stripline Gunn Oscillator	56
IV.	WAVEGUIDE APPROACH	59
	A. General	59
	B. Waveguide Quadrupler and 15 GHz Source	59
	C. Direct Generation of 60 GHz Using Gunn Diodes	61
	D. Direct Generation of 60 GHz Using Avalanche Diodes	62
	1. General	62
	2. Material and Device Fabrication	62
	3. Mounting and Testing	70
	4. Frequency Stability	72

TABLE OF CONTENTS (Continued)

SECTION	TITLE	PAGE
V.	MILLIMETER-WAVE RECEIVER	75
	A. Millimeter-Wave Mixer	75
	B. Receiver Measurements	75
VI.	IF AMPLIFIER	79
	A. General	79
	B. Amplifier Design	79
	C. Hybrid Fabrication and Performance	82
VII.	CONCLUSIONS	87
VIII.	REFERENCES	91

LIST OF ILLUSTRATIONS

FIGURE	TITLE	PAGE
1.	Atmospheric Absorption versus Frequency	2
2.	Integrated Circuit Block Diagram	3
3.	Schematic Diagram of Gunn Diode Structure	6
4.	Top View of Monolithic Gunn Diode	7
5.	Fabrication Process of Schottky Barrier Diode	8
6.	Dielectric Constant of GaAs at 1 MHz	11
7.	Dielectric Constant versus Frequency in X-Band	12
8.	Dielectric Constant versus Frequency in R-Band	13
9.	Antenna Coaxial Transducer	17
10.	Transmission Loss Through Coaxial Antenna Pair	18
11.	E-Band Crossed Waveguide Measurement Jig	20
12.	Waveguide to Stripline Transition Using Tapered Ridges	21
13.	Comparison of Field Distribution in Ridged Waveguide and Stripline	21
14.	Characteristic Impedance of GaAs Microstrip Transmission Lines versus w/h	22
15.	Free-Space to Microstrip Wavelength Ratio versus w/h for GaAs Substrates (k = 13.2)	23
16.	Resonance Measurement on Loosely Coupled Transmission Line	24
17.	Transmission Line Attenuation versus Frequency.	25
18.	Arrangement of Field Pattern Measurements	26
19.	Stripline Wavelength versus Frequency	27
20.	Circular Stripline Cavity	28
21.	Resonant Frequency versus Diameter for Circular Cavity	29
22.	Insertion Loss of $\lambda/4$ Stub	30
23.	Dimensions of $\lambda/4$ Stub	31
24.	Stripline Gunn Oscillator (decoupled, full-wavelength)	32
25.	Stripline Gunn Oscillator (circular cavity)	33
26.	Full-Wavelength Gunn Oscillator (directly coupled)	34
27.	Monolithic Full-Wavelength S-Shaped Oscillator (schematic)	35
28.	Monolithic Circular Gunn Oscillator (schematic)	36
29.	Top View of Actual S-Shaped Oscillator	37
30.	Single-Ended Monolithic Mixer	38
31.	Balanced Monolithic Mixer	38
32.	Current/Voltage Characteristic of Schottky Diode	39
33.	Sensitivity of Single-Ended Mixer as a Detector	41
34.	94 GHz Integrated Microwave Receiver	42
35.	DC Characteristics of Monolithic Diodes	43
36.	Effective Dielectric Constant versus w/h	47

LIST OF ILLUSTRATIONS (Continued)

FIGURE	TITLE	PAGE
37.	Impedance versus w/h	48
38.	Balanced Mixer on Quartz	49
39.	Isolation of Hybrid Coupler versus Frequency	51
40.	Power Division of Hybrid Coupler versus Frequency	52
41.	Input VSWR of Hybrid Coupler versus Frequency	53
42.	Output Phase Difference of Hybrid Coupler versus Frequency	54
43.	Quadrupler on Quartz	55
44.	Waveguide Quadrupler	60
45.	Cross Section of Waveguide Jig	63
46.	Exploded View of Jig	64
47.	Impurity Profile Summary for Avalanche Diode	65
48.	Schematic Diagram of Electric Field in Depletion Region	66
49.	Donor Density versus Depletion Width	67
50.	Diode Capacitance versus Voltage	68
51.	(a) Diode After Separation (b) Diode After Etching to Final Size	71
52.	Side View of Circular Cavity	73
53.	Block Diagram of Receiver	76
54.	IF Amplifier Schematic	81
55.	Performance Data-Breadboard Version, Shunt-L Input	82
56.	Performance Data-Breadboard Version, Shunt-C, Series-L Input	83
57.	Physical Layout of Hybrid IF Amplifier	84
58.	Performance Data-Ceramic Hybrid Version, Shunt-L Input	85

LIST OF TABLES

TABLE	TITLE	PAGE
I.	Balanced-Mixer Results	40
II.	Thermal Conductivity and Expansion Coefficients	45
III.	Comparison of Stripline Characteristics at 60 GHz	48
IV.	Summary of Device Characteristics	65
V.	Hybrid Version Performance Summary	85

SECTION I

INTRODUCTION

For many years there has been considerable interest in extending the utilization of the frequency spectrum to millimeter wavelengths. The basic advantages of using this portion of the spectrum have long been realized: namely, wide, instantaneous bandwidth and high gain from small antenna structures. However, atmospheric attenuation and the lack of suitable and reliable components has limited the utilization of the millimeter portion of the spectrum.

During the past few years, many new millimeter-wave devices in discrete form have been developed using silicon and gallium arsenide materials. The first of these was the GaAs P-N junction varactor developed by Texas Instruments in 1959. This device offered significant improvement in performance over other varactors then available, and continues to find broad application in high-frequency multiplication and low-noise parametric amplification, for ground, airborne, and space-borne radar and communication systems.

More recently, metal-semiconductor or Schottky-barrier devices have been developed using both Si and GaAs material, resulting in mixers and varactors of exceptional quality. Noise figures of 4.7 to 4.9 dB are achieved regularly at 9.3 GHz from mixers. This performance is only 0.2 to 0.4 dB above the minimum possible noise figure of a mixer working into an IF preamplifier having a 1.5 dB noise figure. Conversion loss as low as 4 dB has been obtained from N-type GaAs Schottky-barrier diodes in a millimeter-wave mixer at 58 GHz.[1]

Within the past few years, Copeland[2] and others have carried out extensive work on the higher-frequency-mode (LSA) generation of power, using Gunn devices. Outputs of 20 mW CW between 40 and 90 GHz have been achieved in a waveguide circuit[3]. Both the power and frequency are equal to or higher than that achieved when the device is operated in the transit-time mode. The operating frequency when used in this mode is highly dependent on the resonance of the external circuit. Investigations have been carried out at TI to ascertain the feasibility of initiating this mode in microstripline cavities to achieve the output at millimeter wavelengths directly.

Although these semiconductor elements are of value in themselves, their use in combination with other elements to form functional systems shows even greater advantage. Recent technological advancement has renewed interest in the system application of millimeter-wave components. Molecular resonance absorption by constituents of the atmosphere has been evaluated theoretically and experimentally. The atmospheric absorption line of oxygen occurs around 60 GHz (see Figure 1), and attenuation for transmission through the atmosphere has been measured to be greater than 15 dB/km at sea level. This can afford a high degree of security and privacy for exo-atmospheric systems and short-range atmospheric systems.

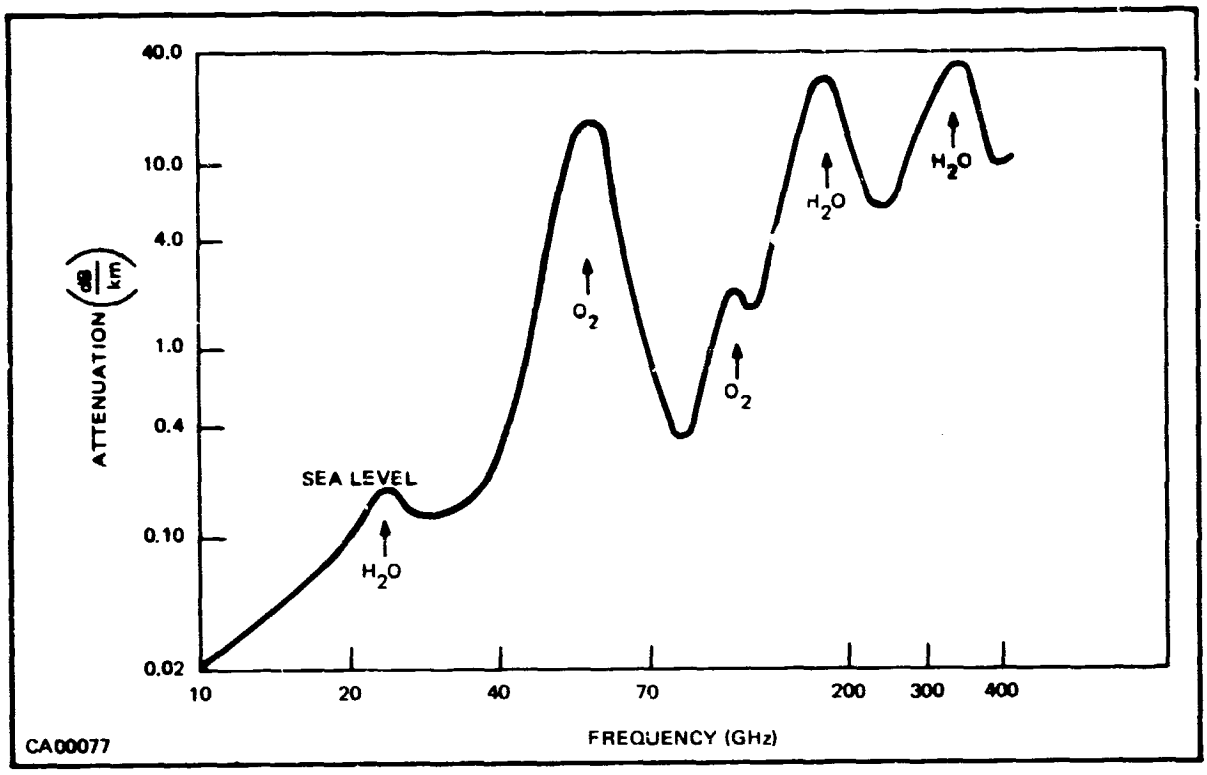

Figure 1. Atmospheric Absorption versus Frequency

With the development of the basic active components, all that is required to achieve millimeter-wave integrated circuits are the passive circuit elements and the interconnections. This capability can be provided by microstriplines constructed on a semi-insulating GaAs substrate material. The use of semi-insulating GaAs means that the active components, such as Gunn diodes and Schottky barrier diodes, may be fabricated on the same substrate by selective epitaxial deposition. This monolithic form of circuit fabrication allows the circuit to be extremely small, and the cost of mass-producing such circuits is also potentially very low.

A considerable proportion of the development studies on monolithic technology was carried out on a contract running concurrently with this study. This contract [AF33(615)-5102] involved the development of a 94 GHz receiver front-end, consisting of a planar 31 GHz Gunn transit-time oscillator, a triplet using a Schottky barrier varactor, and a balanced mixer using two low-loss, planar, Schottky barrier, mixer diodes. These elements were all fabricated on semi-insulating GaAs substrates. The advanced technology developed on this contract would be readily transferable to the fabrication of the 60 GHz integrated receiver.

The specific goal of the proposed program was to develop a reliable, compact, low-noise low-power RF head operating at 60 GHz for use in a space-borne microwave radiometer which would be instrumented for horizon sensing applications. The block diagram of the proposed circuit for this unit is shown in Figure 2. The local oscillator was to take one of two forms:

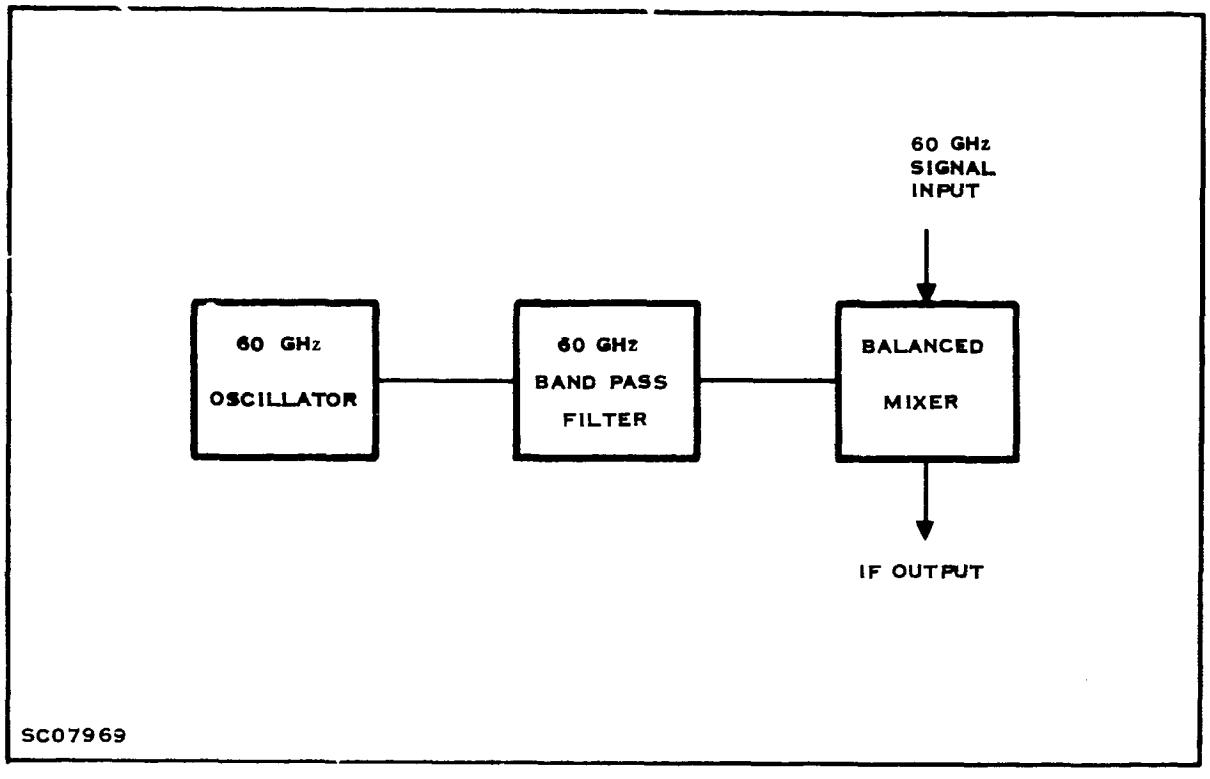

Figure 2. Integrated Circuit Block Diagram

1) Direct generation of the 60 GHz power using a planar bulk GaAs diode operating in the LSA mode.

2) Generation of a 30 GHz signal by means of a Gunn oscillator followed by a frequency doubler to 60 GHz using Schottky-barrier diodes.

The first phases of the contract were used to fabricate discrete devices (Gunn oscillators and Schottky diodes) by the techniques which would be used to fabricate the integrated circuit. The principal Gunn oscillator technologies investigated were attainment of controlled low-carrier-concentration epitaxial GaAs, methods for preparing ohmic contacts, and measurement of device operating characteristics. The Schottky diode problems investigated were the surface preparation procedures prior to metal evaporation and methods for fabricating a planar device. Some preliminary circuit studies were performed to generate the data required to design the circuits to perform the mixing and local-oscillator functions.

During the course of this program, it was found that the monolithic approach was not feasible within the time frame of the contract; therefore, alternative hybrid and waveguide approaches were considered. Previous investigations of the direct generation of millimeter-wave frequencies using avalanche diodes reported[4] outputs of up to 100 mW at 70 GHz, and this approach was finally chosen to be the most appropriate. Using such a device, a complete receiver at 60.8 GHz was developed in waveguide.

The second part of this contract was to develop a very-low-noise preamplifier at 60 MHz. For any very high frequency system it is necessary to reduce the frequency to a level where high gain and bandwidth are available, i.e., a superhetrodyne receiver is necessary. Since the IF noise figure adds directly to the overall noise figure, a very low noise preamplifier (< 1.5 dB) is desired. Also, the bandwidth of the IF was made wide to make the overall system more flexible.

A great deal of experience in the computer design and optimization of amplifier circuits, as well as state-of-the-art transistors were available at Texas Instruments. Previously proved techniques were used extensively in the design and fabrication of this extremely low-noise, high-bandwidth preamplifier.

The authors would like to acknowledge the contributions of the following members of the TI staff:

N. J. Tolar, H. M. Leedy, W. A. Little, G. L. Spence and R. W. Cantrell for the fabrication of the diodes and diode assemblies; S. Mao, E. W. Mehal, R. W. Wacker and R. C. Hooper for work on the monolithic circuits; and to G. L. Spence for testing and evaluation of the source. The suggestions and support of R. R. Webster throughout the program are gratefully acknowledged.

SECTION II

MONOLITHIC INTEGRATED CIRCUIT APPROACH

A. MATERIAL TECHNOLOGY

The initial approach considered for this program was to investigate the feasibility of a fully-monolithic, integrated receiver, on a semi-insulating GaAs substrate. Considerable experience has been gained at Texas Instruments in the material technology (material preparation, epitaxy, metallization, etc.) on contract AF33(615)-5012, which involved the development of a monolithic 94-GHz receiver on GaAs. Work on both contracts was carried out concurrently, with most of the material development work undertaken on the Air Force contract, and translated to 60 GHz as development progressed.

The first phase of contract (NAS12-555) was directed toward development of the technology to fabricate discrete devices (Schottky barrier diodes and Gunn oscillators) by the techniques which would be used to construct the completely integrated circuit. The principal Gunn-oscillator problems investigated were the attainment of controlled, low-carrier-concentration, epitaxial GaAs; methods for preparing ohmic contacts; and measurement of the device operating characteristics. The principal Schottky-barrier-diode fabrication problems investigated were the surface preparation procedures prior to metal evaporation and methods of constructing a planar device.

For details on the preparation of semi-insulating GaAs, doping techniques, epitaxy, low-temperature selective deposition, and ohmic-contact evaluation see the FINAL REPORT of contract No. AF33(615)-5012 (Report AFAL-TR-68-339).

B. FABRICATION OF GUNN DIODE OSCILLATORS

Planar Gunn diodes were fabricated by the selective epitaxial deposition of suitably doped GaAs onto pre-determined areas of the semi-insulating GaAs substrate. A schematic diagram of the procedure is shown in Figure 3. The Gunn diode is essentially made up of an N^+ layer doped usually in the range from 1 to 5 X $10^{18}cm^{-3}$, to a depth of 10 to 15 microns. A second selective deposition, the N^- layer, defines the transit-time frequency of the device. This layer has a doping concentration of from 2 to 8 X $10^{15}cm^{-3}$, to a depth of 2.5 microns for transit-time operation at 60 GHz. To facilitate the deposition of ohmic contacts, a further selective deposition of N^+ material is made, with a doping concentration in excess of $10^{19}cm^{-3}$. Ohmic alloy (AgInGe) contacts are deposited onto the N^+ region and the microstripline cavity is evaporated onto the substrate. The ground plane is evaporated onto the back of the slice after it has been lapped and polished to a thickness of 4 mils.

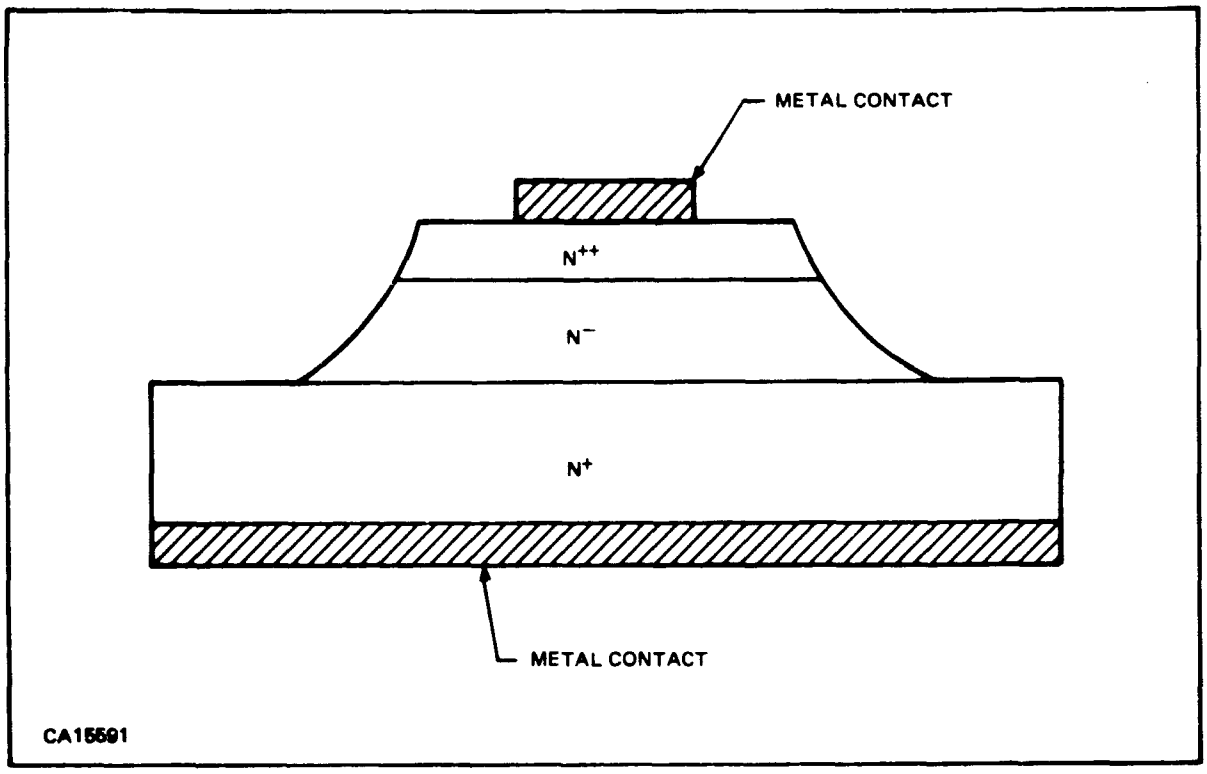

Figure 3. Schematic Diagram of Gunn Diode Structure

Several semi-insulating GaAs substrates were prepared and etched for Gunn diode fabrication. The selective epitaxial operations were performed and the devices tested. A topographical view of the Gunn diode is shown in Figure 4. Due to etch and refill of the top N^+ layer, a 4.5 micron N^- layer was deposited rather than a 2.5 micron layer. This would cause the Gunn diode to operate at 30 GHz in the transit time mode rather than at 60 GHz.

Uniform carrier concentration in the order of $10^{15}cm^{-3}$ is very difficult to obtain on a substrate which has a carrier concentration three orders of magnitude higher. For LSA operation, which has been considered in this contract, the thickness of the N^- layer is not so critical; however, the concentration should be approximately $3 \times 10^{15}cm^{-3}$ for the N/F ratio to be $5 \times 10^{4}sec\ cm^{-3}$ at 60 GHz.

C. FABRICATION OF SCHOTTKY BARRIER DIODES

A schematic diagram of the procedure to fabricate planar Schottky barrier diodes is shown in Figure 5. This process was chosen to isolate the N layer, which reduces the leakage current and keeps the parasitic capacitance smaller. The N^+ region is deposited into holes etched into the semi-insulating GaAs. The impurity concentration in the N layer is typically 0.7 to $2 \times 10^{17}cm^{-3}$ while the thickness is 0.5 to 1.0 microns. This corresponds to a reverse breakdown voltage of 15 to 20 volts.

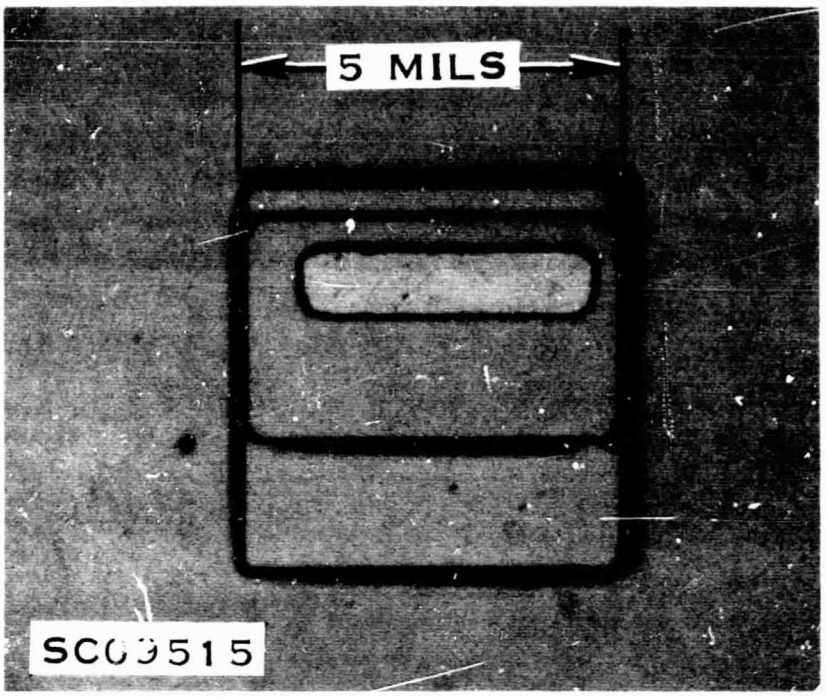

Figure 4. Top View of Monolithic Gunn Diode

The N^+ region is deposited into 1 X 2 mil holes in the semi-insulating GaAs; great care must be taken in the deposition rate, or overgrowth occurs. These raised deposits create difficulties in the definition and alignment of the small geometry contacts as well as the expanded contacts. The actual diode active region was made with four different areas, 0.2 X 0.2, 0.4, 0.6, 0.8 mil^2, to provide diodes with different junction capacitances.

Some difficulty was experienced with the original fly's-eye masks used to define the geometries. Another difficulty was the surface clean-up between various process steps. Increased series resistance (which is undesirable) is seen when surface clean-up is inadequate. The best clean-up method found was the use of concentrated HF and subsequent quenching, but this is not compatible with planar-diode technology. The use of buffered HF solution in the last clean-up instead of concentrated HF also appreciably reduced the series resistance, and, with SiO_2 used for the surface pacification and masking, is preferred over the HF. This buffered HF is presently being used in cleaning all GaAs surfaces.

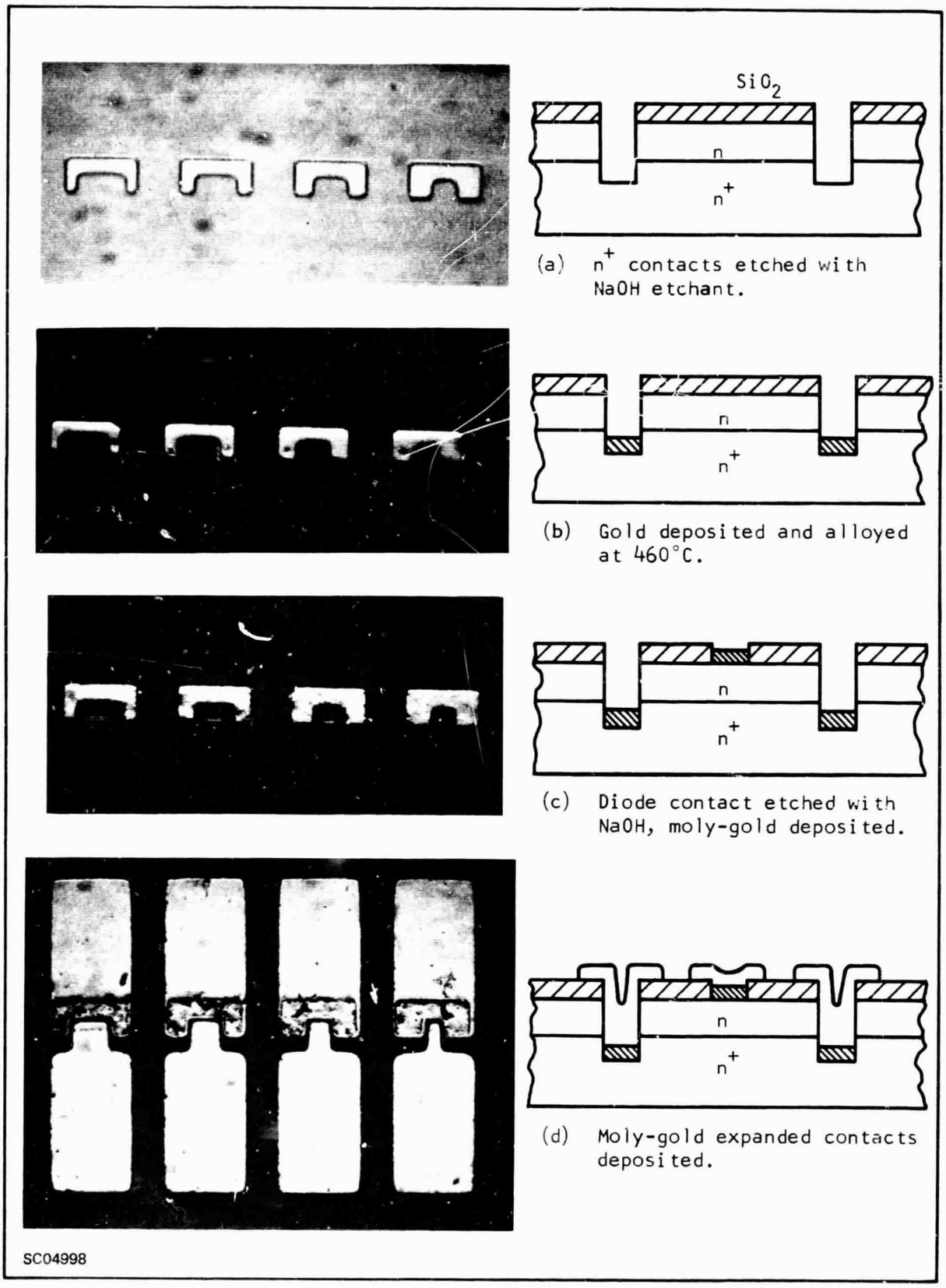

Figure 5. Fabrication Process of Schottky Barrier Diode

D. CIRCUIT DESIGN AND EVALUATION

1. Dielectric Constant of GaAs

Before circuit design can be initiated, certain characteristics such as the dielectric constant and loss in a stripline have to be determined.

Recently it was reported[5] that the real part of the complex dielectric constant of GaAs exhibits a broad resonance between 2.0 and 80 GHz. As there is no known theoretical reason why this phenomenon should exist, some measurements were made to ascertain whether the semi-insulating GaAs produced at Texas Instruments exhibited the same characteristics.

Results showed[6] that from 4 to 40 GHz the dielectric constant did not change. Recently other investigators have also found that the dielectric constant of GaAs is invariant in the microwave region. Champlin et al.[7] measured a dielectric constant of 12.95 between 8.5 and 70 GHz. Braslau[8] has found no significant change in dielectric constant in the range of 1.9 to 13 GHz. Rogers et al.[9] measured a dielectric constant of 12.35 and a loss tangent of 5.6×10^{-4} at 9.4 GHz. They found no significant change in dielectric constant between 7 and 12 GHz. Both the findings of other investigators and the results recorded at Texas Instruments indicate that semi-insulating GaAs substrates will function properly in the microwave and millimeter wave regions.

Following initial work on the nonvariance of the dielectric constant of GaAs with frequency in the microwave range, further investigations were carried out to find a rapid and accurate method of measuring the absolute dielectric constant. It was decided that the most accurate method was to construct parallel-plate capacitors of various areas, using the dielectric in question, and to measure their capacitance at 1 MHz using a bridge. Since GaAs is a semiconductor, special care must be taken when metallizing its surface. Two main methods are available: a) forming a layer of oxide on the surface prior to metallization; or b) using ohmic alloy contacts (AgInGe). Initially method a) was used, but, because of poor metal adhesion and a diodic effect observed when testing the I/V characteristic, ohmic contacts were chosen. These contacts were checked on the curve tracer and found to be purely ohmic.

Certain corrections were used to obtain the actual dielectric constant from the observed capacitance. These are due to: a) fringing effects and b) slight reduction in the metallic area because of imperfections at the perimeter. The latter correction is represented by a length 2x, where $(a - 2x)$ is the true length of one side of the capacitor, and 'a' the measured length. Another source of error is the reduction in thickness of the capacitor due to the metal alloying into the surface. A small correction was made to the thickness to allow for this. The equation describing the capacitance incorporating these corrections is as follows:

$$C = \frac{k_o k_1 (A - \ell x)}{d} + P\ell \qquad (1)$$

where

C = measured capacitance

k = relative dielectric constant

k_o = dielectric constant of free space

A = measured area

ℓ = perimeter length

P = a constant describing fringing effect.

Rearranging Equation (1) we obtain

$$\frac{C}{\ell} = \frac{k_o k_1 A}{d\ell} - \frac{k_o k_1 x}{d} + P \qquad (2)$$

Plotting C/ℓ against $A/d\ell$ should give a straight line of slope $k_o k_1$ and intercept on the C/ℓ axis of $(P - k_o k_1 x/d)$, thus eliminating both errors.

Results are shown in Figure 6 for one sample approximately 0.5 inch square and three samples approximately 0.2 inch square, and they are seen to be a straight line as predicted. The value of dielectric constant from these results is found to be 13.2 ± 0.2. Measurements similar to these have previously been reported,[10] with a value of dielectric constant of 12.5. This difference may be due to the difference in metallization techniques.

The primary purpose of this work was to measure the complex dielectric constant at the frequency of operation. As large samples of the substrate are not always available or are difficult to machine accurately, a perturbation method was used which required only a small sample of the material. The principle of this technique is to perturb a high-Q cavity with a sample so small that the field pattern is not appreciably disturbed. The most convenient method is to insert a small cylinder of material through a hole in the broadwall of a rectangular waveguide cavity. Equation (3) can be derived from well-known basic perturbation theory[11] using the geometry of the sample

$$2\left[\frac{f_{r1} - f_{r2}}{f_{r2}}\right] - j\left[\frac{1}{Q_{L1}} - \frac{1}{Q_{L2}}\right] = (\epsilon - 1)\ \frac{4\pi r^2}{ad} \qquad (3)$$

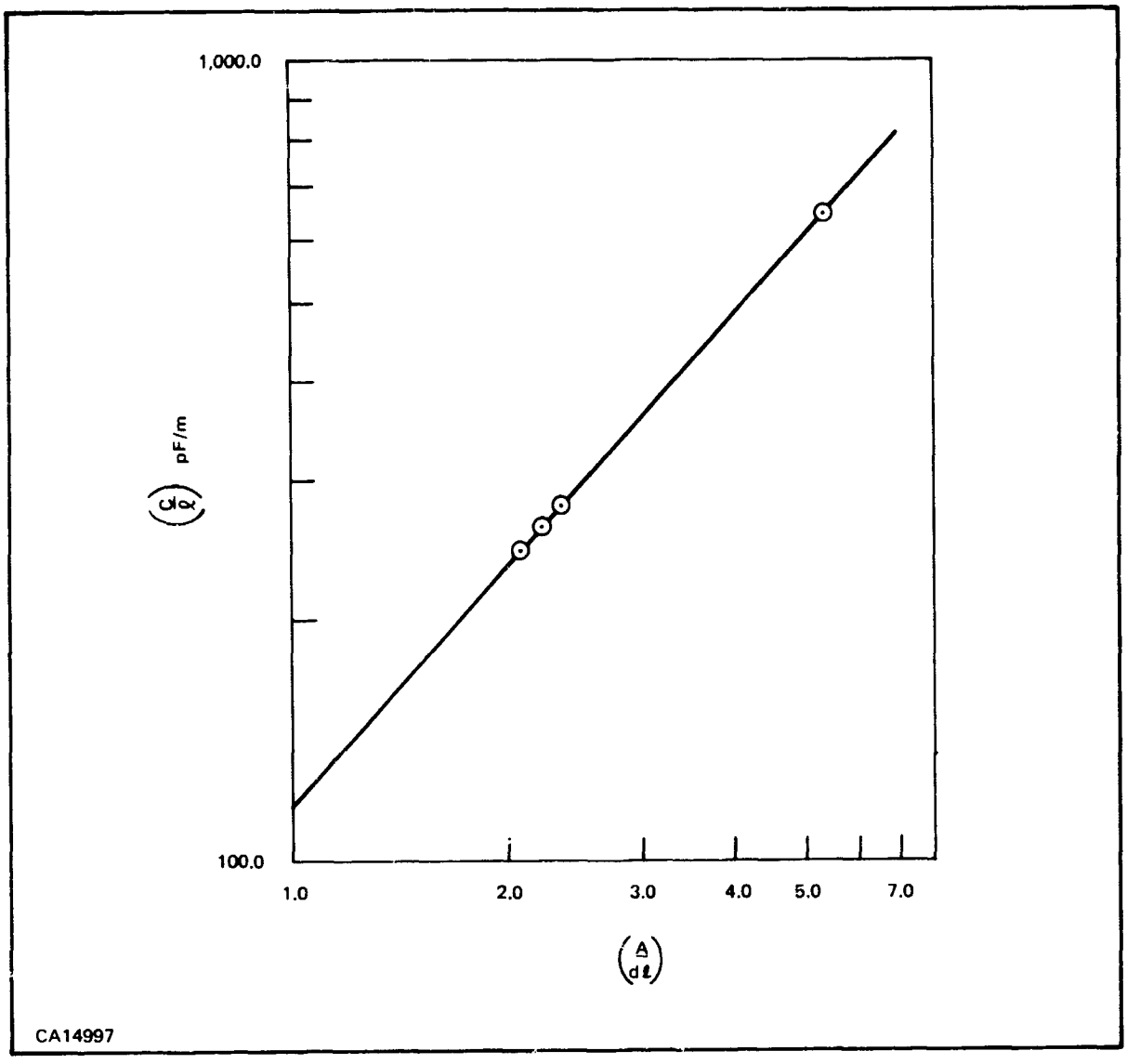

Figure 6. Dielectric Constant of GaAs at 1 MHz

where

f_{r1} and f_{r2} = resonant frequencies before and after perturbation

Q_{L1} and Q_{L2} = "quality factors" of resonance before and after perturbation

r = radius of sample

a and d = width and length of waveguide cavity

ϵ = complex dielectric constant.

Certain important conditions are assumed in the derivation of Equation (3). These are: a) the electric field in the cavity is the same before and after perturbation; b) the electric field is a constant maximum value throughout the sample. Both of these conditions are met, provided the sample is sufficiently small compared to the wavelength at the frequency in question. The size of the rod available was limited by the minimum diameter it was possible for us to achieve using cavitron techniques (approximately 85 mils).

To improve the accuracy a cavity 19 λ/2 was constructed at 10 GHz using X-band waveguide. A hole 90 mils in diameter was drilled in the center of the cavity, and two thin irises with 100-mil-diameter holes were bolted to the extremes. Because of the length of the cavity several resonances were observed in X-band. To check the validity of the assumptions, the rod was inserted and measurements taken of the frequency change. As expected, every odd resonance frequency was shifted—corresponding to the maximum electric field in the sample—and every even resonance was unchanged, showing the sample to be sufficiently small.

In the observed results, shown in Figure 7, the dielectric constant is seen to be 13.3 ± 0.4. Much of this error resulted from our inability to produce a rod of constant dimensions, as a slight taper was unavoidable. When a similar rod of high-resistivity silicon was constructed and tested in similar manner, the resulting dielectric constant was found to be 11.9 ± 0.4, which corresponds well with previously reported values. The dielectric constant of GaAs has previously been measured by perturbation techniques, but the value quoted was somewhat lower (12.35) than we obtained.[9]

The loss tangents of these two materials were measured, but owing to their low loss it was difficult to measure accurately the Q of the resonant response. Results obtained were as follows:

Material	Loss Tangent
GaAs	0.0016*
Si	0.004

* This value is similar to previously reported values.[5,12]

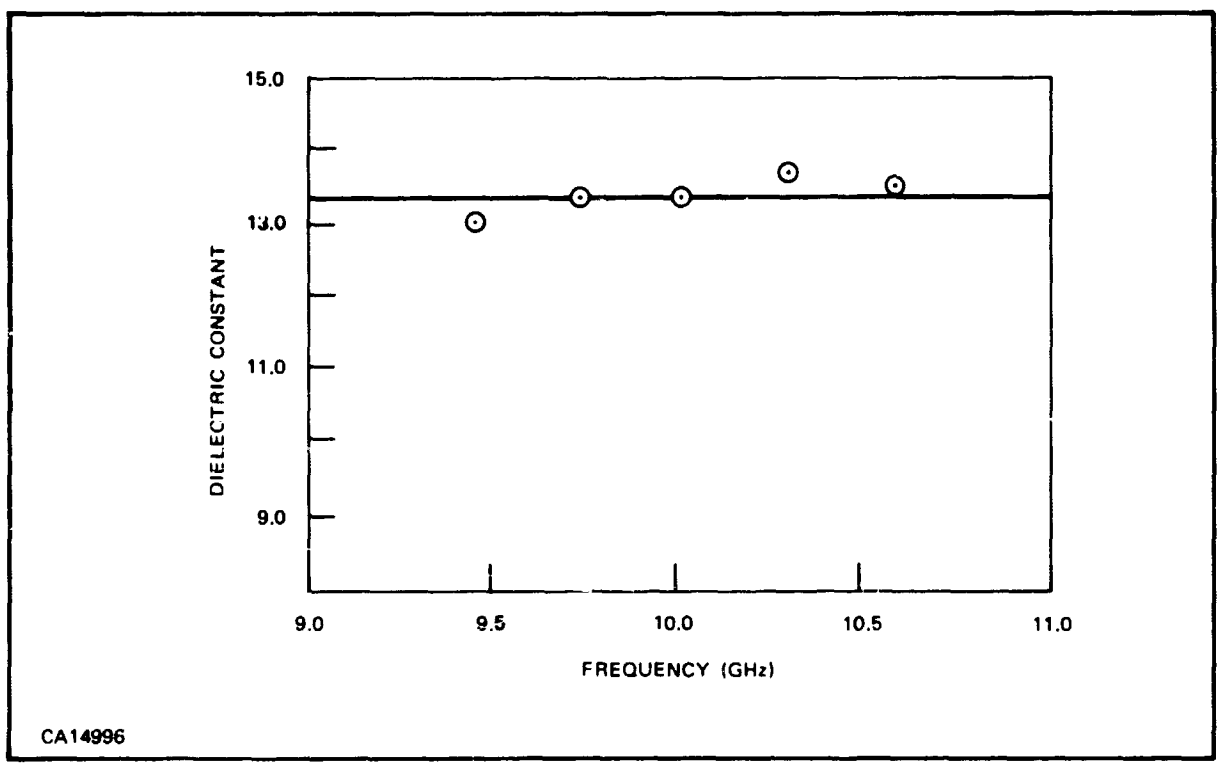

Figure 7. Dielectric Constant versus Frequency in X-Band

Measurements have also been made in R-band (26 to 40 GHz) using a cavity similar to that described above, but being 19 $\lambda/2$ at 33 GHz. In this case 85-mil-diameter rods were too large, and bars of GaAs (22-mils square) were prepared. The results observed are shown in Figure 8. It is seen that the dielectric constant appears to vary slightly in linear fashion about the center frequency of the band in question, because of the limitation set by the conditions assumed in deriving Equation (3). Therefore the results, which are only valid near this center frequency, give a dielectric constant of 13.25 ± 0.5 for GaAs. Due to the high Q of the resonance response, values of the loss tangent in R-band were too inaccurate.

In conclusion, the absolute value of the dielectric constant of GaAs is shown to be 13.2 ± 0.2. This value has also been found at 70 GHz.[13]. The accuracy of the method employed in the microwave range is limited by the assumed conditions, but corrections can be made to improve this accuracy. The method described is very simple to perform once a cavity has been constructed in the required frequency range, if samples of the correct dimensions are available. The results are sufficiently accurate to permit the construction of stripline circuits using the material in question as the substrate, and seem suitable for dielectric constants in the range from 5 to 100. For high-resistivity material, however, loss-tangent measurements are only approximate.

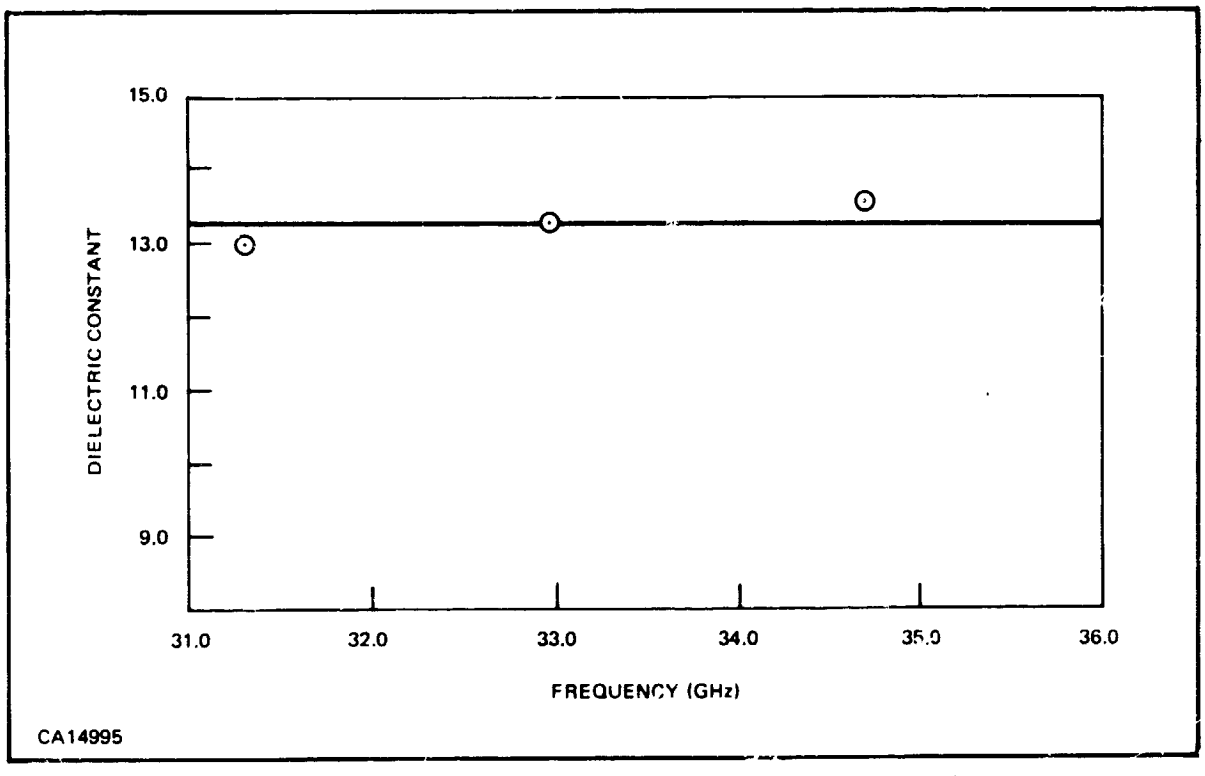

Figure 8. Dielectric Constant versus Frequency in R-Band

2. Theoretical RF Power Loss of Striplines on GaAs

Microstripline attenuation is caused by both dielectric and conductor losses. For low-loss dielectrics the attenuation is primarily caused by conductor losses. Since the dielectric loss tangent of semi-insulating GaAs is not accurately known in the millimeter-wave region, the total attenuation can only be estimated.

a. Dielectric Loss

The theoretical dielectric loss for microstripline deposited on an imperfect dielectric has been derived by Welch and Pratt.[14] Since semiconductors are imperfect dielectrics ($\alpha \neq 0$), the dielectric loss is composed of both internal polarization loss and ohmic loss (not to be confused with conductor loss described in the following section). The dielectric loss tangent is given by

$$\tan \delta = \tan \delta_\epsilon + \tan \delta_\sigma \tag{4}$$

$$\tan \delta_\sigma = \frac{\sigma}{\omega \epsilon} \tag{5}$$

At low frequencies the ohmic term dominates. At higher frequencies the total dielectric loss tangent asymptotically approaches $\tan \delta_\epsilon$. The crossover frequency is defined where $\tan \delta_\epsilon$ equals $\tan \delta_\sigma$ and is given by

$$\omega_c = \frac{\sigma}{\epsilon \tan \delta_\epsilon} \tag{6}$$

For high-resistivity Si of 10^3 Ω-cm resistivity and a $\tan \delta_\epsilon$ of 0.001, the crossover frequency is 150 GHz. For high-resistivity GaAs of 10^5 Ω-cm resistivity and a $\tan \delta_\epsilon$ of 0.001 this frequency is 1.3 GHz. Walsh has measured a $\tan \delta_\epsilon$ of 0.0001 in 10^6 Ω-cm GaAs from 2.5 GHz to 10 GHz. Although the dielectric loss tangent of GaAs in the millimeter-wave region is unknown, as there are no resonance effects, the total dielectric loss tangent may be assumed to be ~0.001.

The attenuation (in units of nepers/meter) due to dielectric loss is given by

$$\alpha_d \cong \frac{\omega}{2} (\mu k)^{1/2} \tan \delta \left(\frac{k}{k'} \right)^{1/2} q \tag{7}$$

where q is the effective filling factor given by Wheeler.[15]

For a 50-Ω line on 4-mil GaAs the following parameters were used to estimate the attenuation given by Equation (7):

$$\mu = 4\pi \times 10^{-7} \text{ Henry/meter}$$

$$k = \frac{13.2}{36\pi \times 10^{9}} \text{ Farads/meter}$$

$$q = 0.613 \frac{\omega}{h} = 0.8$$

$$\frac{k}{k'} = 13{\cdot}2/8{\cdot}48$$

Substituting in Equation (7):

$$\alpha_d = 2{\cdot}92\, f \cdot 10^{-12} \text{ nepers/meter}$$

$$= (2{\cdot}92\, f \cdot 10^{-12} \text{ nepers/meter})\ (8{\cdot}686 \text{ dB/nepers}) \left(\frac{3 \times 10^{8}}{f \times 2{\cdot}91} \cdot \frac{\text{meter}}{\lambda g} \right)$$

$$= 0.026 \text{ dB}/\lambda g$$

The dielectric attenuation is independent of frequency and very low, provided the loss tangent remains low at millimeter-wave frequencies.

b. Conductor Loss

Conductor loss may be approximately calculated by assuming a uniform current distribution across the width of the microstripline, and assuming that the ground-plane current is distributed uniformly under the conductor. When the conductor thickness is appreciably greater than a skin depth the conductor attenuation (in nepers/meter) becomes

$$\alpha_c \cong \frac{\sqrt{\pi f \mu \rho}}{Z_o w} \tag{8}$$

where ρ is the conductor resistivity (not the reciprocal of σ in the previous section). Using the parameters for a 50-Ω line on 4-mil GaAs

$$w = 3.6 \text{ mils}$$

$$\rho = \frac{1}{4.1 \times 10^{7}} \quad \Omega - \text{meter}$$

and substituting in (8) gives

$$\alpha_c = 0.687 \times 10^{-4} \sqrt{f} \text{ nepers/meter}$$

$$= \left(0.687 \times 10^{-4} \sqrt{f} \frac{\text{nepers}}{\text{meter}}\right)\left(8{\cdot}686 \frac{\text{dB}}{\text{nepers}}\right)\left(\frac{3 \times 10^8}{f \times 2{\cdot}91} \frac{\text{meter}}{\lambda_g}\right)$$

$$= \frac{6{\cdot}07 \times 10^4}{f} \text{ dB}/\lambda_g$$

At 60 GHz, $\alpha_c = 0{\cdot}25$ dB/λ_g.

A recent paper by R. A. Pucel[16] et al. gives a more accurate value of the conductor attenuation, by assuming a current pattern more nearly that found in practice. The conductor attenuation is reported to be approximately 45% lower under these circumstances. The example above was recalculated using this reference and the attenuation factor α_c was reduced to 0.14 dB/λ_g.

For the calculation of conductor loss, a single layer of gold several skin depths thick, has been assumed. In reality a thin layer (~ 3 μ inches) of molybdenum is applied prior to deposition of the gold layer. As shown in a previous report,* the additional RF loss associated with the multilayer metal system produces a second-order correction. For example, if the molybdenum layer is one-fourth of a skin depth thick (~ 4 μinches at 94 GHz), the RF loss is increased by only 6 percent.

3. Transitions

The evaluation of discrete components at 60 GHz presents a special problem because of the difficulty of obtaining good transitions from waveguide to stripline. Commercial transitions are limited to ~ 18 GHz at present, so an acceptable transition at millimeter wave frequencies had to be developed.

Because of the extremely small size of the millimeter-wave integrated circuits, great difficulty was found in the construction of these waveguide-to-microstrip transitions. Three methods of construction have been used, as described below:

a. Antenna-Coaxial Transducer

The antenna-coaxial transducer consists of an antenna formed by the center conductor of a miniature semi-rigid coaxial cable, which protrudes through the broadwall (i.e., in the E-Plane) of the waveguide. The waveguide is terminated in an adjustable short circuit. The other end of the coaxial cable is connected to the microstripline circuit by bonding gold wires (Figure 9).

* Contract AF33(615)-5012

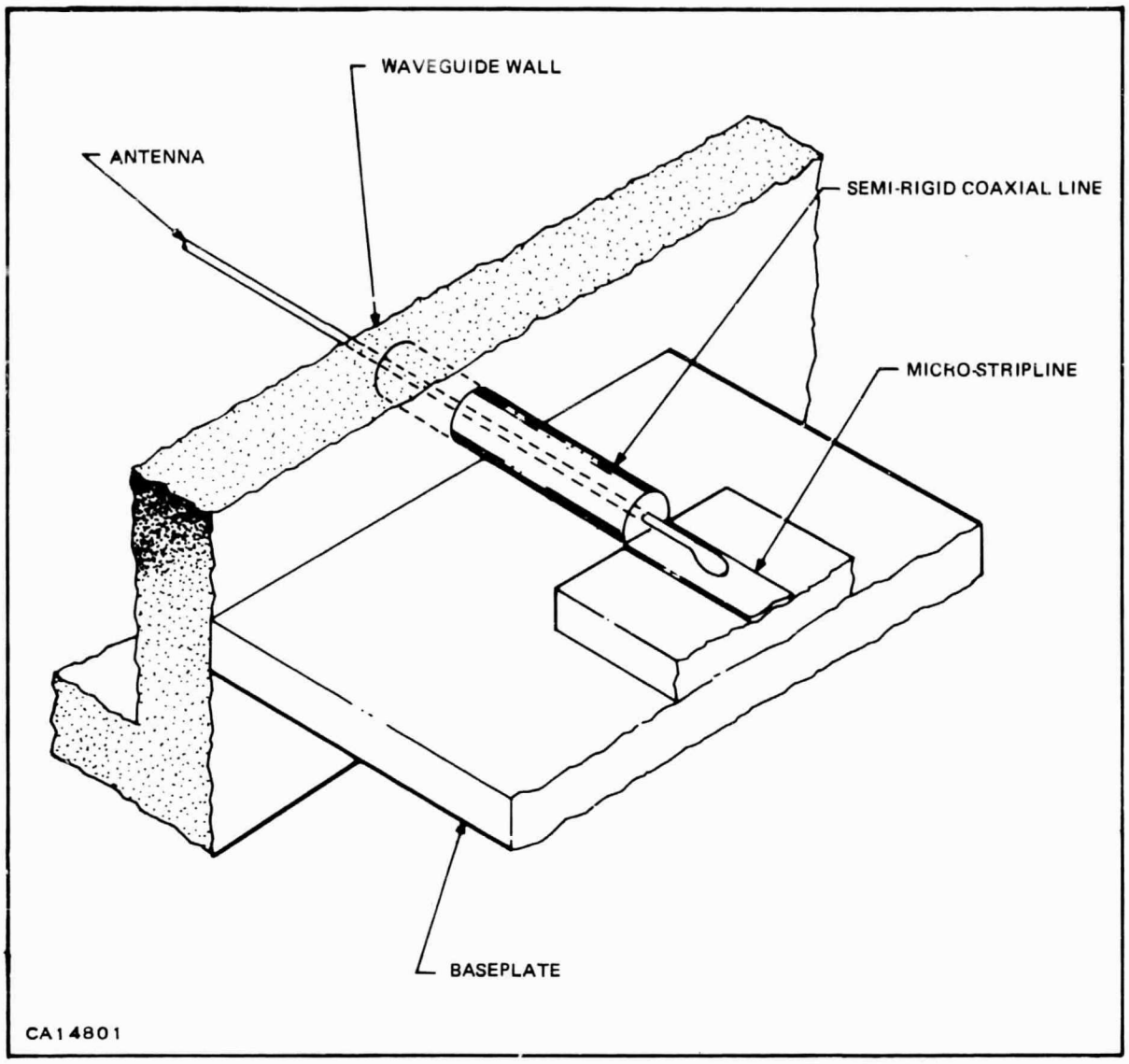

Figure 9. Antenna Coaxial Transducer

The optimum position for the antenna in the waveguide was found by using the design process of Mumford[17] in which the impedance of the probe-piston combination is matched to the coaxial line impedance. A minor revision of Mumford's impedance relation shows:

$$Z_o = Z_g \sin^2 \frac{2\pi L}{\lambda_g} \cos^2 \frac{\pi d}{a} \qquad (9)$$

where

Z_g = characteristic impedance of waveguide

a = waveguide width

d = probe distance from waveguide center

L = distance between piston and probe.

One condition for optimum bandwidth is to pick the piston location giving the least change of Z_o with frequency change. A study of the first derivative of Equation (9) set to zero shows that L/λ_g should be 0.23 to 0.218, as λ/a varies from 1.2 to 1.5 (the usual dominant-mode frequency range). To evaluate this method, a transition was constructed in E-band. A value of $d/a = 0.32$ was selected with an L/λ_g ratio of 0.22, to transduce to the 0.013-inch, miniature, 50-ohm, coaxial line. Measured insertion loss for a transducer pair is shown in Figure 10 to be less than 1 dB at 60 GHz. This form of transition has been used for the input and output of the 30-to-90-GHz tripler.

The assembly of a jig is facilitated by using coaxial transitions, since the circuit and coaxial lines can be mounted onto a base plate and the gold wires bonded in place, thus simplifying insertion into the waveguide.

b. Antenna Feedthrough Transducer

The antenna feedthrough transducer consists of a 1- or 2-mil gold wire antenna protruding through the broadwall of the waveguide at the optimum position as previously discussed. The other end of the wire is bonded directly onto the test circuit, keeping the length as short as possible. The short distance through the waveguide wall forms a coaxial line with air dielectric. Again, the waveguide is terminated in an adjustable short circuit. This transition has given preliminary insertion loss values of approximately 4 dB for a transition pair in E-band (60 GHz to 90 GHz).

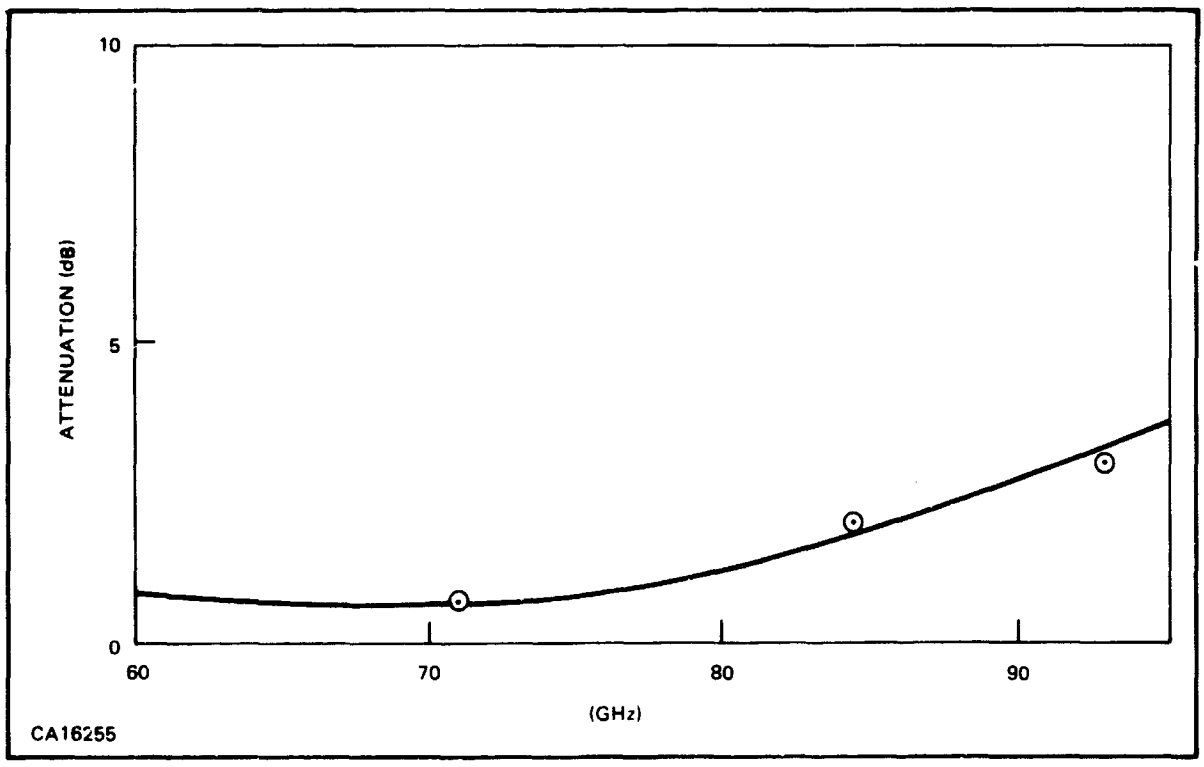

Figure 10. Transmission Loss Through Coaxial Antenna Pair

This form of transition has been used successfully for the measurement of the microstripline cavity and quarter-wave stub described in this section, and of the balanced mixer and single-ended mixer to follow. For measurement, the circuit to be tested was mounted between crossed waveguides, as shown in Figure 11 (this greatly reduces direct leakage due to proximity of the two waveguides). Unfortunately this presents some difficulty in the assembly of the jig. Some experiments were initiated in mounting Gunn oscillators on the outside wall of a waveguide, using the above transition from Gunn device to waveguide.

c. Ridged Waveguide Transducer

The ridged waveguide transducer is shown diagrammatically in Figure 12 and consists of a tapered, single-ridge waveguide. This transforms the signal sent into the waveguide into a field pattern closely matched to the microstripline field distribution, as shown in Figure 13, thus giving a good impedance match. More than 75 percent of the power can be concentrated under the ridge, depending on the width of the ridge relative to the waveguide width. When measured at R-band the tapered ridges had an insertion loss of less than 2 dB for a transition pair.

This form of transition has been used for measurements of microstriplines and cavities at R-band, and recently in E-band. Certain difficulties arise when using these transitions: the direct leakage of power from the open end of the waveguide, which can be minimized by using lossy material at the waveguide mouth and by constructing the two waveguides at right angles, and the destruction of the 4-mil GaAs substrates due to the pressure of the ridge, since a good electrical connection is necessary.

4. Striplines and Passive Stripline Circuit Elements

To design striplines and stripline circuits, it is necessary to know the effective dielectric constant of the substrate for a given line geometry, i.e. accounting for the fringing effect. This has been done by Wheeler[15], and curves computed by us for GaAs are shown in Figures 14 and 15.

Microstrip circuits consisting of transmission lines, disc cavities and tuning stubs, for measurement from 30 GHz to 90 GHz, have been fabricated on semi-insulating GaAs substrates.

One problem is the handling of thin GaAs slices. To avoid spurious modes of propagation and minimize radiation loss, the thickness of the dielectric substrate as well as the width of the strip conductor should be less than 1/8 wavelength. At 94 GHz, the wavelength is approximately 0.044 inch. Therefore, the semi-insulating GaAs substrate should be less than 0.005 inch thick. However, GaAs is brittle, and it is difficult to handle thin, 0.50 X 0.25-inch slices. In spite of the difficulty, we are currently processing 0.004 inch thick slices with reasonable success.

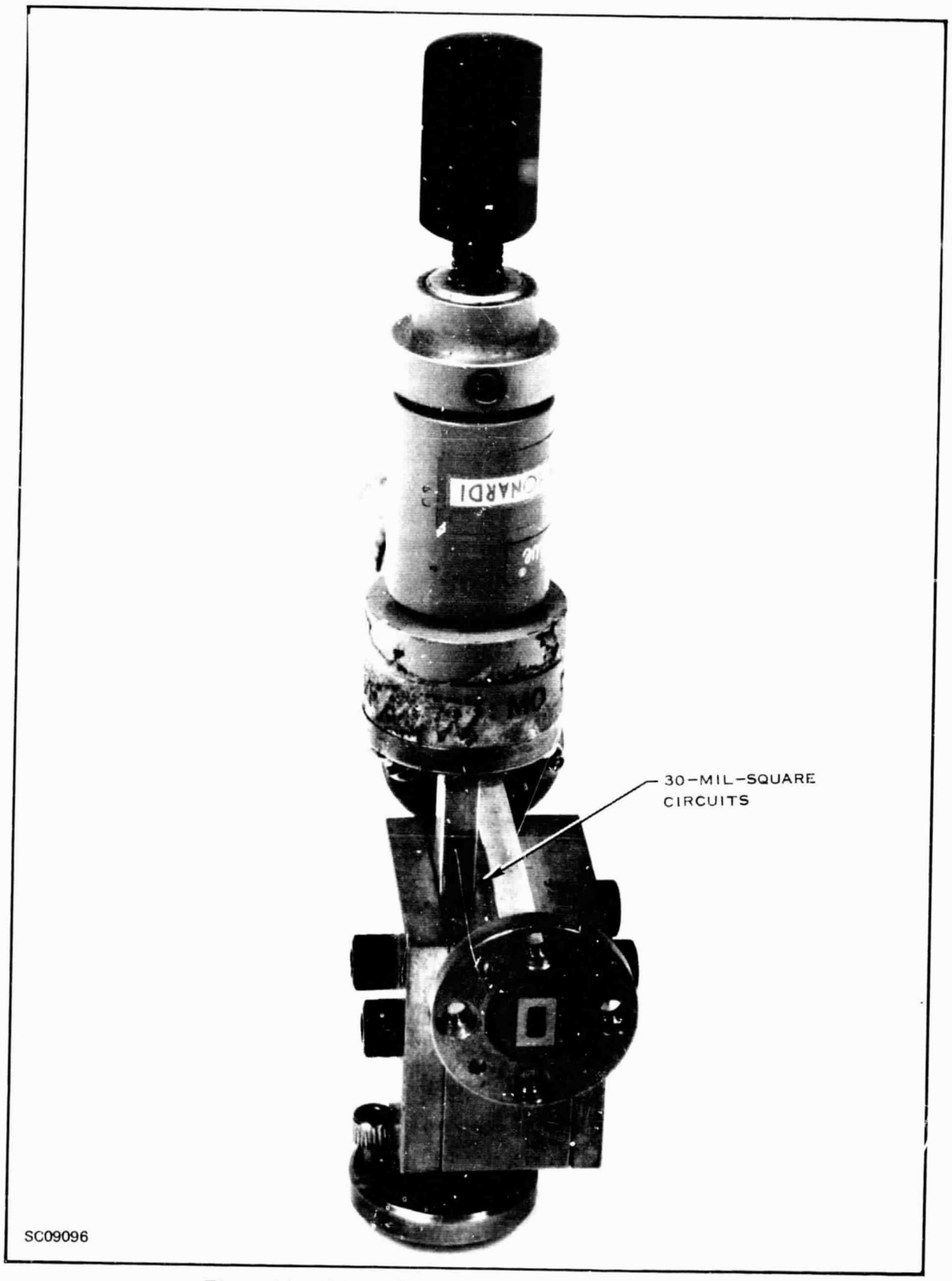

Figure 11. E-Band Crossed Waveguide Measurement Jig

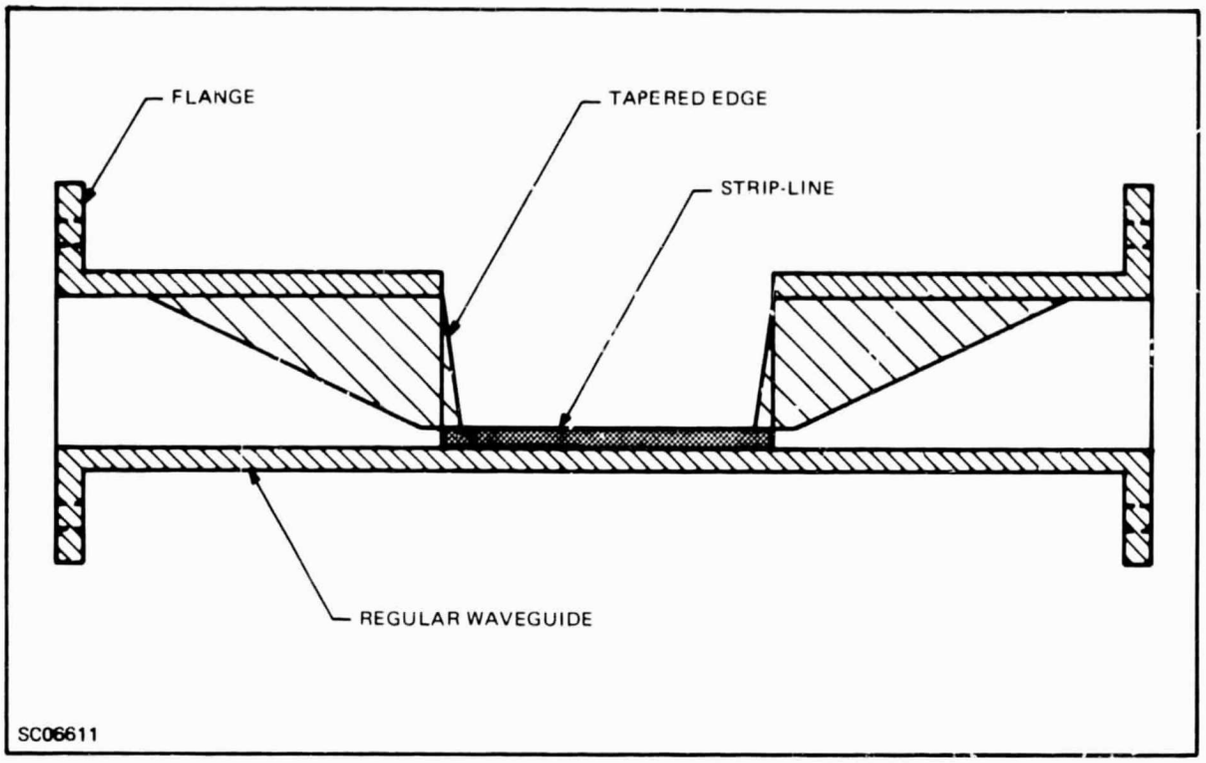

Figure 12. Waveguide to Stripline Transition Using Tapered Ridges

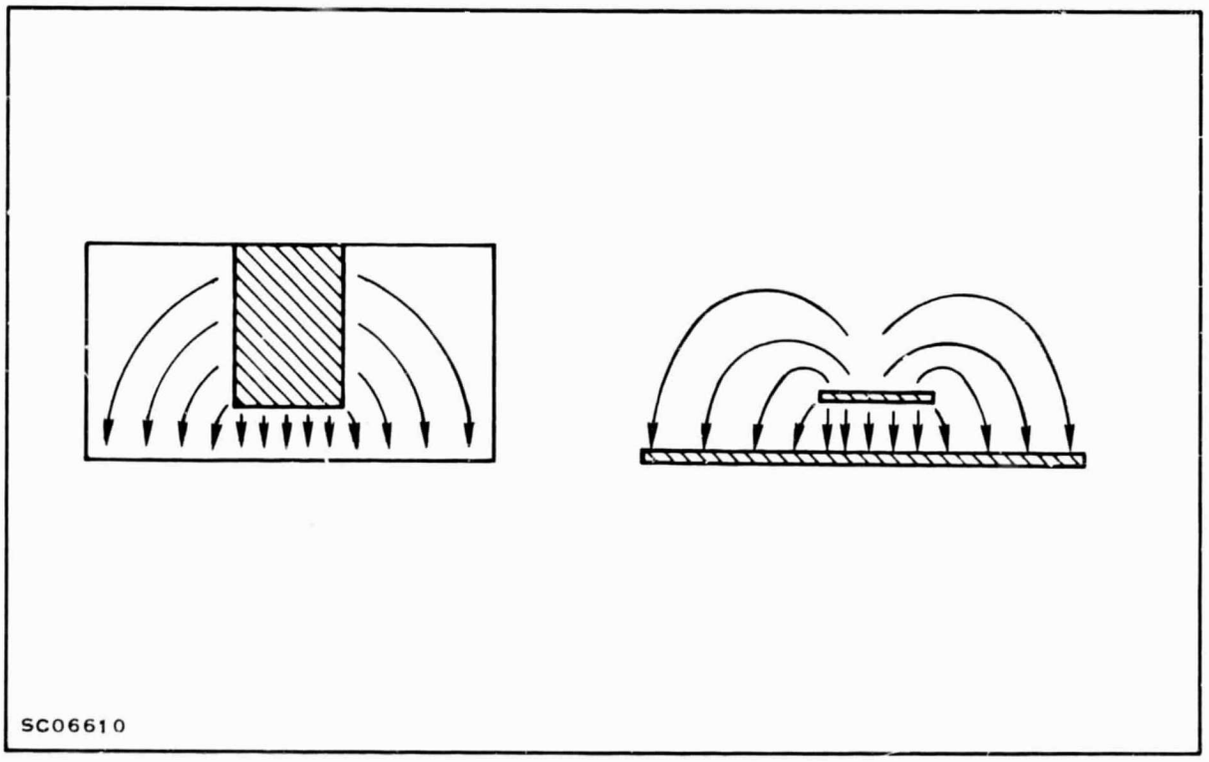

Figure 13. Comparison of Field Distribution in Ridged Waveguide and Stripline

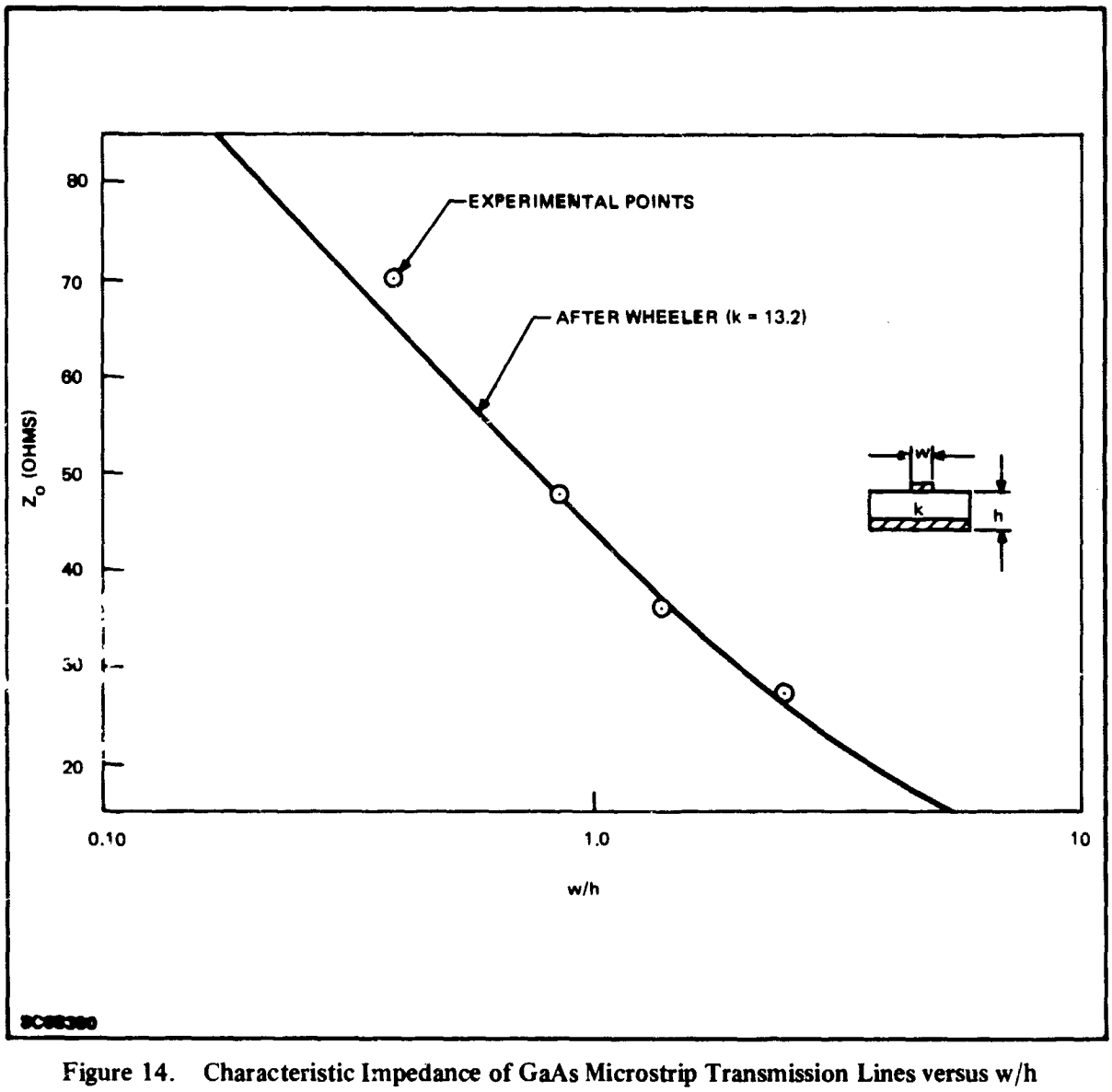

Figure 14. Characteristic Impedance of GaAs Microstrip Transmission Lines versus w/h

The striplines fabricated have included the following (all on 4-mil-thick semi-insulating GaAs):

- Disc Cavities: 1/2-inch-long lines, 2 and 4 mils wide, with circular cavities of various diameters from 4 to 50 mils.
- Tuning Stubs: 1-inch-long lines, 3 mils wide, with 8-mil-wide stubs of various lengths from 25 to 50 mils.
- Variable-Width Lines: 1-inch-long lines, 100 mils apart, with widths varying from 4 to 16 mils; 1/2-inch-long lines, 50 mils apart, with widths varying from 2 to 4 mils; 1/4-inch-long lines, 100 mils apart, with widths from 0.4 to 8.0 mils.

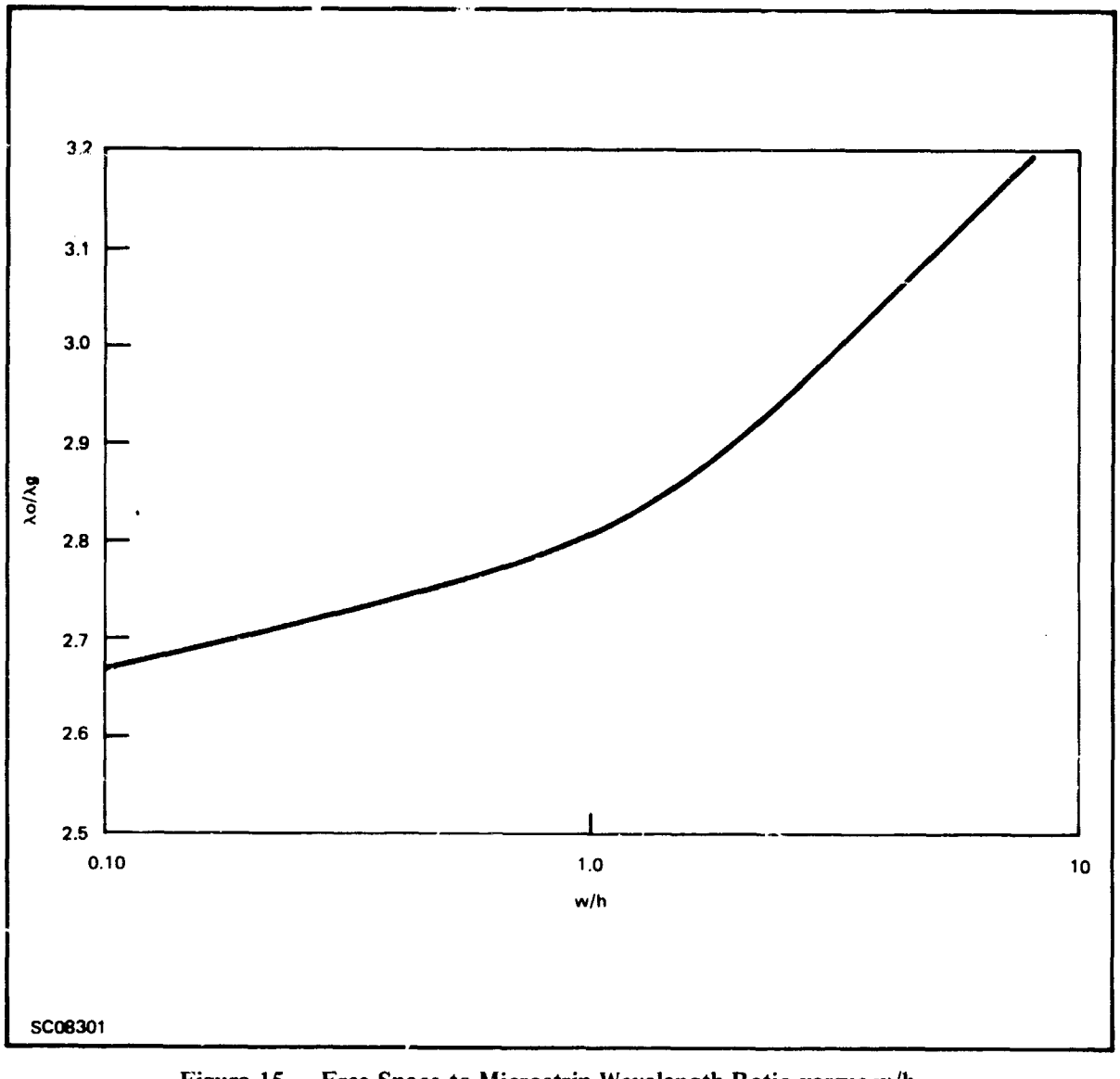

Figure 15. Free-Space to Microstrip Wavelength Ratio versus w/h for GaAs Substrates (k = 13.2)

a. Striplines

The characteristic impedances of microstrip transmission lines have been measured with a time domain reflectometer (TDR). The measured data, shown in Figure 14, agree with the theoretical values predicted by Wheeler.[15]

A 3.5-mil-wide microstripline has been evaluated on semi-insulating GaAs substrates from 60 GHz to 90 GHz. The microstripline was centered on a 30-mil-square GaAs substrate that was 4 mils thick. The microstrip and waveguide transition consisted of a 1-mil antenna which extended to about two-thirds of the waveguide height through a 13-mil hole in the waveguide. The circuit was evaluated in the 90 GHz waveguide jig of Figure 11.

The loss is quite sensitive to both input and output tuning and the mechanical rigidity of the holder.

Owing to the small losses in the stripline (a few tenths of a dB) the results were not conclusive. However, since the overall transmission loss was less than 2 dB from 60 to 80 GHz, (including the transitions) then the stripline itself did not have excessive loss.

To make more accurate measurements of the attenuation/wavelength, longer lines were used at lower frequencies (26-40 GHz). The attenuation in microstripline can be obtained from the Q of the resonance of a loosely coupled transmission line, as shown in Figure 16. The attenuation loss can be determined by a method based on that of Ginzton[18], and from the relation:

$$\frac{1}{Q_L} = \frac{1}{Q_u} + \frac{2\beta'}{Q_e} \tag{10}$$

where Q_L is the loaded Q of the transmission line, Q_u the unloaded Q, and Q_e the external Q. The coupling factor β', was experimentally determined (as outlined by Ginzton) to be approximately one, indicating critical coupling. The loaded (measured) Q_L was found from the usual 3 dB-down response; that is, Δf is the frequency difference between points on the response curve for which the voltage amplitude response is down to $1/\sqrt{2}$ of its maximum value, such that $\Delta f/f_o = 1/Q_L$. The insertion loss through the resonant two-port line is in decibels.

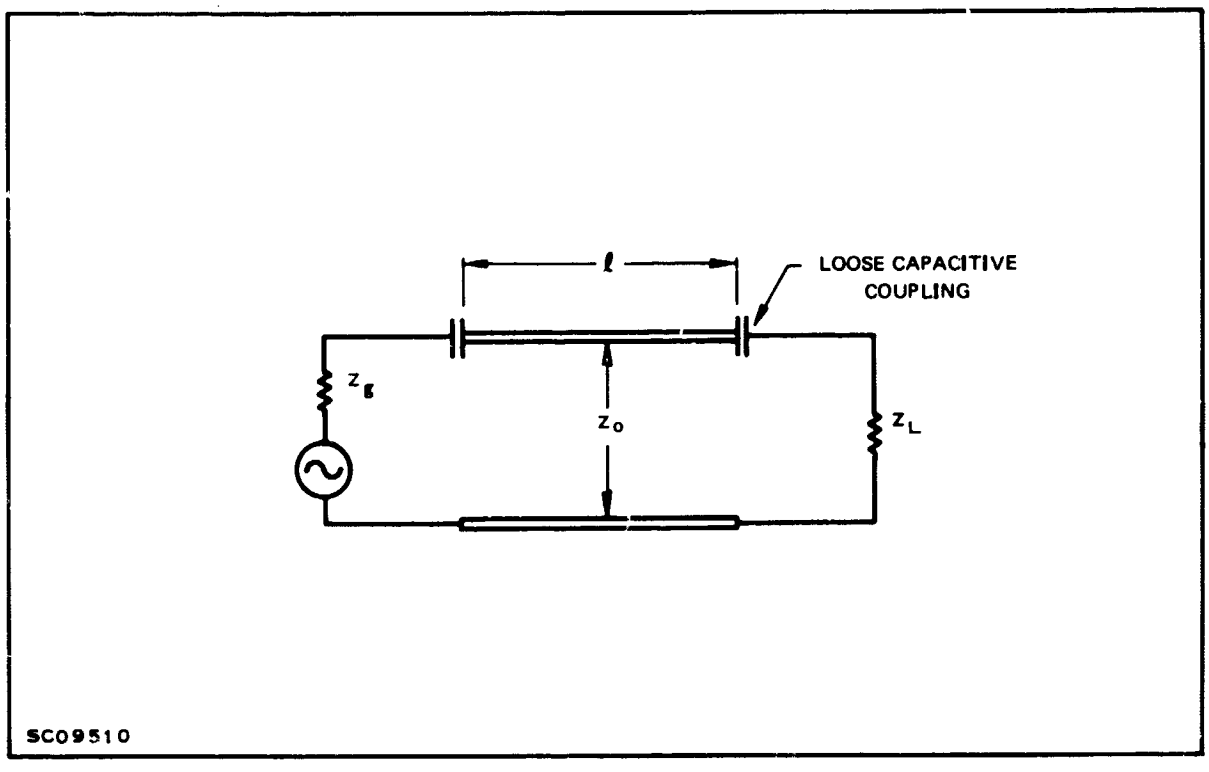

Figure 16. Resonance Measurement on Loosely Coupled Transmission Line

$$I = 20 \log_{10} \left(1 + \frac{Q_e}{2Q_u} \right) \tag{11}$$

From the measured values of Q_L and insertion loss, I, we find the unloaded Q (Q_u) from Equations (10) and (11). Hence the attenuation constant is found from:

$$\alpha = \beta/2Q_u \text{ nepers/length}, \quad \beta = 2\pi/\lambda_g \tag{12}$$

$$\alpha = \frac{27.3}{Q_u} \text{ dB}/\lambda_g$$

Measured values of attenuation by the Q method are shown in Figure 17 with values found by direct insertion loss measurements, and theoretical values derived similarly to those in Paragraph D.2. From these results it is seen that measurements by the two different methods differ somewhat, due to the very small quantities being measured. However, the values obtained show that the insertion loss has a maximum 0.3 dB/λ_g in this frequency range, which is quite acceptable for stripline circuitry.

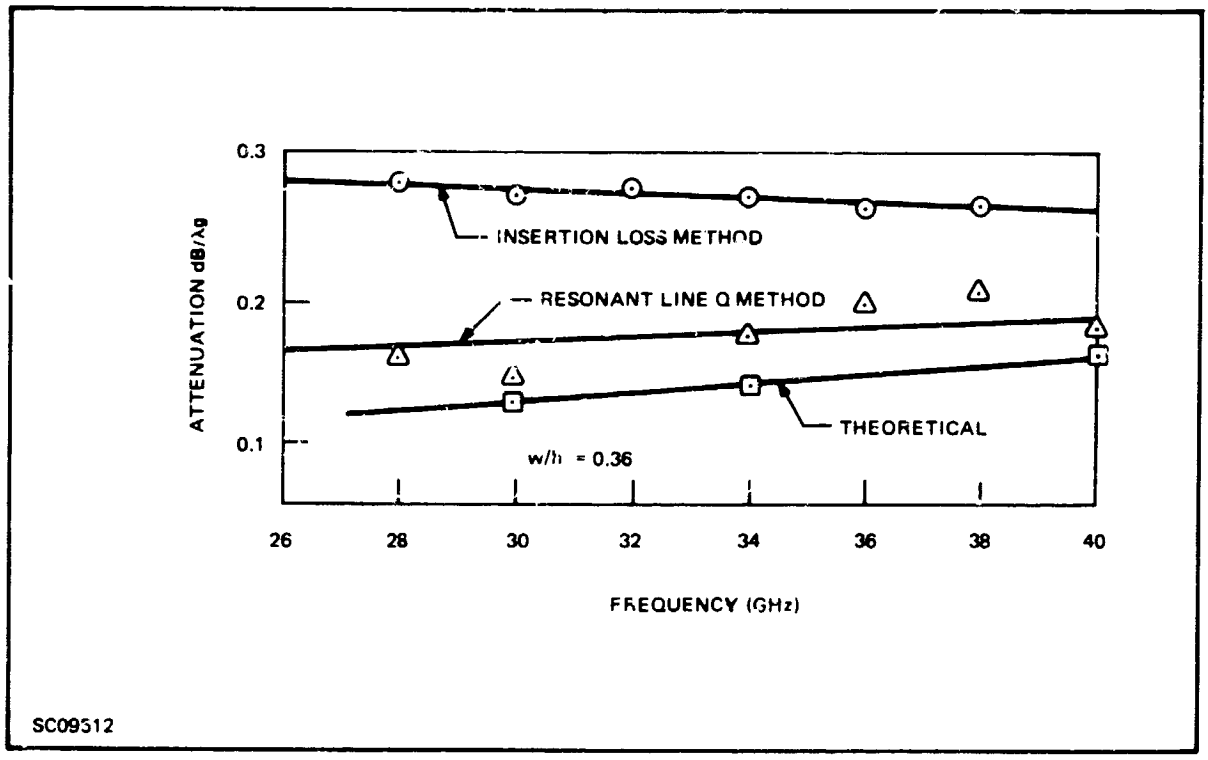

Figure 17. Transmission Line Attenuation versus Frequency

Some measurements have also been made of the field pattern above the stripline which enabled the slowed wavelength to be verified. The arrangement for these measurements is shown in Figure 18 and the results obtained in Figure 19. The results of the slowed wavelength obtained by the resonant line method are also plotted for comparison. The agreement between the two methods and the theoretically predicted results is better than 8 percent.

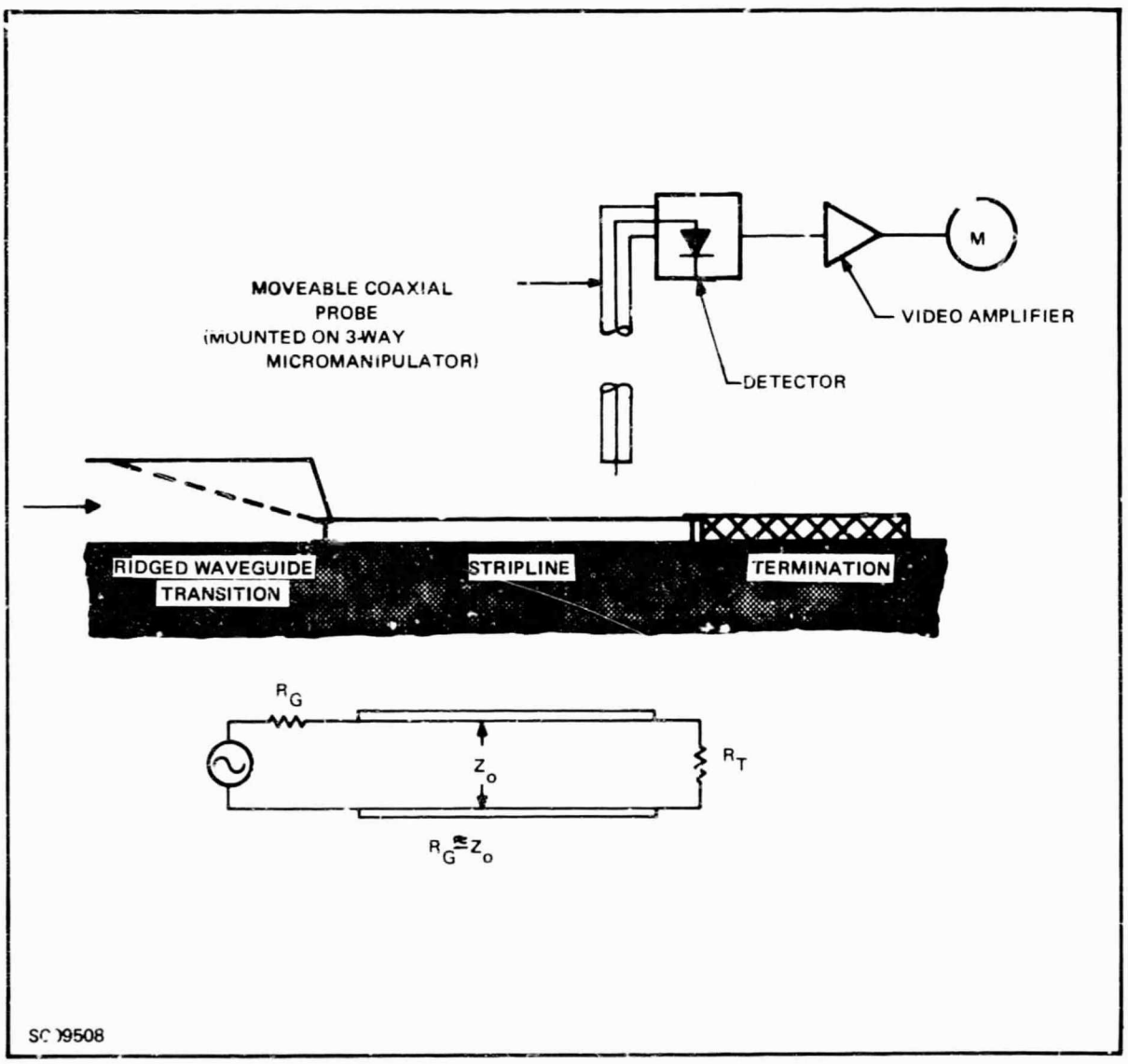

Figure 18. Arrangement of Field Pattern Measurements

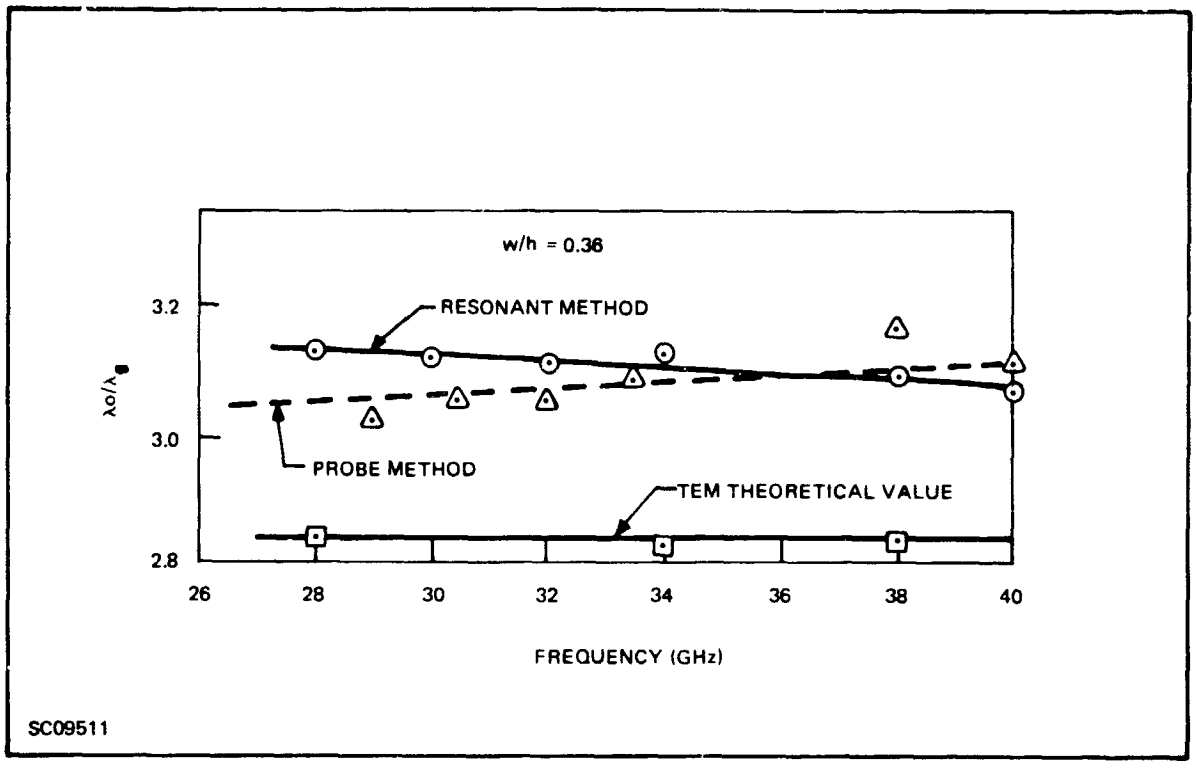

Figure 19. Stripline Wavelength versus Frequency

b. Microstripline Resonant Cavities

The fundamental resonant frequency of a circular microstripline cavity is given by the following relationship:

$$f \approx \frac{0.6\,c}{\sqrt{k}\,d} \quad \text{for } h << d \tag{13}$$

where d is the diameter of the cavity, h is the substrate thickness, k is the dielectric constant, and c is the velocity of light.

Power is coupled into and out of the cavity by means of 50-ohm microstriplines, and the degree of coupling is predetermined by the gap between the cavity and the ends of the microstripline, as shown in Figure 20.

Preliminary measurements on microstripline cavities were carried out using ceramic substrates and adhesive aluminum tape for the metallization. Resonant frequencies of several circular cavities were measured and the results are shown in Figure 21. The theoretical results are plotted for comparison and coincide within ~ 10 percent. Some of this discrepancy is due to the dielectric constant of the ceramic being somewhat different from the manufacturers value of (9.5), and to the fact that fringing at the edges is not negligible.

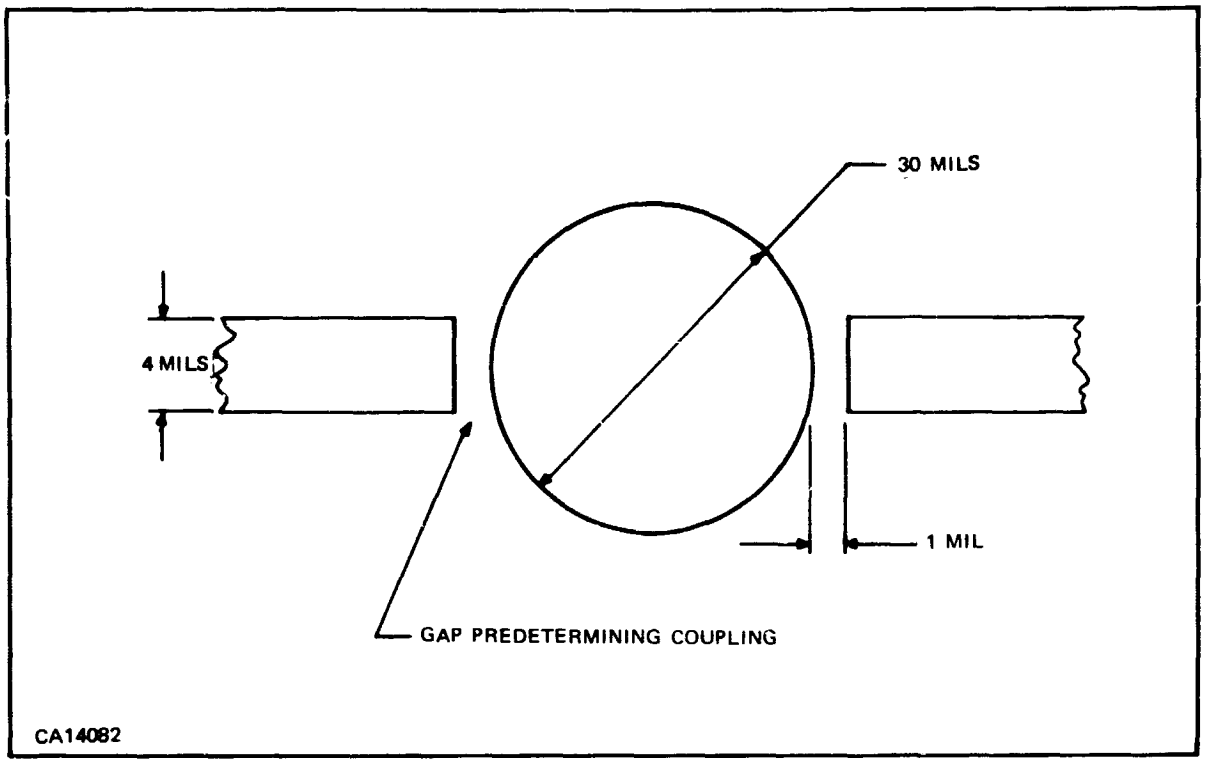

Figure 20. Circular Stripline Cavity

Measurements were then made on a circular cavity on semi-insulating GaAs. For the cavity in question, the gaps were 1 mil wide and the cavity diameter was 30 mils. The substrate was 4-mil-thick semi-insulating GaAs. Equation (13) predicts a resonant frequency of 65 GHz for this case.

The circuit was mounted between crossed waveguides, using antenna feedthrough transducers as described in Paragraph D.3b. The results observed showed an insertion loss of 5 dB with a center frequency of 70 GHz and a loaded Q of 100. Much of this insertion loss is due to the transistion loss, but an insertion loss of at least 3 dB for a cavity with a Q of 100 is expected. Again, the measured resonant frequency is higher than the predicted frequency, in this case by ~ 8 percent. The effect of fringing in a circular cavity is expected to be much the same as in a stripline, i.e., to decrease the effective dielectric constant. This would cause the resonant frequency to increase, as is observed.

c. Microstripline Rejection Filter

The main difficulty in designing a quarter-wave stub on stripline at millimeter wavelengths is that the width of the line is not negligible compared to the length. The actual electrical length of the line is thus in doubt. To clarify this problem a simple microstrip rejection filter, exhibiting the characteristics of a resonator, was fabricated on 4-mil semi-insulating GaAs and evaluated around 90 GHz. The circuit, used for the single-ended mixer to be described later, consisted of a 35-ohm, quarter-wave-length, open-circuited stub which shunted a 50-ohm input and output line on a

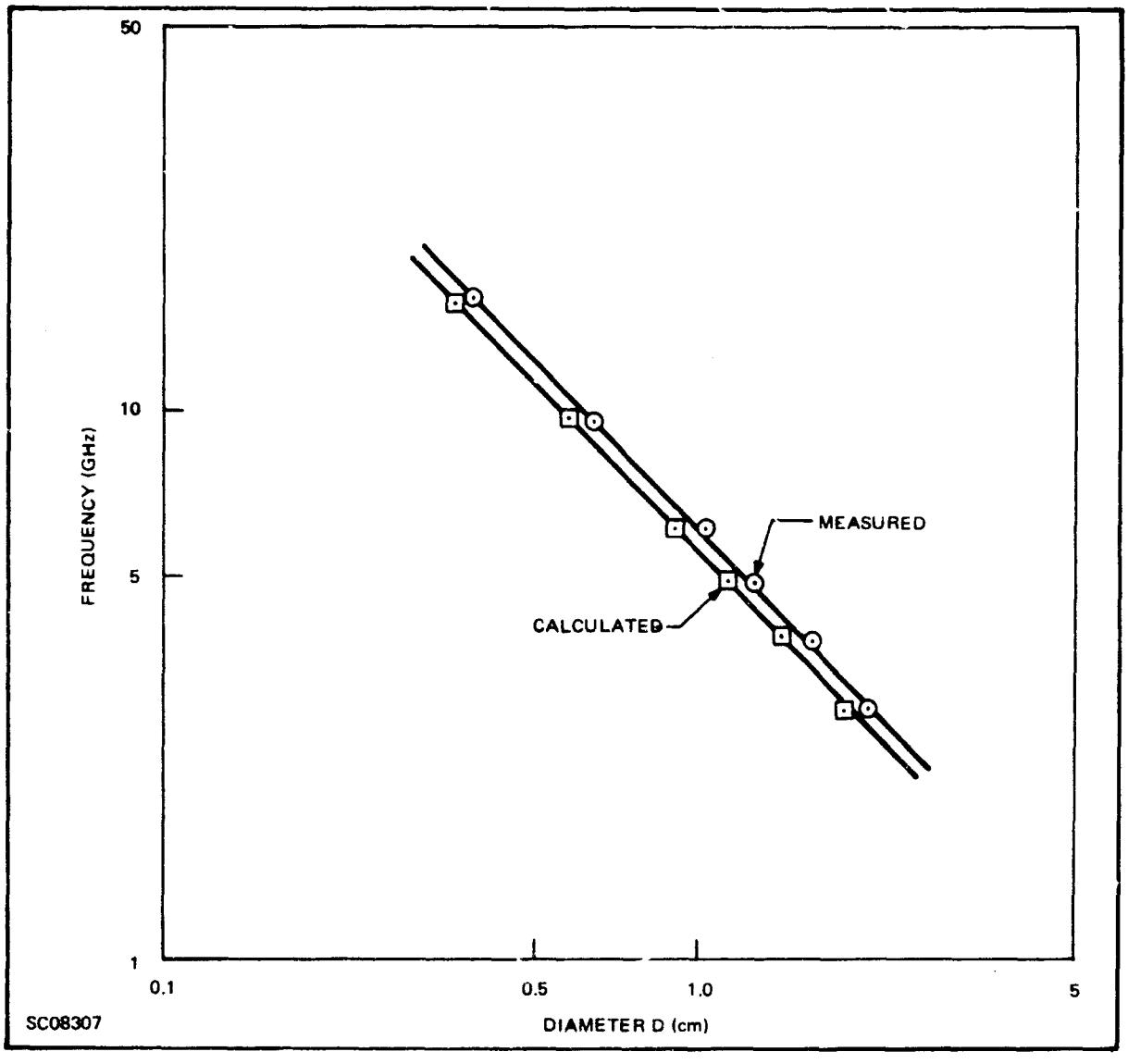

Figure 21. Resonant Frequency versus Diameter for Circular Cavity

30-mil-square substrate. The circuit was mounted between crossed waveguides as shown previously in Figure 11. The insertion loss was measured as a function of frequency and is shown in Figure 22. The frequency of resonance was found to be 96.5 GHz.

Figure 23 shows the actual dimensions of the rejection filter measured. For a 35-ohm line on semi-insulating gallium arsenide the effective dielectric constant is given by

$$k' = 1 + q(k - 1) \tag{14}$$

$$= 1 + 0.665(13.2 - 1) = 9.12 \qquad \left(\sqrt{k'} = 3.02\right)$$

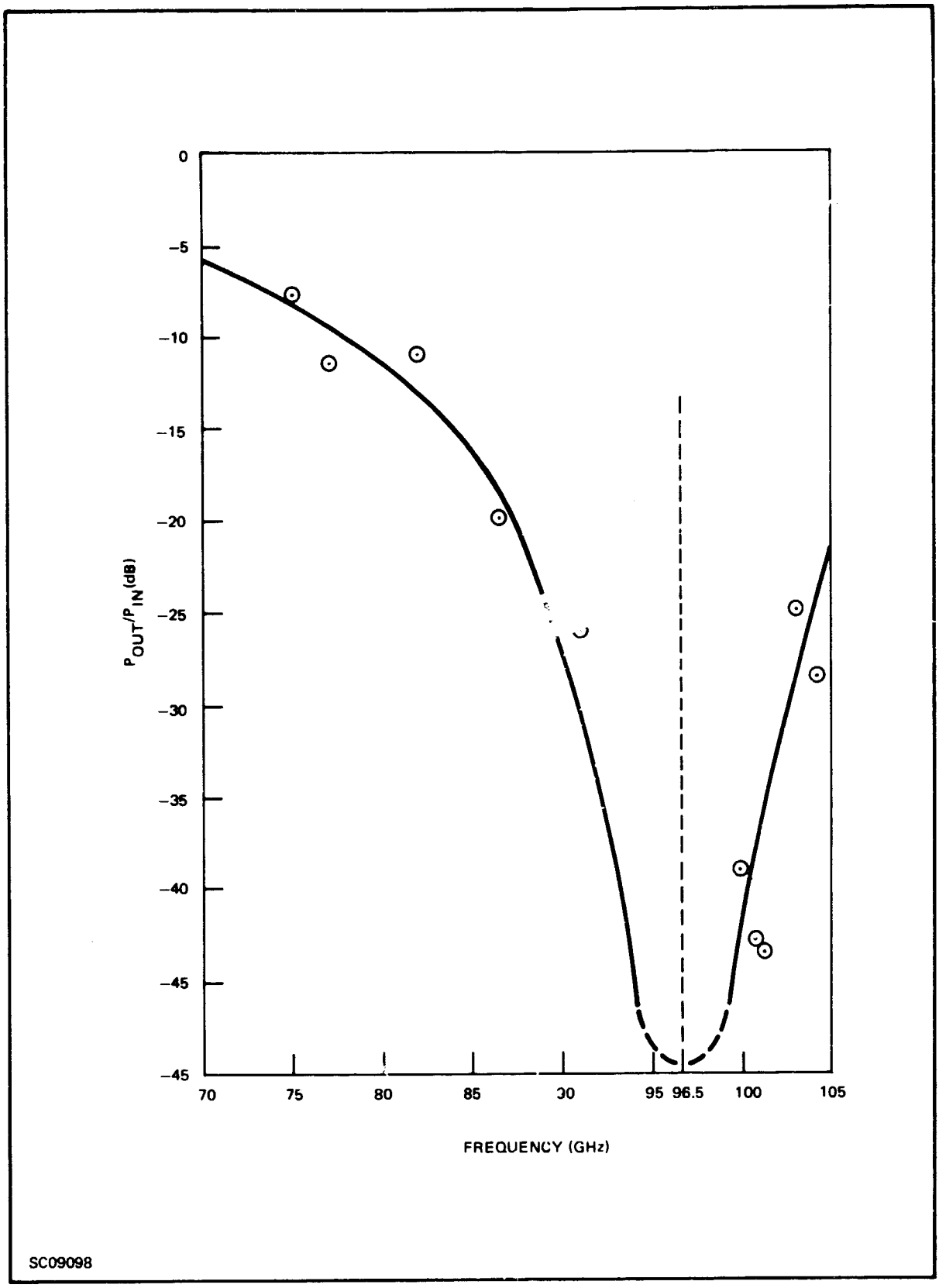

Figure 22. Insertion Loss of λ/4 Stub

Thus for a resonant frequency of 96.5 GHz, the stub length is given by

$$\ell = \frac{\lambda_g}{4} = \frac{3 \times 10^{10}}{4 \times 2.54 \times 10^{-3} \sqrt{k'} \times 96.5 \times 10^{7}} \qquad (15)$$

$$= 10.1 \text{ mils}$$

The actual physical length of the line is seen to be 9.9 mils, thus the apparent reference plane is very close to the plane where the stub joins the 50 stripline (within 2 percent). Results similar to this have also been found at lower frequencies.

5. Gunn Diode Circuits

Initial investigation of the stripline application of Gunn diodes was carried out at lower frequencies using ceramic substrates. Gunn diodes are prone to multi-frequency oscillation, particularly in stripline, and care has to be taken to keep the Q of the resonant cavity as high as possible.

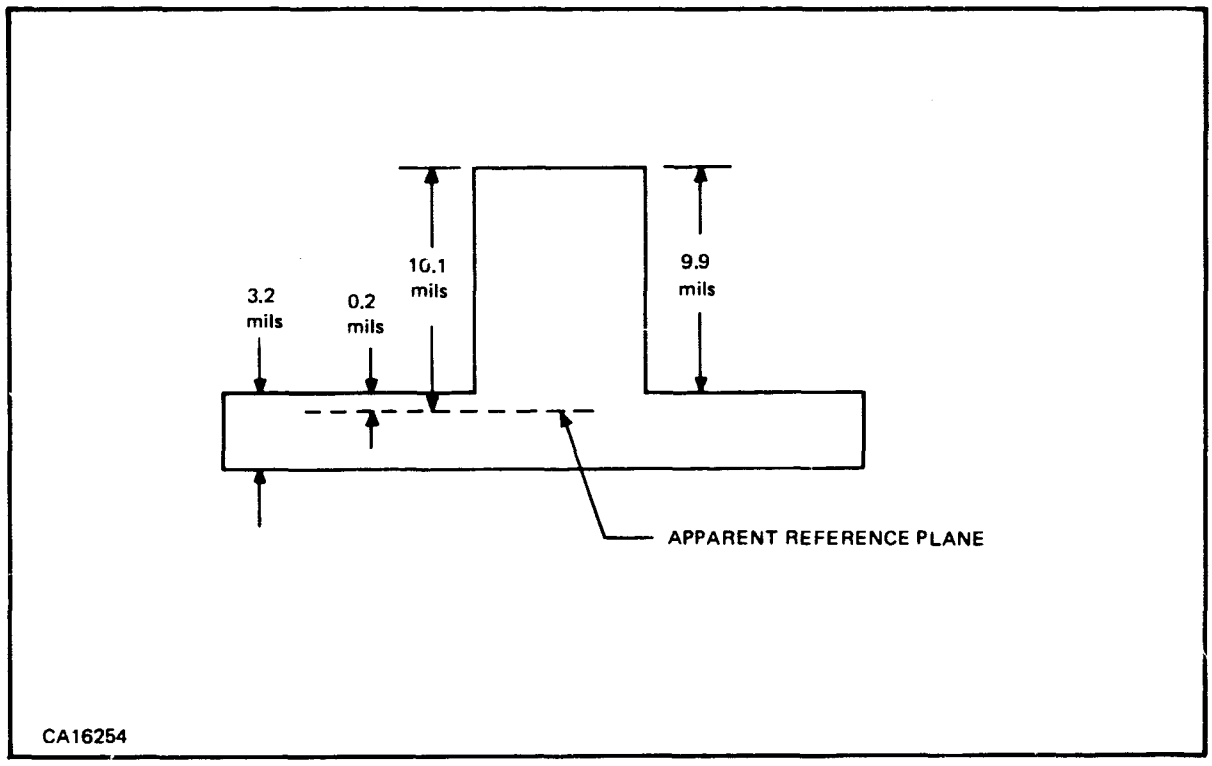

Figure 23. Dimensions of λ/4 Stub

Initially the Gunn diode was incorporated in shunt in a ceramic strip-transmission line, and the bias was applied through the top line and the ground plane. However, multi-frequency oscillation was observed. With a high impedance bias line connected to a low impedance line, single-frequency oscillation was obtained.

An open-circuit full-wavelength cavity also was investigated. The bias was placed 1/4 wavelength from the open circuit and the Gunn diode was placed 1/4 wavelength from the other open end, as shown in Figure 24. The output was capacitively coupled to the cavity. Single-frequency oscillation was easily obtained and the frequency was well defined by the cavity length. The bias circuit still had slight effect on the oscillating frequency.

This circuit is not directly applicable to planar integration, since the planar diode has to be surface oriented, not through the substrate.

A second form of cavity investigated was the circular cavity, as shown in Figure 25. The advantage of a circular cavity is that it is smaller; however, the full wavelength rectangular cavity could be folded to reduce its size. The diode used in this investigation was the 583-16 which oscillated at 6 GHz and had a maximum power output of about 20 mW with an efficiency of 2.2

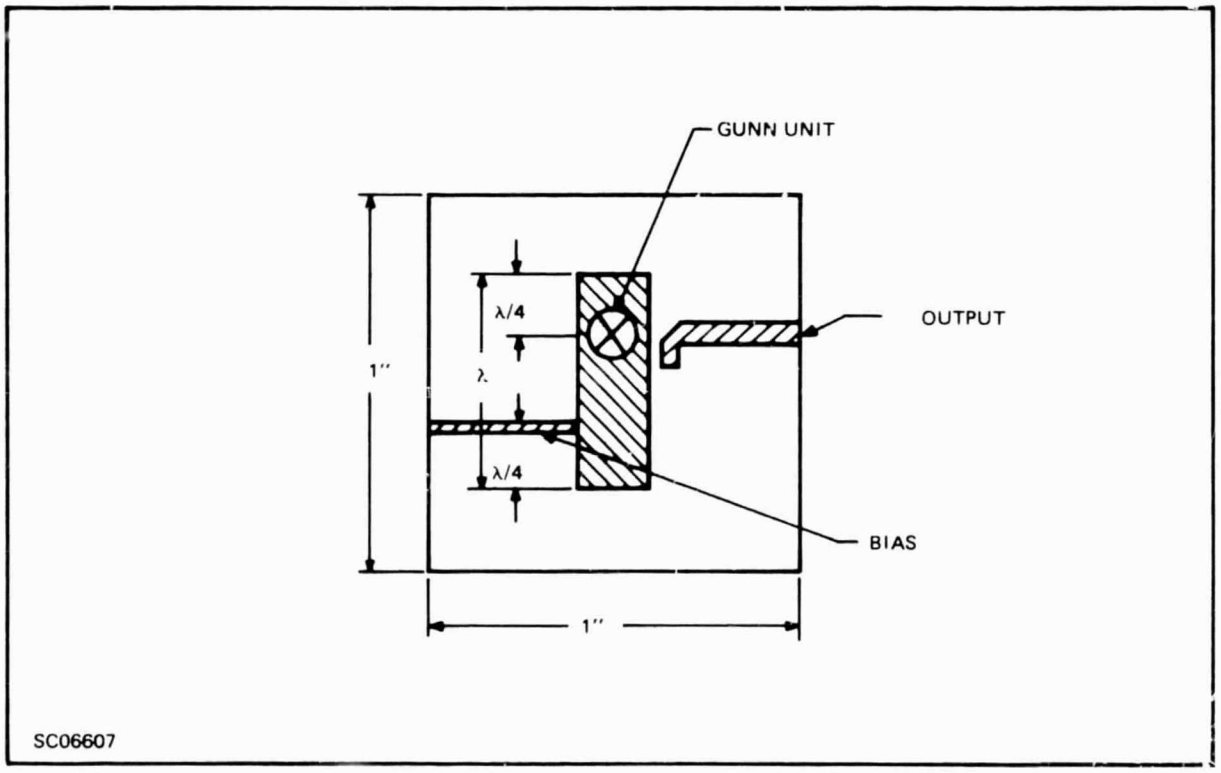

Figure 24. Stripline Gunn Oscillator (decoupled, full-wavelength)

percent in waveguide when biased at 10 volts. The 583-16 is contained in a modified pill package with a pure copper heatsink. Because of the direct connection to ground, there was no need for a quarter-wavelength open stub to provide RF ground. The bias was provided through the RF output terminal by an inductive choke and dc block. The maximum power output obtained at 6 GHz was 16 mW when the unit was biased at 6 volts. The efficiency of this operation is about 2.6 percent, which is higher than that obtained in waveguide circuits.

Substantially higher efficiency, about 3.2 percent, was obtained when the same unit was integrated into a full-wavelength cavity. This rectangular cavity was somewhat different from the one previously described and is shown in Figure 26. The diode was located roughly at the center of the cavity. Maximum power output at 6 GHz was 20 mW with the unit biased at 6 volts. That the power drops when the bias is beyond 6 volts is thought to result from insufficient heatsink in the microstrip circuits. Direct coupling was used in this case to achieve maximum power output.

One major conclusion obtained from the results of the J-band testing of integrated Gunn oscillators is that, at the proper bias, no further tuning is necessary to intiate the oscillation after the cavity is adjusted to the right frequency for the Gunn unit. This eliminates an original concern that the oscillation has to be initiated by tuning, which is difficult to accomplish in the microstrip circuits. However, if the cavity resonance frequency is very far from the transit time frequency, the

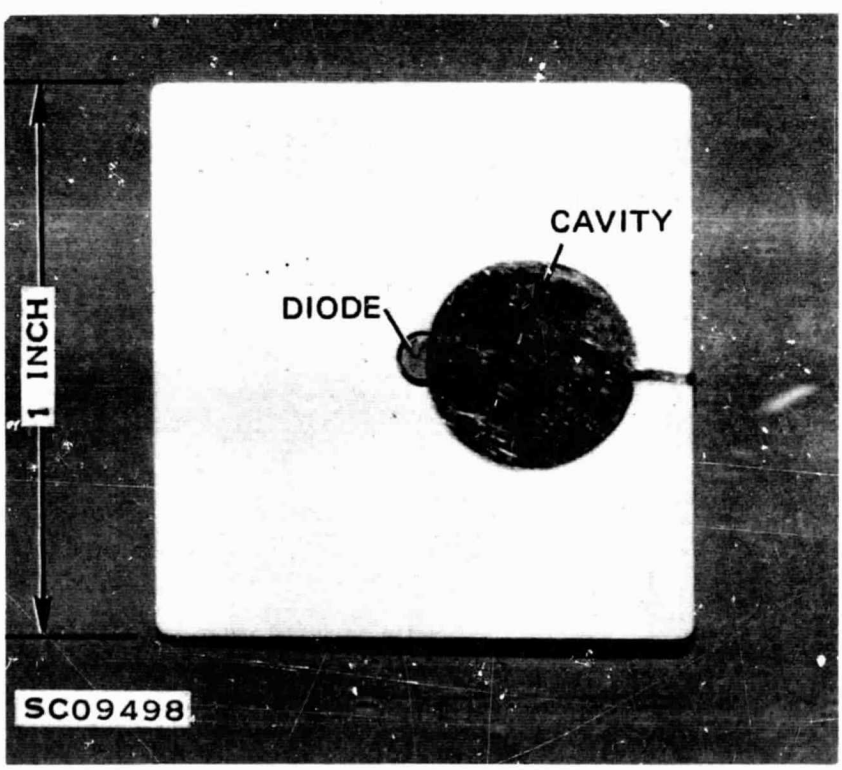

Figure 25. Stripline Gunn Oscillator (circular cavity)

power output will be degraded. Therefore, the match of the Gunn transit-time frequency and the cavity resonance frequency is thought to be somewhat critical, particularly in the millimeter-wave region in which the sample thickness is very small, of the order of 5 μm at 30 GHz. The exact thickness is hard to control or even measure. A plus or minus one micron variation will change the transit-time frequency from 25 GHz to 37.5 GHz, or ± 25 percent.

Because of this limitation, it was hoped that the limited space charge accumulation (LSA) mode of operation might be applicable to this contract. This mode is not based upon a transit-time phenomenon, but does—like the regular Gunn effect—require a material with two mobility states.

The characteristics of the LSA mode are:

- Frequency of operation higher than the reciprocal of the carrier transit time
- Frequency of oscillation determined by the resonant frequency of the circuit
- Power-impedance product can be much higher for this mode than for the regular Gunn mode, and
- Power output and efficiency equal to or higher than when the same device is operated in the normal Gunn mode.

It was hoped to trigger the LSA mode of operation by fabricating a lower frequency Gunn diode into a 60 GHz stripline cavity. However, LSA operation was not observed.

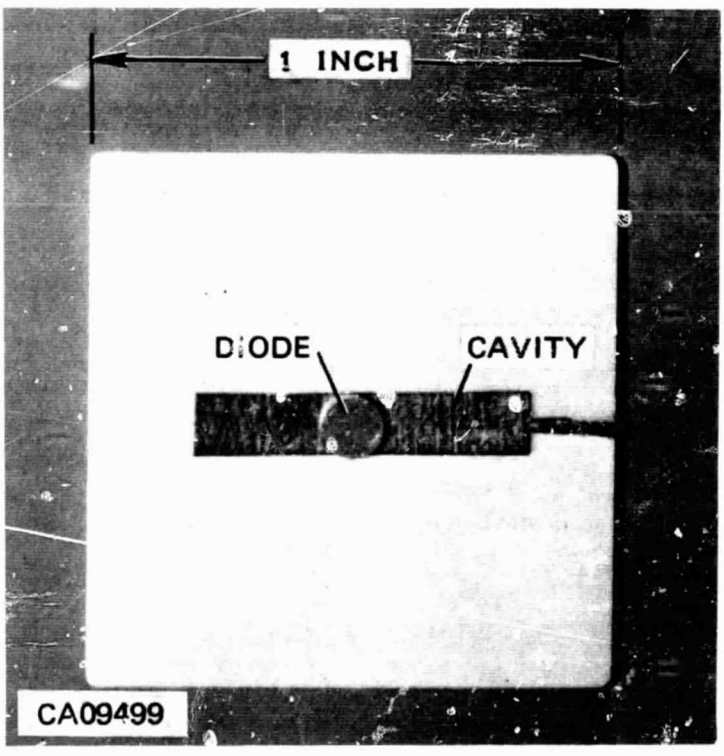

Figure 26. Full-wavelength Gunn Oscillator (directly coupled)

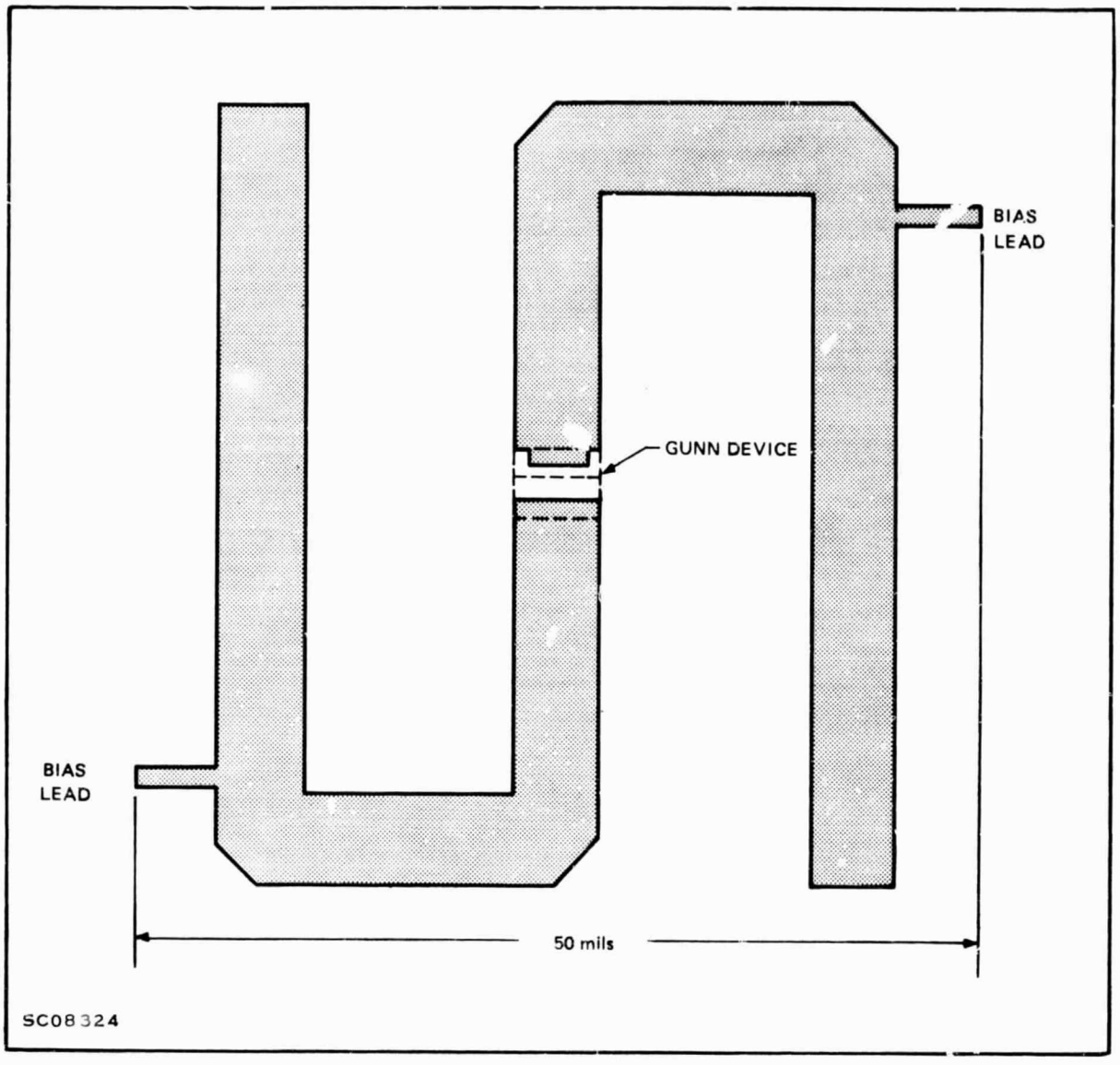

Figure 27. Monolithic Full-Wavelength S-Shaped Oscillator (schematic)

The two microstripline cavities investigated at lower frequencies were used for the integration of Gunn oscillators: one with a full-wavelength, open-circuited resonance cavity and another with a disk cavity.

A full-wavelength, open-circuited resonance cavity was designed for integrating Gunn oscillators at 60 GHz and 30 GHz. The one-sided Gunn oscillator is placed close to the center of the cavity. The configuration, shown in Figure 27, occupies an area 50 mils by 50 mils square.

A circular microstrip resonance cavity was also designed for integrated Gunn oscillators at 60 GHz and 30 GHz. An effective RF ground was formed by the use of a 1/4-wavelength, open-circuit stub. Figure 28 shows this configuration with the biasing arrangement employing 1/4-wavelength, high-impedance stubs with capacitive areas at their ends to provide RF isolation. This oscillator circuit occupies a rectangular area 90 mils by 100 mils.

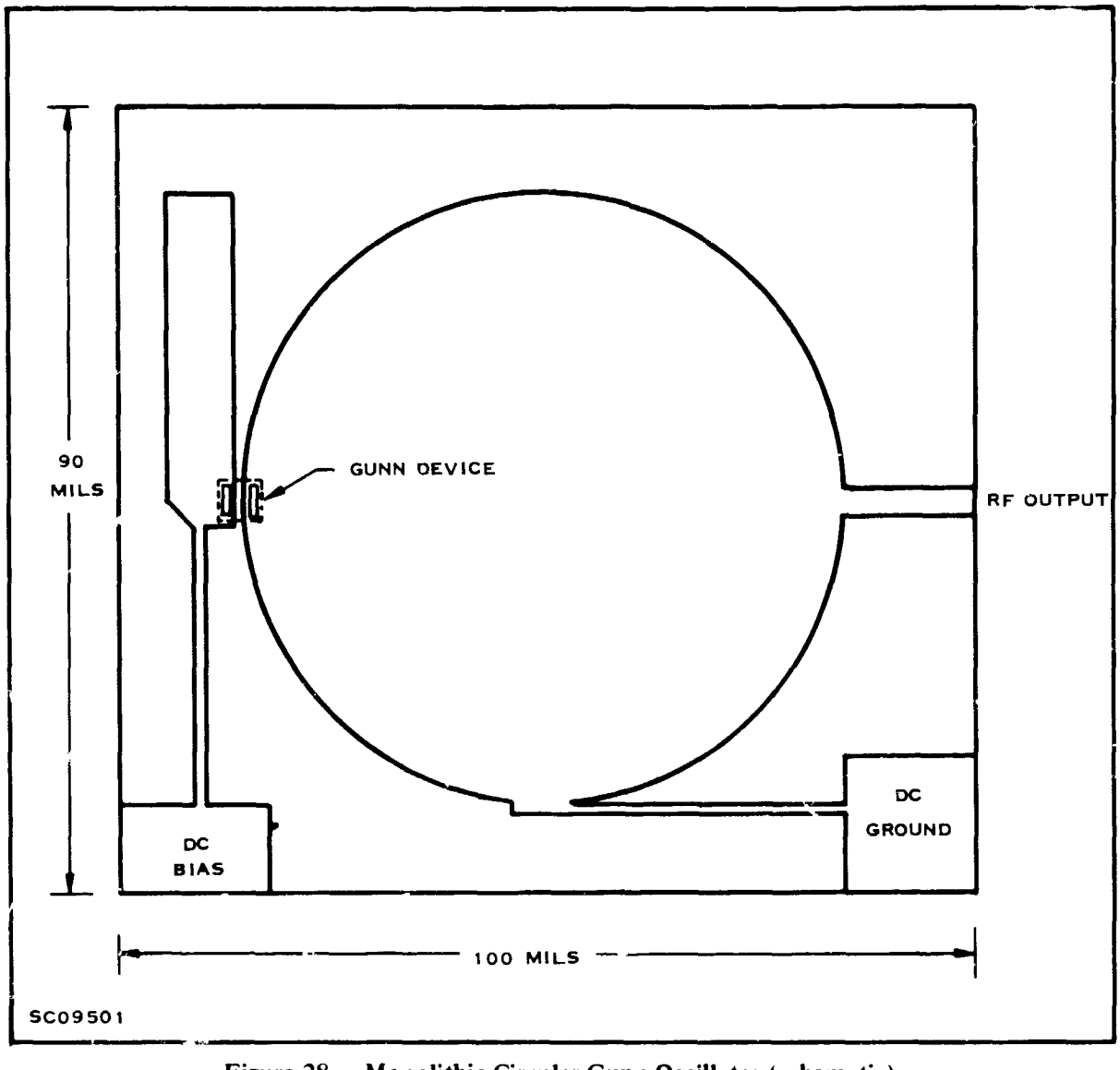

Figure 28. Monolithic Circular Gunn Oscillator (schematic)

Only the full-wavelength, folded, rectangular cavity was fabricated (Figure 29). Owing to the difficulty in controlling the thickness of the N^- layer and its concentration, this monolithic oscillator did not operate successfully. Results from 9 completed slices showed excessive current and higher threshold voltage than anticipated. However, Gunn diodes fabricated in the same fashion on semi-insulating GaAs were mounted in hybrid circuits and operated at 28 GHz with 1.5 mW of output power. This output power was coupled to the waveguide by an antenna feedthrough transition described previously. The threshold voltage for operation at 60 GHz is 0.7 volt, corresponding to an N^- layer 2.5 microns thick. The observed threshold voltage was ~ 2 volts corresponding to an N^- layer of 4.5 microns and a transit-time frequency of ~ 30 GHz.

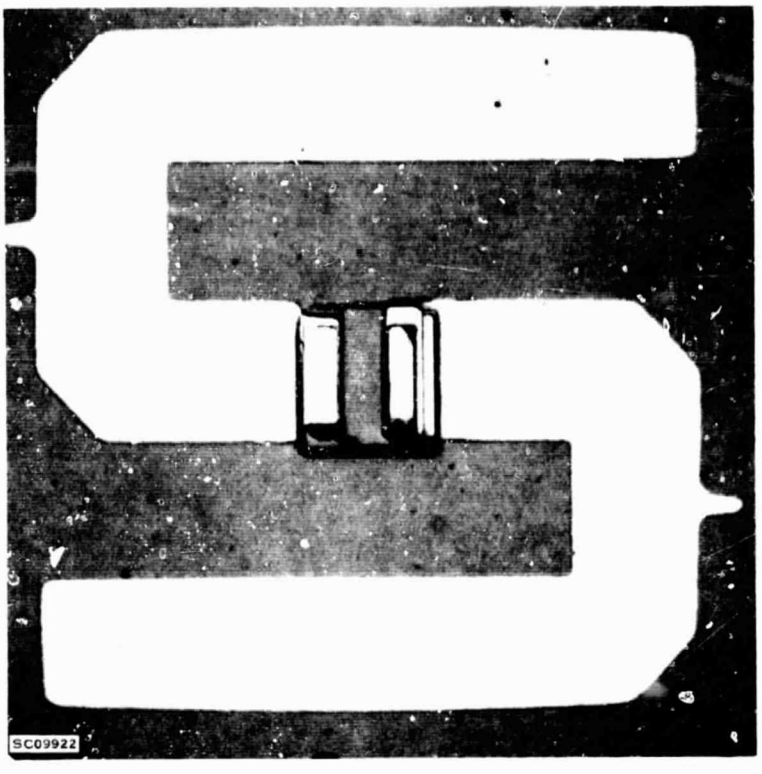

Figure 29. Top View of Actual S-Shaped Oscillator

6. Mixer Circuits

Both single-ended and balanced mixers have been investigated by TI. They are shown in Figures 30 and 31, respectively. The designs were based on a gallium arsenide Schottky barrier diode with the following parameters:

$$C_J(0) \cong 0.02 \text{ pF}$$
$$f_{co} \cong 300 \text{ GHz} \qquad (16)$$

This diode has an RF impedance of approximately 50 ohms at 92 GHz. Therefore, no RF matching is required in the mixer circuit.

The single-ended mixer consists of a Schottky barrier diode followed by a quarter-wave open stub for RF ground, and 50 ohm input and output lines. The substrate was 4-mil-thick semi-insulating gallium arsenide. The diode occupies an area of 0.2 X 0.1 mils and the circuit size is 30 mils square.

The balanced mixer consists of two Schottky barrier diodes, a branch-line coupler, and a quarter-wave open stub for RF ground. Identical Schottky barrier diodes will be used in the single-ended and the balanced mixer. The balanced mixer circuit size is also 30 mils square on a 4-mil-thick substrate.

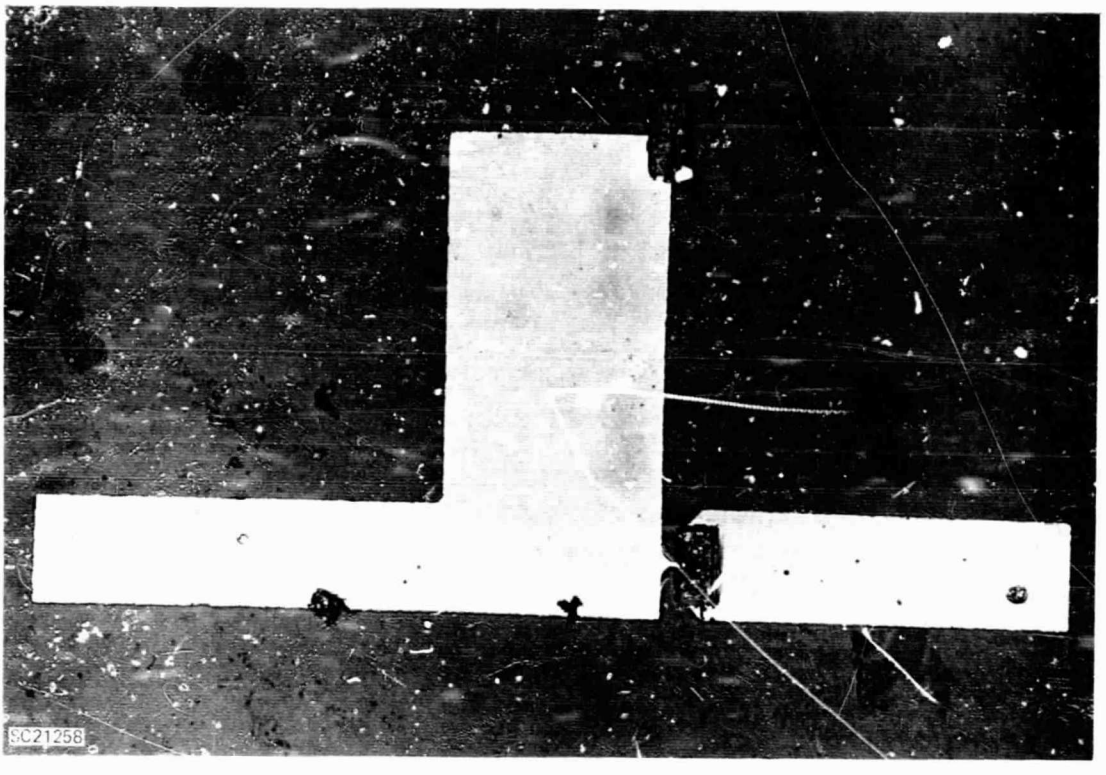

Figure 30. Single-Ended Monolithic Mixer

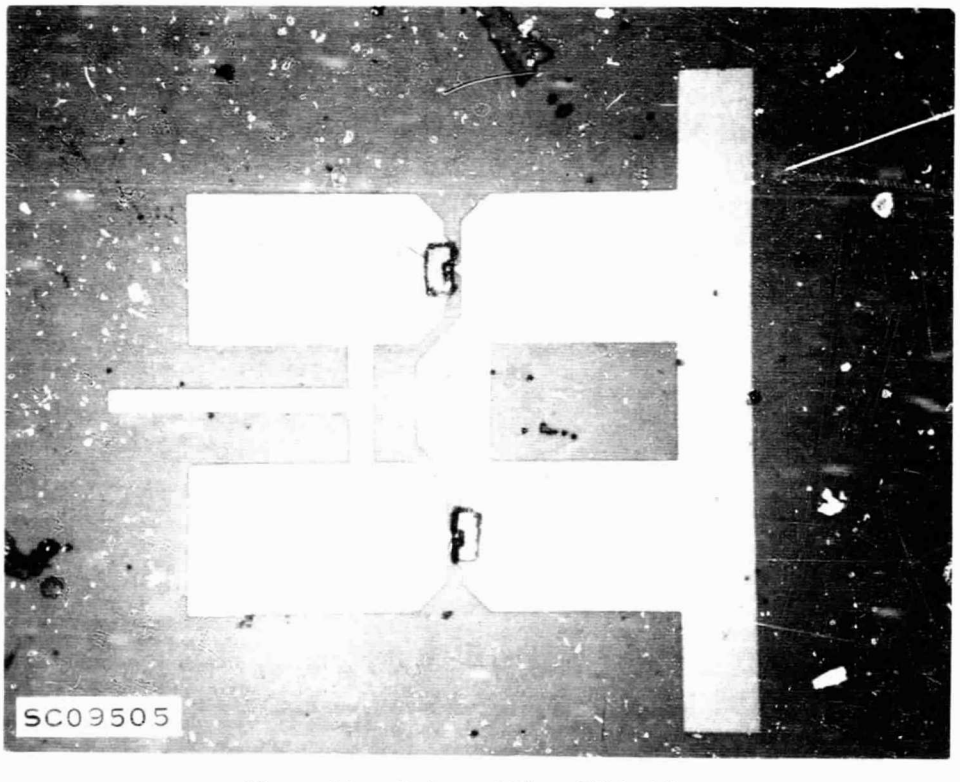

Figure 31. Balanced Monolithic Mixer

Measurements on the Schottky barrier diodes have been made at X-band, where a noise figure of 6.2 dB was obtained for a device of area 0.2 X 0.6 mil having a series resistance of 20 ohms, cut-off frequency of 140 GHz, and zero bias capacitance of 0.056 F. The I/V curve of these devices is shown in Figure 32. The dotted lines are given by the equation:

$$I = I_S \left[\exp \frac{qV}{nkT} - 1 \right] \tag{17}$$

where

n = dimensionless number equal to 1.00 for an ideal Schottky-barrier diode.

To carry out measurements on the complete circuits, it was necessary to use the antenna feedthrough transitions from the 60- to 90-GHz waveguide to the microstriplines, described previously. Initially the single-ended mixer was tested as a detector. The circuit was mounted on the outside wall of the waveguide, and a 40-mil, 50-ohm coaxial line was employed to extract the demodulated output. A ground return was provided to complete the IF circuit, since there is no IF ground return via the waveguide. It was also possible to apply bias through the IF coaxial cable. A high resistance was provided in the bias loop to prevent loading the IF circuit.

To test the balanced mixers two transitions were necessary, so the circuit was mounted between two crossed waveguides. The IF output was extracted through a 50-ohm ceramic microstripline followed by a 40-mil, 50-ohm coaxial line. Two adjustable waveguide shorts were used to maximize the transmission of local oscillator and signal powers.

Examination of the I/V curves of some single-ended mixers indicated that the forward characteristics were similar for most devices, with a current of 50 μA at forward bias voltages between 0.44 and 0.48 volt. In the reverse direction, however, the characteristics were quite different, with currents ranging from 8 to 40 μA at 1.0 volt. Devices with almost symmetrical forward and reverse characteristics operated as detectors when high forward bias voltages were applied, as expected; but the minimum detectable signal was poor because of this high bias current. The more asymmetric devices were found to operate in a satisfactory manner with no applied bias. The improvement in conversion efficiency upon application of 20 μA forward bias was only 2 dB, and the minimum detectable signal is degraded by the forward bias current. The minimum detectable signal at 87 GHz was found to be better than – 54 dBm/Hz, as shown in Figure 33. Conversion efficiency is seen to be 5 dB better than that of a 1N53 diode in a Phillips mount.

Two different frequency conditions were used in testing the balanced mixers, as indicated in Table I. Unfortunately the loss of local-oscillator power through the transitions is excessive, and optimum drive power was not achieved at the diode in either case. Results show that the balanced mixers are not as sensitive as expected, but further improvements should increase the sensitivity by several orders of magnitude. The major problem at present is the critical requirements of the masks, since very small misalignment causes imbalance of the two diodes.

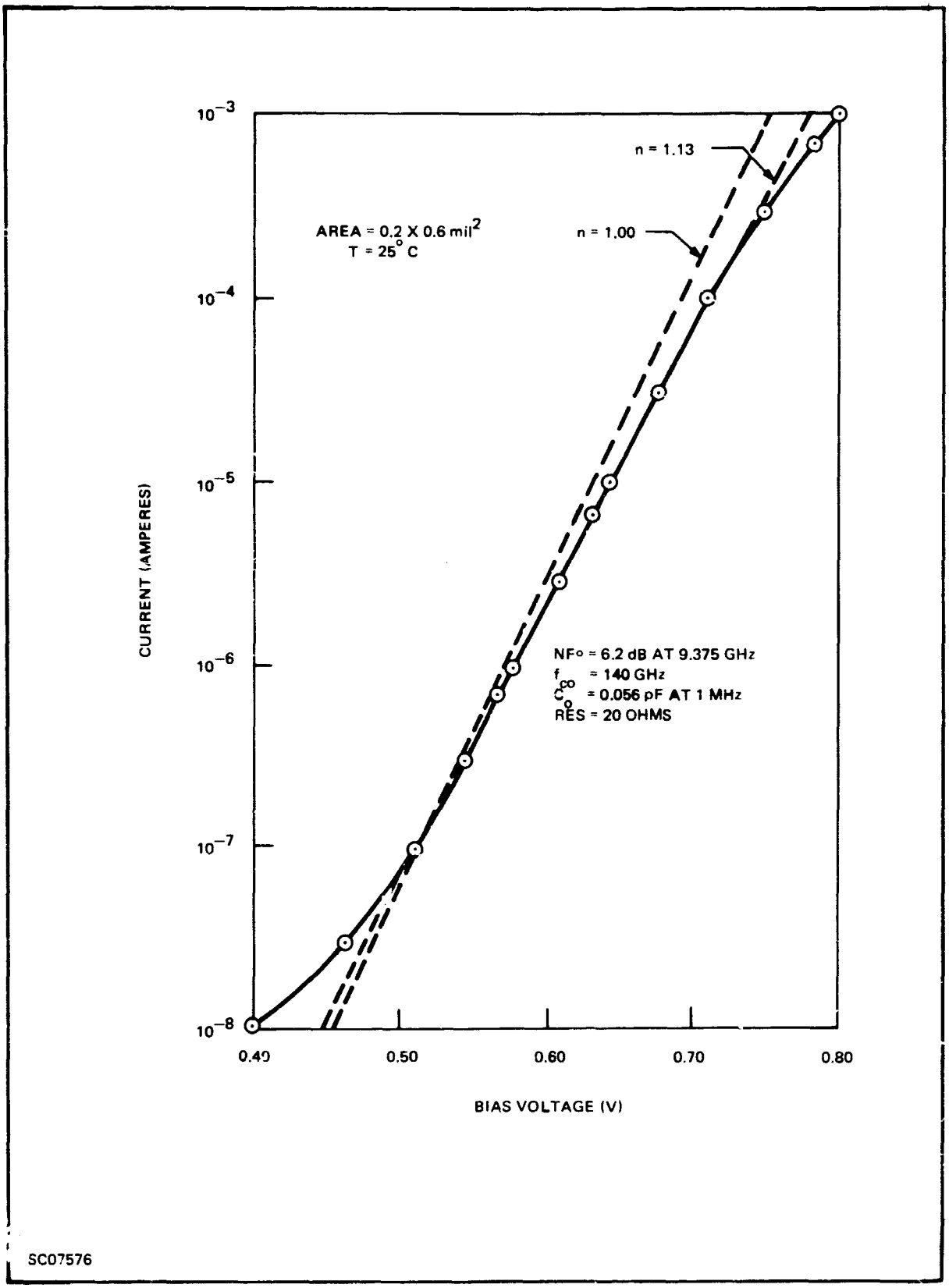

Figure 32. Current/Voltage Characteristic of Schottky Diode

Table I. Balanced-Mixer Results

Case	Signal Frequency (GHz)	Local-Oscillator Frequency (GHz)	Minimum Detectable Signal For 1 Cycle Bandwidth (dBm)
1	71.0	68.5	-125.5
2	90.0	87.5	- 93.5

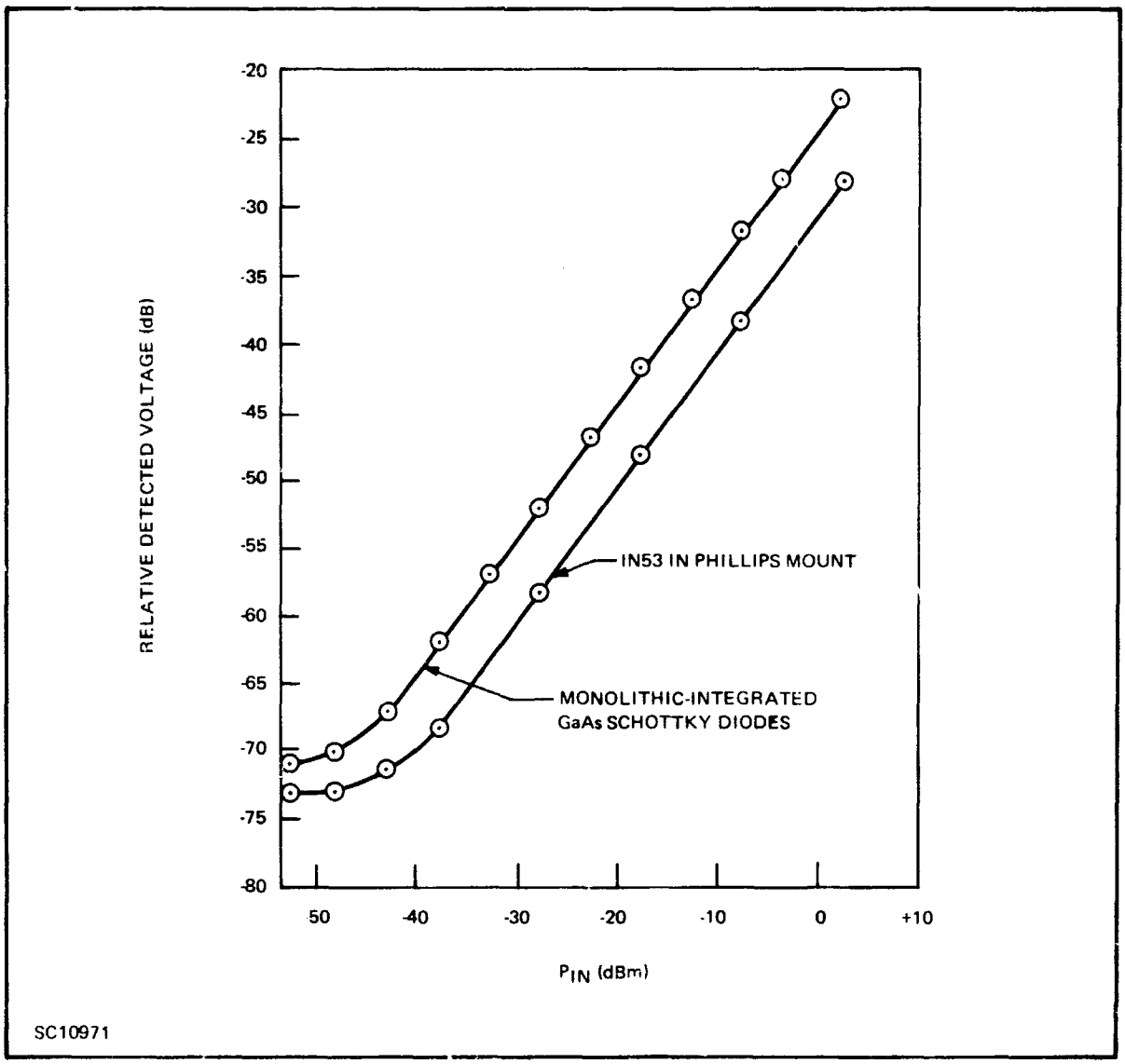

Figure 33. Sensitivity of Single-Ended Mixer as a Detector

7. Complete Receiver

A completely integrated front end at 94 GHz was fabricated for Contract AF33(615)-5102 on semi-insulating GaAs (Figure 34). Because of the present limits in GaAs technology, spurious growth during epitaxial depositions was apparent, and the masks for metal contacts and circuit definition did not make direct contact to the surface of the substrate. Thus the fine geometry required for high-frequency devices could not be obtained. Since many devices were still short-circuited by the unremoved metal, the yield on the completed receiver was very low.

Some of the active devices in the final circuit were operative, and I/V curves were taken for these. The results are shown in Figure 35 for a single Schottky barrier diode, and a pair of Schottky diodes back-to-back for the balanced mixer. Results were encouraging, but no circuit with four operative devices was obtained.

At this point, it was felt that there was insufficient time remaining to permit a successful completion of the project using GaAs monolithic technology, and it was mutually agreed by NASA and TI to pursue an alternative hybrid approach.

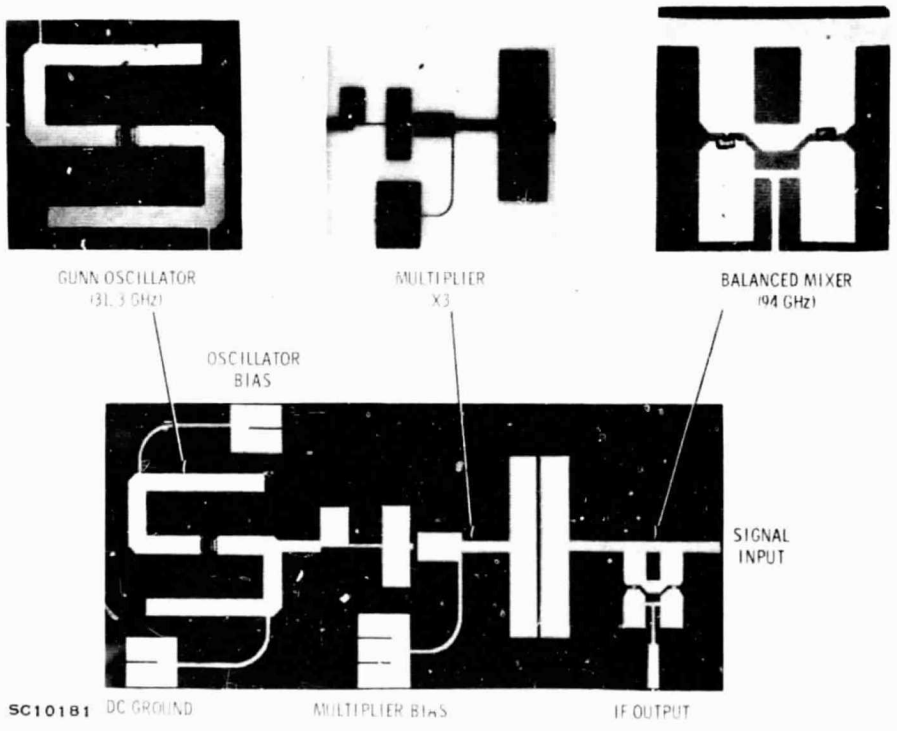

Figure 34. 94 GHz Integrated Microwave Receiver

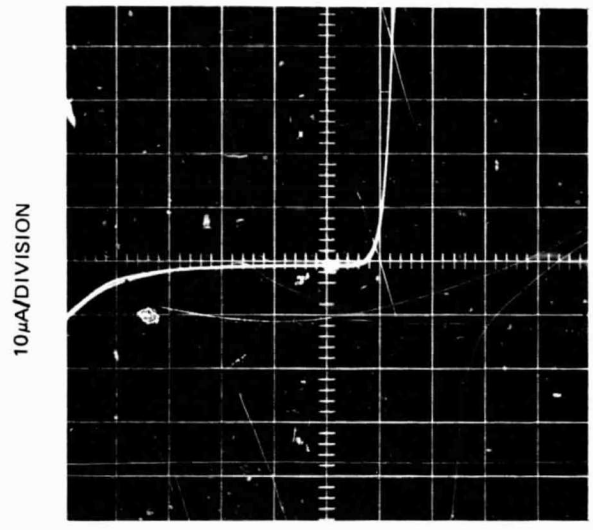

0.5 V/DIVISION
a. I/V CURVE OF SCHOTTKY DIODE

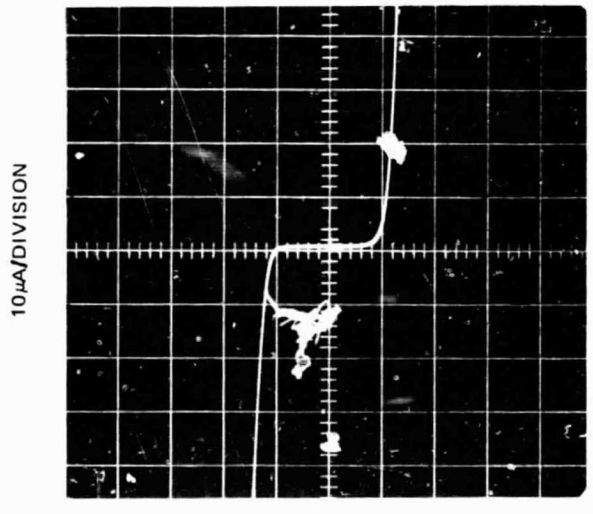

0.5 V/DIVISION
b. I/V CURVE OF BALANCED PAIR OF DIODES

CA16253

Figure 35. DC Characteristics of Monolithic Diodes

SECTION III

HYBRID CIRCUIT APPROACH

A. SUBSTRATES[19]

It was proposed to fabricate the 60 GHz receiver front-end in the hybrid form, i.e., using discrete devices bonded onto microstriplines. Using this method the size and weight are very much smaller than the waveguide counterpart.

Several different substrates are commonly used for the fabrication of microwave hybrid circuits, viz, alumina, sapphire, quartz and beryllia. Table II shows the thermal expansion and conductivity of several materials for comparison. For high frequency-stability with temperature, the thermal expansion should be as low as possible; for high power handling capability the thermal conductivity should be as high as possible. However, these two characteristics are rarely found together in one material. Comparing these materials, quartz is seen to have a very low thermal expansion, while for alumina, it is quite high. Quartz is not a good thermal conductor while beryllia is.

Table II. Thermal Conductivity and Expansion Coefficients

Thermal Conductivity	
Sapphire	0.065 cal/sec cm °C
Copper	0.9 cal/sec cm °C
Quartz	0.0035 cal/sec cm °C
Alumina	0.05 cal/sec cm °C
Beryllia	0.45 cal/sec cm °C
Diamond	4.5 cal/sec cm °C
Thermal Expansion	
Sapphire	8×10^{-6}
Copper	16.7×10^{-6}
Quartz	0.55×10^{-6}
Alumina	8×10^{-6}
Beryllia	7×10^{-6}
Diamond	1.2×10^{-6}

The second limitation governing the choice of substrate is the very short wavelength at millimeter-wave frequencies. At 60 GHz the wavelength in alumina and sapphire (which have dielectric constants of approximately 10) is 70 mils while in beryllia it is about 85 mils. To use discrete devices such as Schottky barrier diodes on a substrate such as alumina, the microstrip-line width should be about 10 mils to allow these devices to be mounted easily and directly. For a 50-ohm stripline with this width, the height of the substrate is also ~ 10 mils. However, $\lambda/16$ in the substrate is only 4.5 mils which makes this thickness undesirable, since $h < \lambda/16$.

It is therefore preferable to use a substrate with a lower dielectric constant, such as quartz ($k = 3.75$). A comparison of the impedance, line widths and wavelength, derived from Figures 36 and 37, is shown in Table III. For the hybrid coupler used in the balanced mixer it is necessary, for optimum performance, that negligible unguided coupling be permitted between opposite lines. From the geometry, the restriction that the separation between lines must be greater than a constant, K, multiplied by the substrate thickness (h) gives the relation:

$$\frac{\lambda_g}{4} - w = Kh.$$

Calculations of this frequency restriction show that either 4 mil quartz ($K = 3.5$) or sapphire ($K = 2.5$) are usable at 60 GHz. To increase the limiting frequency, the arms could be made $n\lambda_g/4$, but losses will also increase. It is noted that an alternative to the $3\lambda/4$ hybrid would be a high impedance $\lambda/4$ hybrid with transformers on the input ports. This would reduce the line widths as shown in Table III.

B. QUARTZ MICROSTRIPLINES

A detailed study of the electrical characteristics of quartz microstriplines has been carried out by TI. The curves shown in Figures 36 and 37 for quartz and alumina were computed using the method of Wheeler[15] and were used extensively in microstripline design.

The RF loss of the striplines can also be calculated as described previously, i.e.,

$$\alpha_c = \sqrt{\frac{\pi f \mu \rho}{Z_o W}} \qquad (18)$$

$$\alpha_d = \pi f \sqrt{\mu k} \tan \delta$$

where

f = frequency,

μ = permeability of the substrate

ρ = resistivity of the metal

$\tan \delta$ = loss tangent of the substrate

k = dielectric constant

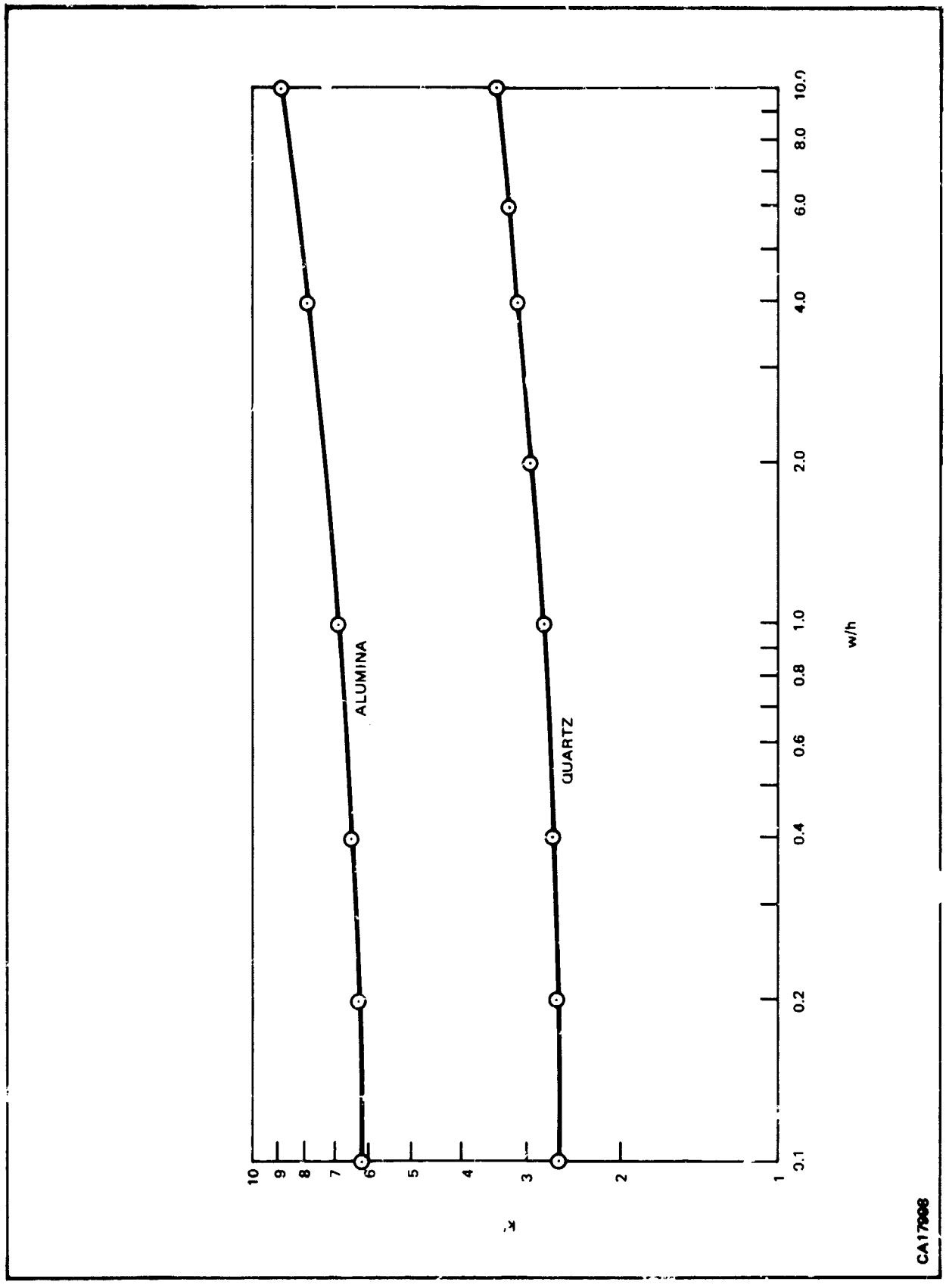

Figure 36. Effective Dielectric Constant versus w/h

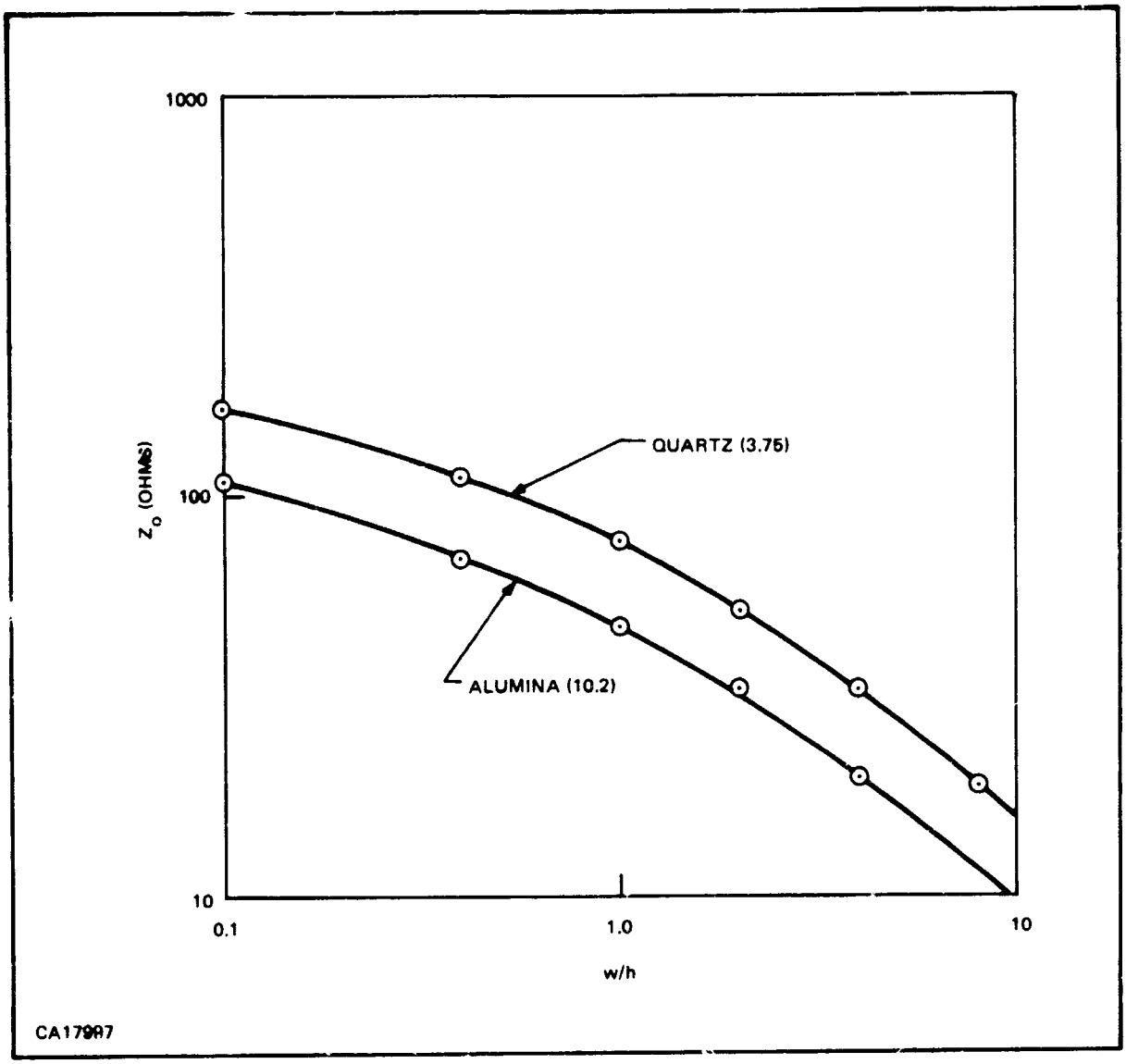

Figure 37. Impedance versus w/h

Table III. Comparison of Stripline Characteristics at 60 GHz

Substrate	k	λ/4 (50 Ω Line)	w (35 Ω Line)	w (50 Ω Line)
10 Mil Ceramic	10.2	19.0 Mils	18.0 Mils	9.2 Mils
10 Mil Quartz	3.75	28.0 Mils	37.0 Mils	21.2 Mils
4 Mil Quartz	3.75	28.0 Mils	14.8 Mils	8.5 Mils

Conditions

$h << \lambda/4$, generally assumed $h < \lambda/16$

$(2n + 1)\ \lambda/4 >$ w + Kh for hybrid coupler

Substituting values for 4-mil thick quartz using gold metallization and a 50-ohm line, we obtain at 60 GHz:

$$\text{Attenuation } (\alpha_t) = 0.17\ (\alpha_c) + 0.03\ (\alpha_d)\ \text{dB}/\lambda_g \tag{19}$$

$$\text{Total Attenuation} = 0.2\ \text{dB}/\lambda_g$$

Experimental measurements of the loss in quartz stripline have also been made at 60 GHz. The stripline was mounted between crossed waveguides using antenna transitions as described previously. The length of the stripline was 4.4 λ_g (0.5 inches) and the measured loss was 4.2 dB at 60 GHz. Substracting 2 dB for the nominal loss in the transitions, the stripline loss becomes ~ 0.5 dB/λ_g. This shows that the loss in quartz is not excessive at this frequency.

C. BALANCED MIXER

The reason a balanced mixer was chosen rather than a single-ended mixer is the reduced L.O. noise contribution at the IF. The mixer considered is shown in Figure 38. It is based on a 3-dB hybrid coupler with two mixer diodes, each terminated in an RF short, as shown. The discrete diodes used are designed to have an RF impedance of approximately 50 ohms.

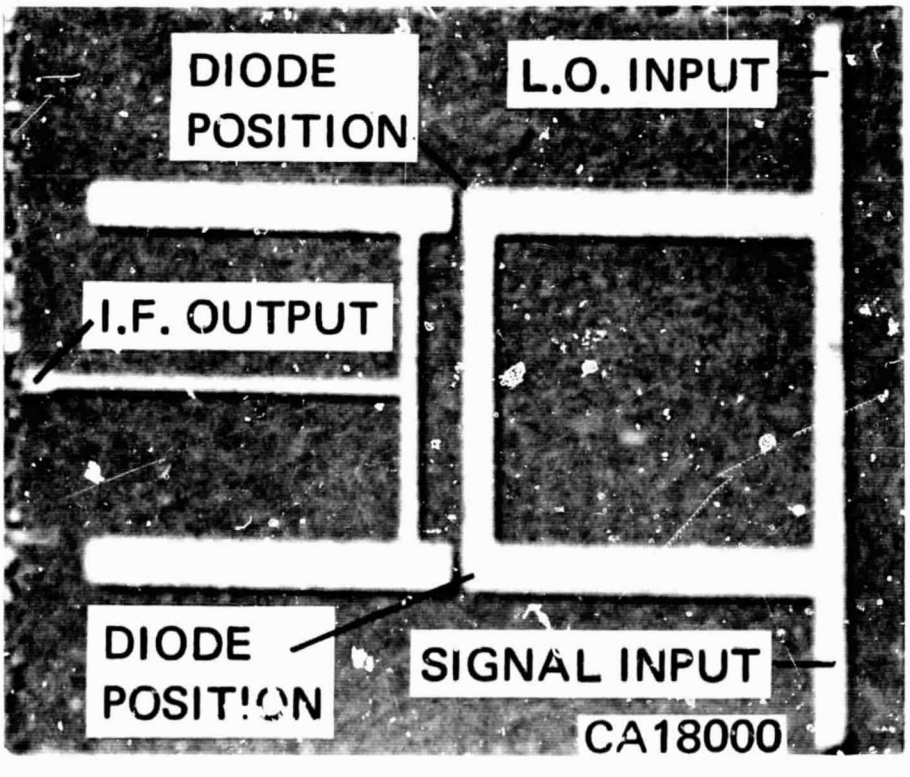

Figure 38. Balanced Mixer on Quarts

The diode impedance at 60 GHz is given by the relation $Z = R_{s(p)} + 1/j\omega C_{j(p)}$ where $R_{s(p)}$ is the RF series barrier resistance and $C_{j(p)}$ is the pumped capacitance. This capacitance is related to the zero bias capacitance $C_{j(o)}$ by:

$$C_{j(p)} = C_{j(o)}/(1 - 0.1 \log 125\, I_d)^{1/2}$$

where I_d is the diode operating current in μA. A typical value of I_d is 4 mA, hence $C_{j(p)}/C_{j(o)} = 1.5$. At the RF frequency, optimum conditions exist where $R_{s(p)} = 1/j\omega C_{(p)}$. Thus for a 50-ohm RF impedance, $C_{j(p)} = 0.075$ pF and $C_{j(o)} = 0.05$ pF. A reasonable value for R_s (the series resistance of the diode excluding the barrier resistance, at 60 GHz) is $\approx 13\Omega$. Considering $R_s = 13\Omega$ the relation

$$\frac{1}{2\pi R_{dc} C_{j(o)}}$$

gives the result $f_{co} = 240$ GHz.

It was decided that GaAs Schottky barrier diodes would be the most suitable for the balanced mixer. These have very low noise figures due to the nigh electron mobility in GaAs. A noise figure of 6.1 dB has been measured at X-band (9.375 GHz) for these Schottky barrier diodes, and a parametric amplifier noise figure of ~ 3 dB at 16 GHz has been obtained. The diodes selected were commercially available and designated TIX VO6. These consist of a 3 X 3 array of various-area diodes on a 15 mil^2 chip. The diode selected for the mixer had a nominal zero-bias capacitance of 0.1 pF and f_{co} of 400 GHz. Using selected diodes the required capacitance could be obtained.

The characteristics of the balanced mixer are limited by the characteristics of the integral 3 dB hybrid coupler. An analysis of this coupler has been made by TI, and the results are shown in Figures 39, 40, 41, 42 for both a $\lambda/4$ and $3\lambda/4$ circuit. The lines were assumed to be lossless and the diode ports matched. Since the balanced mixer had arms $3\lambda/4$ long, the bandwidth was reduced somewhat compared to the fundamental ($\lambda/4$) coupler. The isolation from port 1 to port 2 is in excess of 20 dB between 59 and 61 GHz; the input VSWR is less than 1.5 and the coupling is within $\pm$ 0.15 of 3 dB and within 1° of 90° between 58 and 62 GHz.

A mixer was constructed at 60 GHz as shown in Figure 38. The diodes were bonded onto the stripline and a 1 mil wire was used to bond from the top contact to the opposite stripline, across the gap. The additional inductance contributed by this wire was kept low by keeping the wire as short as possible. The circuit was mounted onto a baseplate and coaxial-antenna transitions were used to couple the L.O. and signal to their respective ports. The balanced mixer was tested initially by measuring the IF impedance at 60 MHz using an R-X meter. With zero L.O. power applied to the mixer, the impedance was found to comprise a real part of approximately 50 k-ohm in parallel with a capacitance of 11.1 pF. When L.O. power was applied, the real part of this impedance did not vary, although it would be expected to be reduced to a value approaching 500 ohms or less. This indicates that insufficient L.O. power is reaching the diodes. Using a small probe it was found that there was excessive radiation from the circuit. A simple modification could be made to the circuit to correct this.

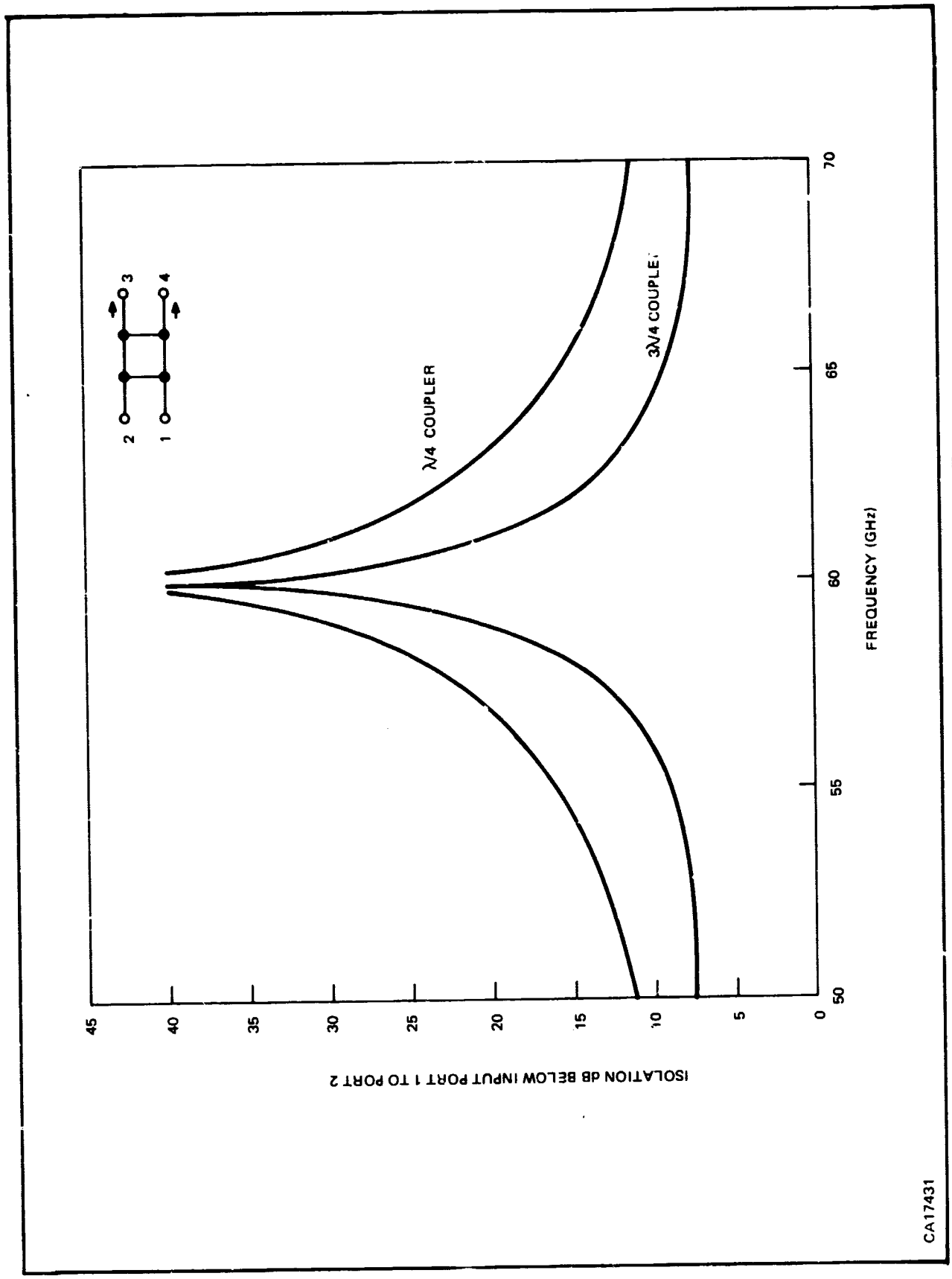

Figure 39. Isolation of Hybrid Coupler versus Frequency

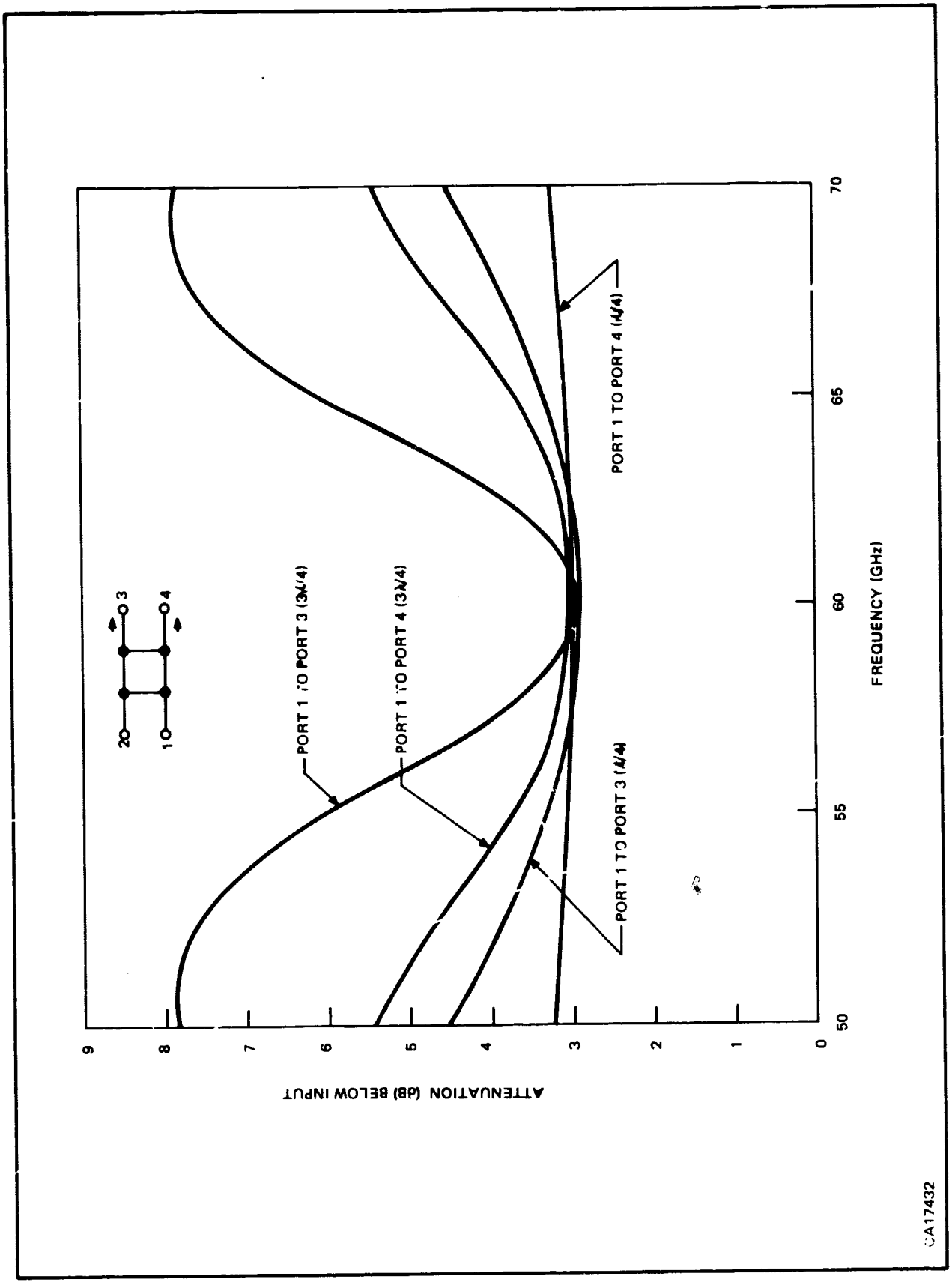

Figure 40. Power Division of Hybrid Coupler versus Frequency

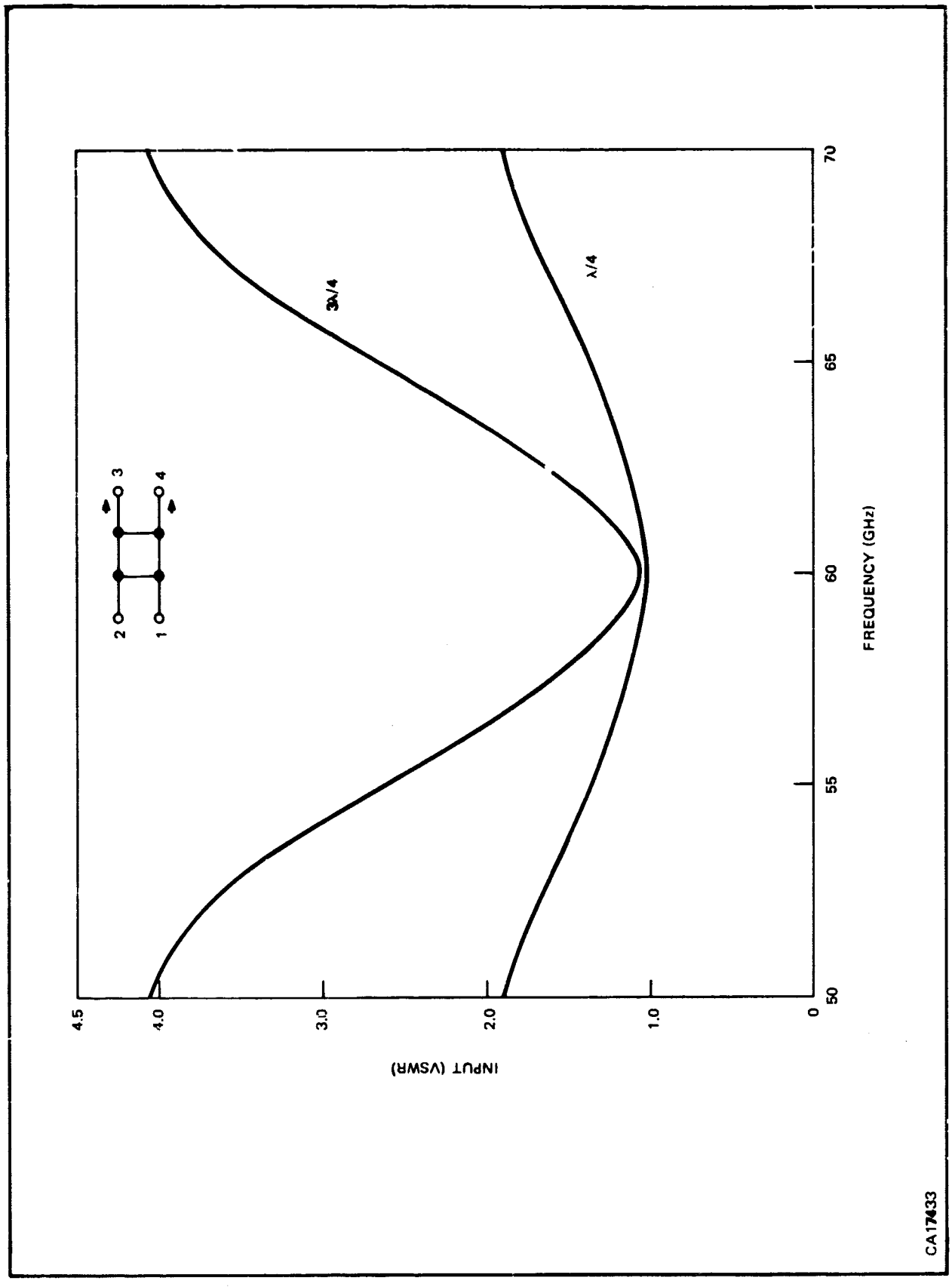

Figure 41. Input VSWR of Hybrid Coupler versus Frequency

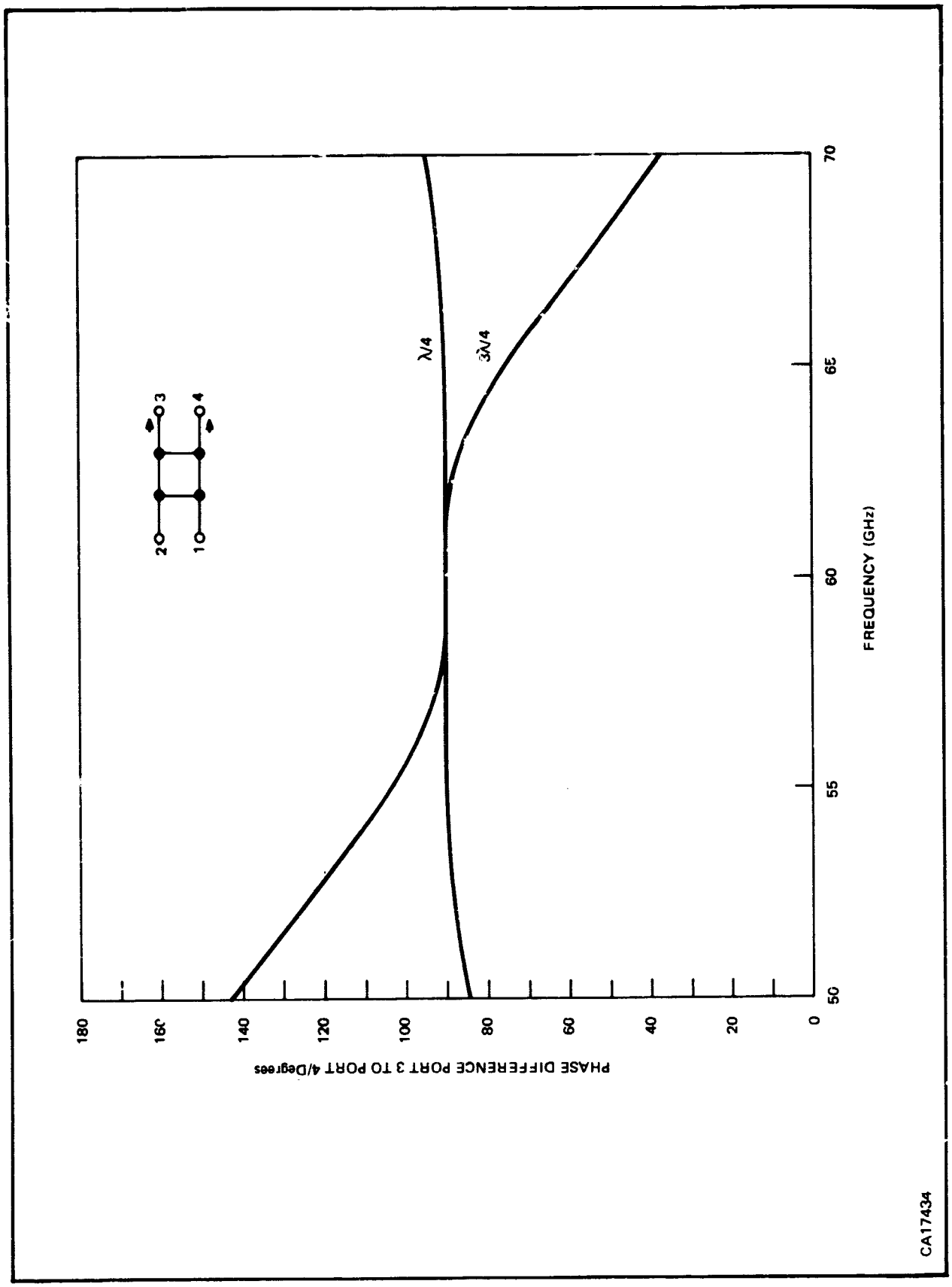

Figure 42. Output Phase Difference of Hybrid Coupler versus Frequency

D. LOCAL OSCILLATOR SOURCE

The local oscillator source had to be capable of delivering at least 5 mW at 60 GHz to the balanced mixer. At this time, this power level had not been achieved at this frequency directly at TI. It was decided to use a Gunn Oscillator at 15 GHz, followed by a quadrupler, and the complete circuit was to be constructed in microstripline on quartz substrate.

1. Multiplier

The stripline quadrupler was designed assuming a varactor diode with the following parameters: cutoff frequency (f_{co}) = 600 GHz and zero-bias capacitance (C_o) = 0.07 pF. This is based on the same Schottky barrier diode array described previously, but the smallest size diode is now considered. From the paper by Burckhardt[20] the pumped capacitance at a reverse bias of 10 volts is 0.042 pF.

A photograph of the quadrupler on quartz is shown in Figure 43. It is made up of a low-pass, Chebychev, input filter, and a high-pass output filter, with the diode connected in series. The diode is resonated at 60 GHz with the package inductance and the input capacitance of the low-pass filter. The diode impedance (12 ohms) is then transformed to the 50-ohm output line. The 30 GHz component is resonated by a correctly positioned quarter-wavelength open-circuited stub at 30 GHz, and the 15 GHz component is resonated by making the 50-ohm output line the correct length. (The output filter is an open-circuit to 15 GHz).

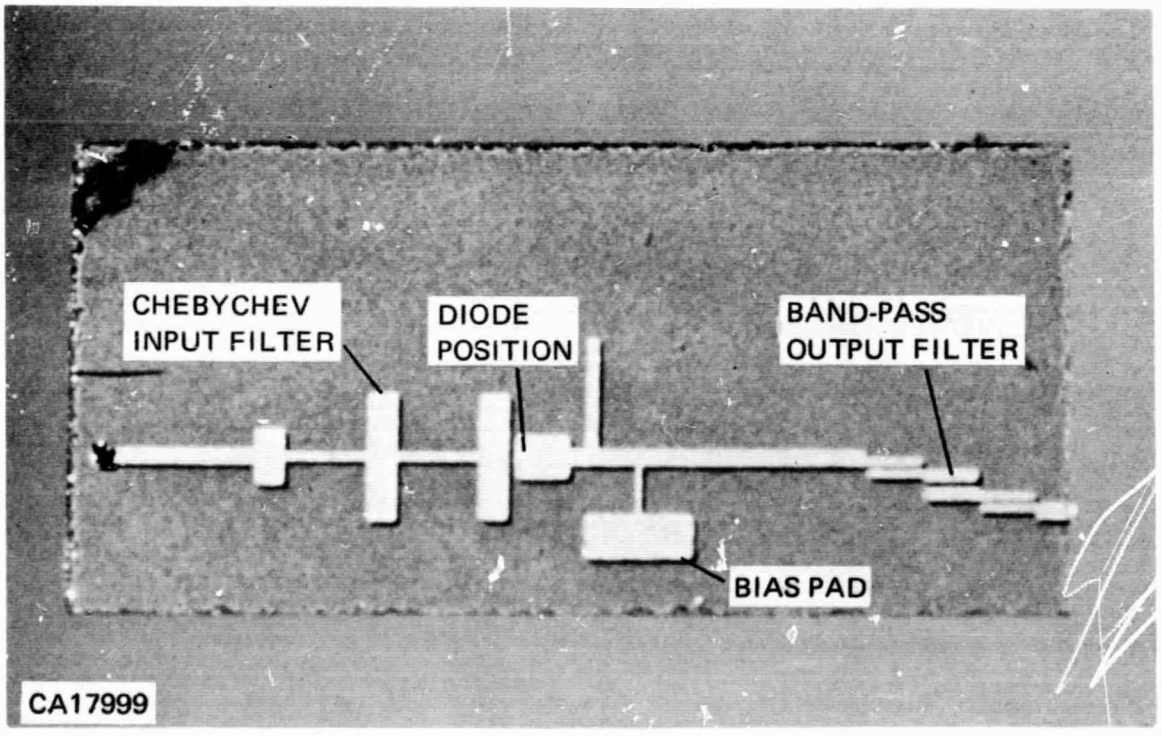

Figure 43. Quadrupler on Quartz

The quadrupler was constructed on quartz substrate (Figure 43), and a GaAs Schottky barrier diode was bonded onto the circuit, again bonding a 1 mil gold wire from the top contact to the opposite stripline. The input at 15 GHz was applied through a commercial waveguide-to-stripline transition, and the output at 60 GHz was removed via an antenna-coaxial transition. The best result obtained was a conversion loss of ~ 20 dB multiplying from 12.75 to 51 GHz. The reasons for the rather high conversion loss and lower operating frequency are as follows:

- The diode lead inductance was too high, causing the resonant frequency of the diode to be lower than expected.
- The thickness of the substrate was nearer 8 mils which caused the pass band of the input and output filters to be incorrect. This was verified by measuring the input VSWR which did not exhibit a low value between 10 and 18 GHz as was expected.
- For optimum results with a stripline quadrupler the length of various stubs need to be modified for maximum output at 60 GHz. With 4 mil quartz substrates this is more difficult, but can be done with small tuning chips (scribed pieces of metallized substrate), or by shortening the lines with a diamond scribe. To date no modifications of this type have been made.

Recently beam-leaded silicon Schottky barrier varactor diodes with capacitances of less than 0.06 pF at −6 volts and cut-off frequencies around 560 GHz have been fabricated. Using these devices the multiplier and balanced mixer would be expected to have greatly improved performance.

2. Stripline Gunn Oscillators

Work on the integration of discrete diodes into stripline circuits was continued for this phase of the contract.

To facilitate the design of the oscillator cavity, measurements have been made on the impedance required to be presented to a pill-packaged Gunn diode for maximum output. This was done by constructing a 7 mm coaxial holder for the pill-packaged Gunn diodes and measuring the impedance of the circuit necessary to tune the Gunn diode for maximum power output, using a slotted line and short-circuit reference.

Considering a series tuned equivalent circuit, the real part of this impedance remains relatively constant over the frequency range studied (6 – 12 GHz in this case), with a widely varying imaginary part. Examples of the impedances are 12 + j40(8.5 GHz) and 12 + j11(11.0 GHz). It has also been shown that the real part is relatively constant for a given batch of diodes but varies from batch to batch; e.g., Batch 594, No. 91, Z = 14 + j22, Batch 594, No. 95, Z = 12 + j23, Batch 596, No. 48, Z = 6 + j10, all at 10.0 GHz.

It would appear therefore that a fixed-tuned circuit could be designed for a Gunn diode from a given batch, at a given frequency, while only one degree of tuning would be necessary for a band of frequencies. However, to achieve the maximum output from diodes of different batches, the circuit would need two degrees of tuning (for real and imaginary parts). It is likely that tighter control of fabrication processes in the future will produce diodes which are similar from slice to slice. Consequently, a TI funded program was initiated and an oscillator circuit has been constructed which verifies the above results.[21]

The hybrid approach using 4-mil thick quartz substrate appears very promising. However, alloyed and wire-bonded diode chips were not suitable for use at millimeter-wave frequencies. An internally funded program to develop beam-leaded devices has been initiated, and the hybrid approach to millimeter-wave circuitry will be re-evaluated when these become available. However, to obtain a demonstration model for the present contract, it was mutually agreed by NASA-ERC and TI to concentrate our effort on the microminiature waveguide approach.

SECTION IV

WAVEGUIDE APPROACH

A. GENERAL

It was proposed to investigate two distinct methods of developing the necessary 5 mW at 60 GHz in waveguide, and after initial evaluation, the most promising approach would be selected. The two methods were:

- The generation of > 30 to 40 mW at 15 GHz using Gunn or avalanche diodes, followed by a waveguide quadrupler.
- The generation of 60 GHz directly with Gunn[2] or avalanche diodes.[4]

B. WAVEGUIDE QUADRUPLER AND 15 GHZ SOURCE

A harmonic generator was designed in waveguide to multiply from 15 to 60 GHz. Basically it was a section of Ku-band waveguide with a section of M-band waveguide inserted at right angles. The Ku-band waveguide was reduced in height, using a linear taper, to the diode, and a short was located behind it. The quadrupler is shown in Figure 44.

The 15 GHz input to the multiplier would be either a Gunn diode, if the conversion loss of the multiplier was less than 10 dB, or an avalanche diode if the conversion loss was between 10 and 20 dB. Both would be in waveguide mounts. An output power of 25 mW has been achieved at 15 GHz using Gunn diodes, and initial tests on avalanche diodes showed an output of 80 mW at 16 GHz. Waveguide mounts at 15 GHz were available.

Initially the active device used in the quadrupler was a pill-packaged, silicon Schottky barrier diode. Measurements showed a conversion loss of less than 20 dB from 15 to 45 GHz. However, due to the resonance of the diode and package parasitics, no output at 60 GHz was observed. A modification was made to the quadrupler so that unpackaged diodes could be used. Initially, avalanche diodes with breakdown voltages of 17 V were used as varactors. The quadrupler gave an output at 60 GHz with 15 GHz input, but at a very low level. However, this shows that unpackaged devices will work at 60 GHz, whereas the packaged Schottky barrier diodes were limited to below 50 GHz.

Analysis showed that the major problem was the relatively low cutoff frequency of the diodes for our application. It is necessary to have a diode with a zero-bias capacitance of less than 0.1 pF with a cut-off frequency of several hundred GHz for operation at 60 GHz. The only diodes available at present approaching these limitations are:

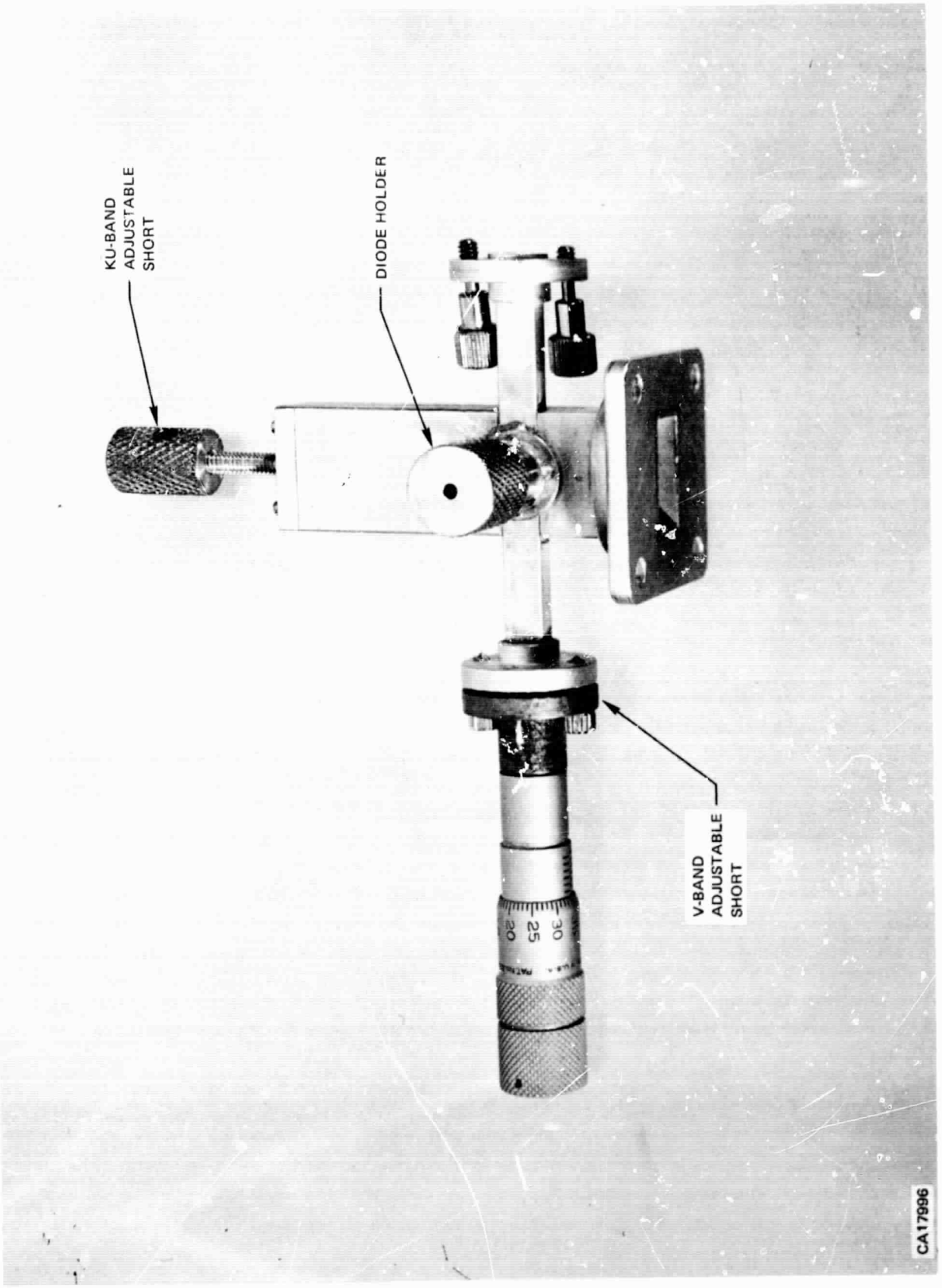

Figure 44. Waveguide Quadrupler

- GaAs varactors specially fabricated and etched
- Beam-lead silicon varactors
- 3 X 3 GaAs Schottky varactor arrays.

The 3 X 3 GaAs Schottky varactor arrays are unsuitable for unpackaged operation in the waveguide jig; and, since the package parasitics will inhibit operation at 60 GHz, as was previously shown, these diodes could not be used.

Several specially constructed GaAs varactors (single diodes mounted on 0.5-mil thick Kovar strips) were obtained having breakdown voltages between 15 and 25 V and zero bias capacitances of 0.1 pF. When mounted in the jig, an output of 0.1 mW was obtained at 60 GHz with 100-mW input power. This low conversion efficiency is thought to be due to the lack of resonance of the diode and inductive post at the second harmonic (30 GHz).

Accordingly, different posts were tried and the output was increased to 0.3 mW. At this point, work was terminated on the quadrupler since success of the avalanche diode approach was proved.

C. DIRECT GENERATION OF 60 GHz USING GUNN DIODES

It has been reported[3] that CW outputs of ~ 20 mW have been achieved between 40 and 90 GHz using a Gunn diode in a high-frequency mode. It was hoped that the jig used for the avalanche diode (Section D), or a modification thereof, would be suitable for the initiation of this mode.

The donor density (η) of the material used for the Gunn diodes at present is approximately $1.2 \times 10^{16} cm^{-3}$, giving an n/f ratio of 2.5×10^5. From a consideration of reference 3 it is expected that the n/f ratio should be between 10^4 and 2×10^5 for high-frequency mode operation. Gunn diodes with various donor densities within and near this range have been mounted onto the gold-plated studs, in the same manner which was used for the avalanche diodes described below, but without being etched. Typical threshold voltages for these diodes were 3 to 6 volts, and operating conditions ~ 7 volts and ~ 80 mA. Output was detected in the required frequency band (50 to 75 GHz), but the level was estimated to be below 0.1 mW. Further tests showed this to be the 5th harmonic of the fundamental Gunn mode. Tuning elements were incorporated into the oscillator circuit to enhance this harmonic oscillation, but no appreciable increase in power was observed.

At this time appreciable outputs were being achieved from avalanche diodes, accordingly the Gunn diode effort was terminated.

D. DIRECT GENERATION OF 60 GHz USING AVALANCHE DIODES

1. General

The direct generation of 60 GHz using an avalanche diode has been described by Misawa.[4] The diode is mounted in the center (high current position) of a circular cavity. This circular cavity is formed inside a section of 50 to 75 GHz waveguide, so that the output is coupled from the edge of the cavity to the waveguide. A cross section of this jig is shown in Figure 45.

The diode is mounted onto a 1/8" gold-plated copper slug, then the diode is etched to the required diameter. This slug is mounted into a massive, copper holder so that the diode base is on the same level as the bottom of the waveguide (to reduce mismatches in the waveguide). This copper holder also provides a good heat sink. The cavity is formed between the bottom level of the waveguide, and a disc which is introduced through a hole in the top of the waveguide. The bias is also introduced on this disc, as shown. An exploded view of the jig is shown in Figure 46, also showing the short-circuit used to maximize the output.

2. Material

From suitable curves[23] of depletion width at breakdown as a function of the impurity concentration it is found that the N-region of the diode should have an impurity concentration of $\sim 5 \times 10^{16} cm^{-3}$ for generation at 60 GHz. This corresponds to a resistivity of about 0.15 ohm-cm in the N-region. The breakdown voltage will be ~ 19 volts. The impurity profile for the avalanche diode is summarized in Figure 47.

Initially some epitaxial Si material was fabricated, based on the above requirements. This was then metallized, scribed, mounted and etched to form 1-mil-diameter diodes. Capacitance vs voltage plots were made on several of the Si diodes, which showed the zero bias capacitance to be between 0.2 and 0.4 pF, the breakdown voltage to be approximately 20 to 25 volts, the width of the depletion layer to be between 0.3 and 0.6 microns, and the doping density to be approximately $1 \times 10^{16} cm^{-3}$. The slope of the doping density vs thickness curve was not as abrupt as expected. Compared to the published results of Misawa (devices with a doping density of $6 \times 10^{16} cm^{-3}$ and a breakdown voltage of 19 volts) our devices differ primarily at three levels: doping density, junction abruptness, and breakdown voltage.

Based on these results, new material was used to fabricate diodes having nearer the required electrical characteristics. Slices from two of these new diffusion runs have yielded reasonable results. These are the IMP 6 and IMP 4. The characteristics of these are shown in Table IV. A few devices from slice IMP X were also available and these are included, along with the published results of the avalanche diode oscillator (ADO) fabricated by Bell Telephone Laboratories.

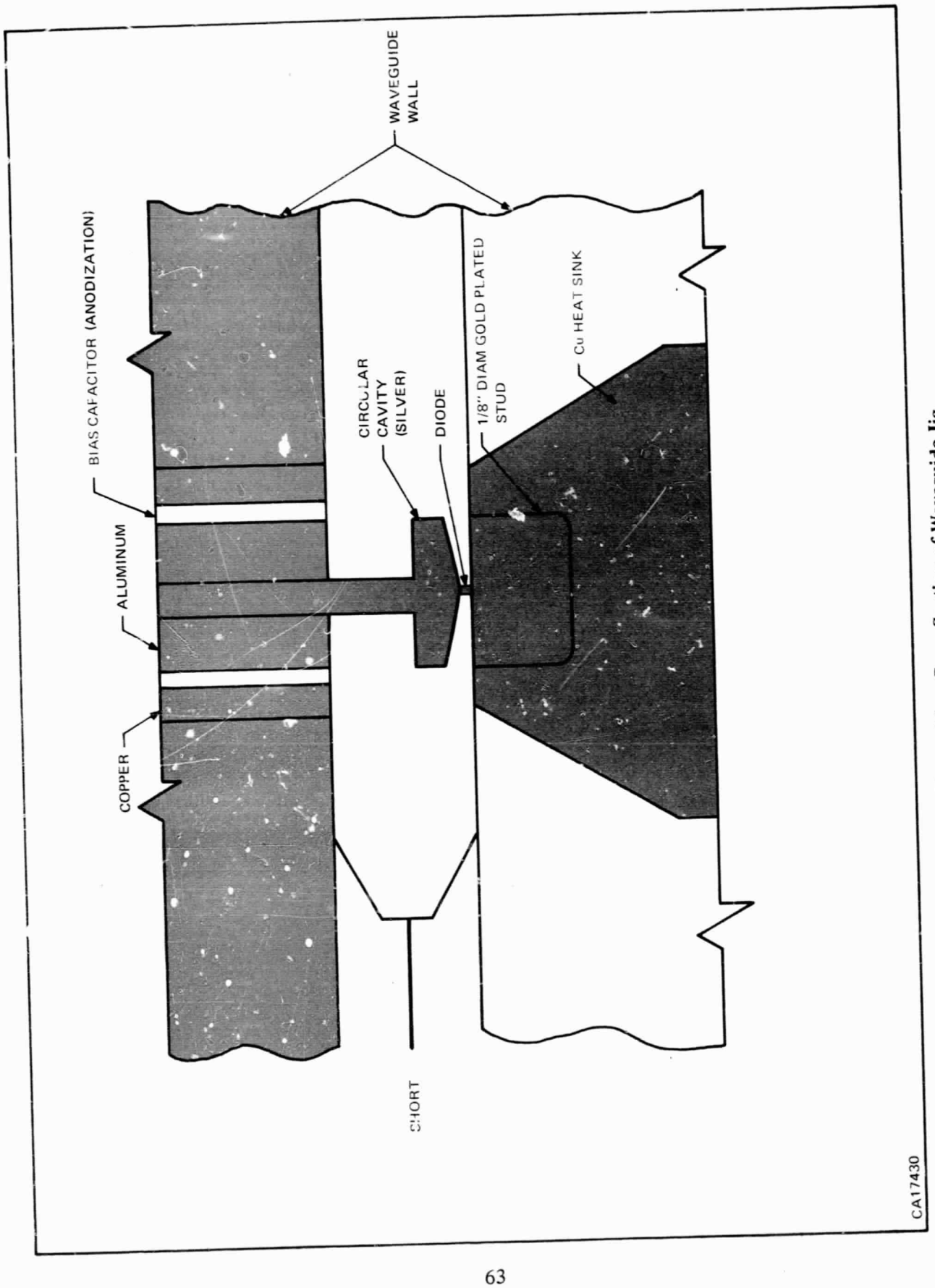

Figure 45. Cross Section of Waveguide Jig

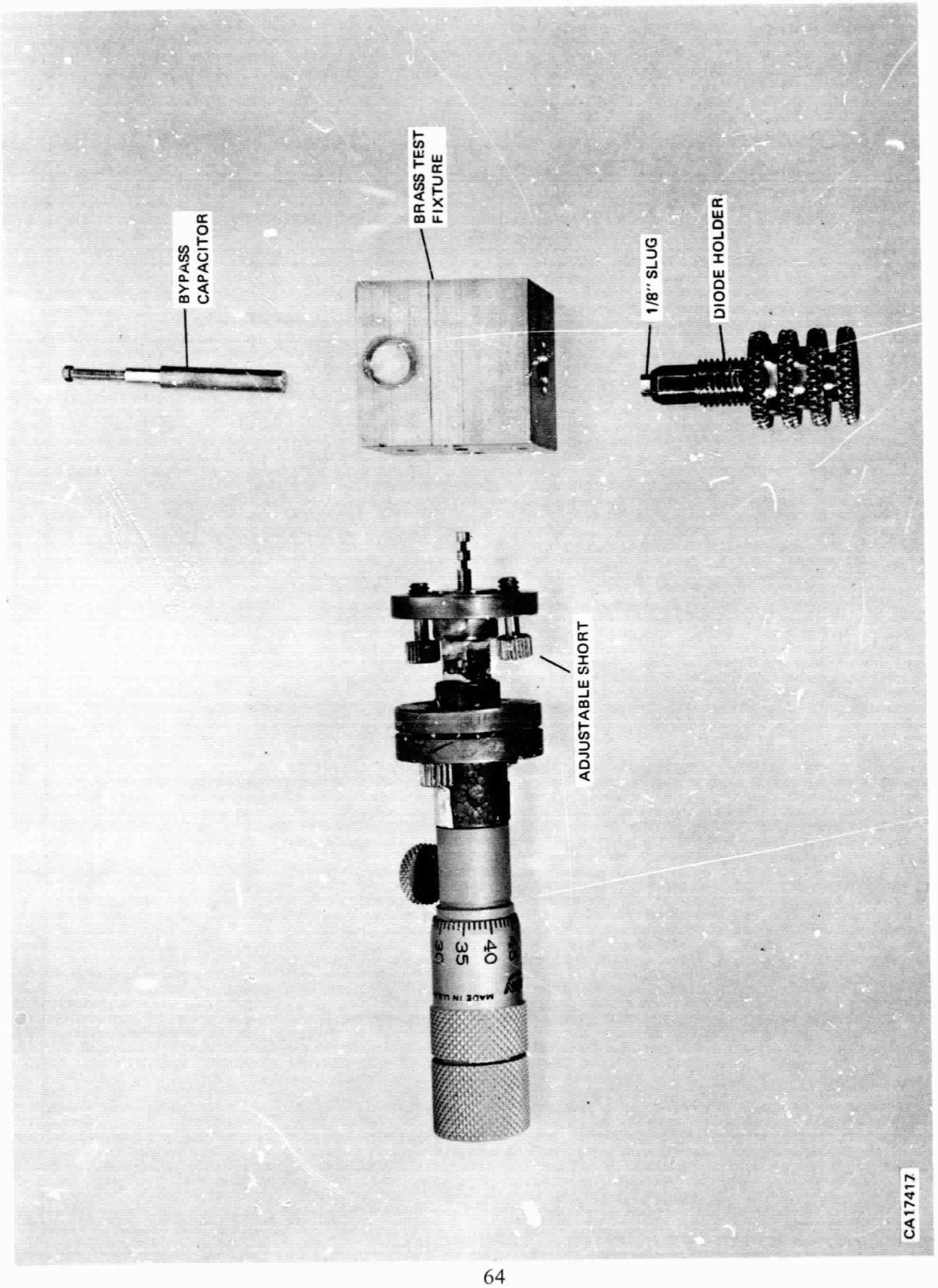

Figure 46. Exploded View of Jig

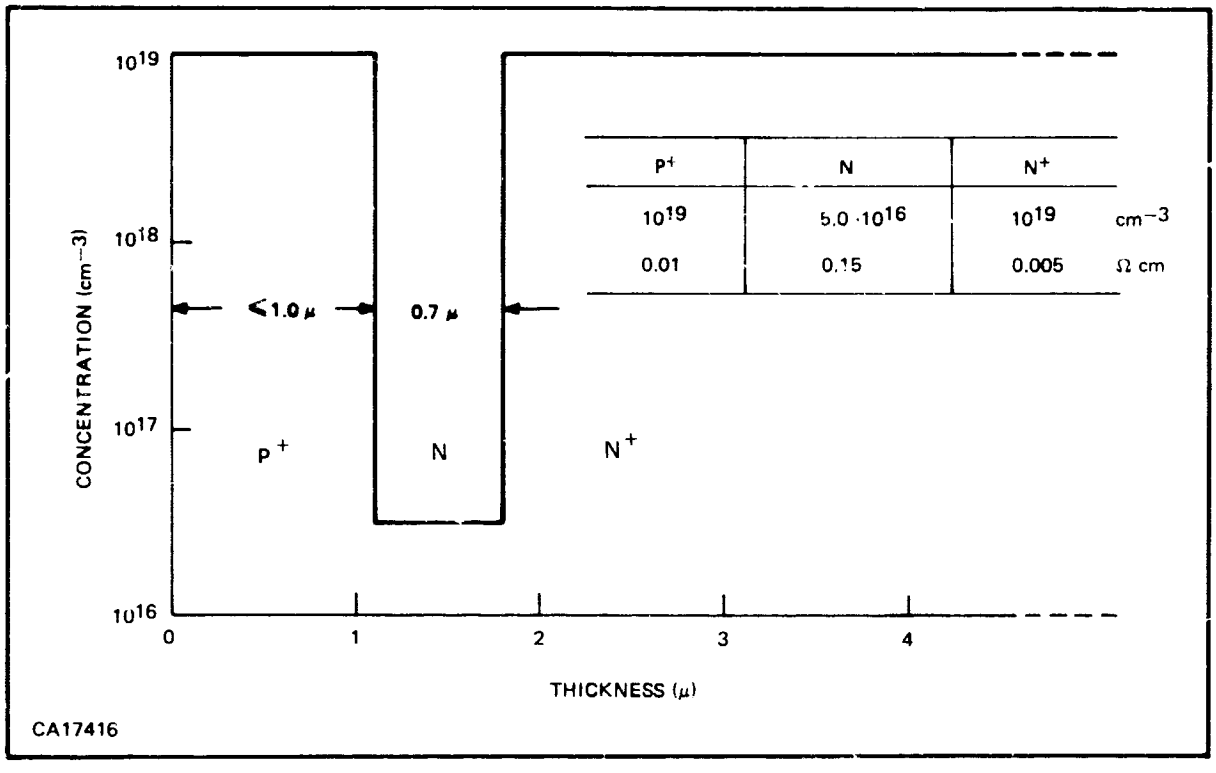

Figure 47. Impurity Profile Summary for Avalanche Diode

Table IV. Summary of Device Characteristics

Type	V_B (V)	Eff. (%)	Density (cm^{-3})	Width (μ)	Frequency (GHz)
IMP X 1B	15	1.0	1×10^{16}	0.7	~57
IMP 4	17	0.3	1×10^{17}	0.6	50 to 55
IMP 6	12	0.3	2×10^{17}	0.35	60 to 70
BTL (LO1175)	17	2.8	9×10^{16}	0.55	55 to 60

The reason for the increased efficiency of IMP X devices can be seen in Figures 48, 49, and 50. Figure 48 shows diagrammatically the electric field distribution in the depletion region of an avalanche diode. Figure 48(a) illustrates a device which breaks down upon depletion. Figure 48(b) shows device breakdown before depletion through to the substrate. This is mainly due to an excessively high donor density in the N-region. Figure 48(c) shows the device depleting somewhat before breakdown, mainly caused by too low donor density in the N-region.

The efficiency in both cases, (b) and (c), is reduced from that of (a). In case (b) there is the series resistance due to the undepleted N-region which reduces the efficiency, while in case (c) there is a fraction of the voltage across the device which is wasted, also reducing the efficiency.

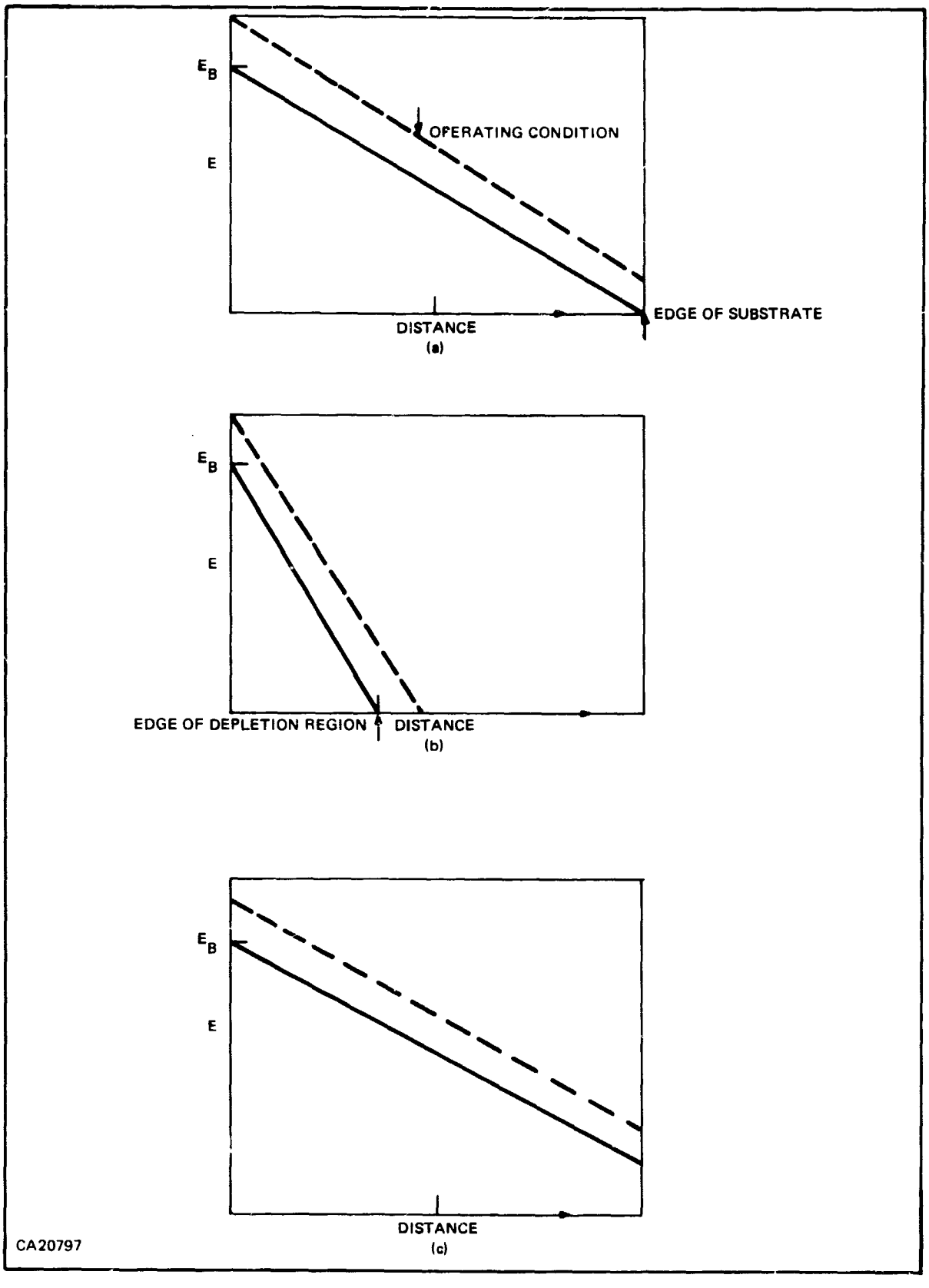

Figure 48. Schematic Diagram of Electric Field in Depletion Region

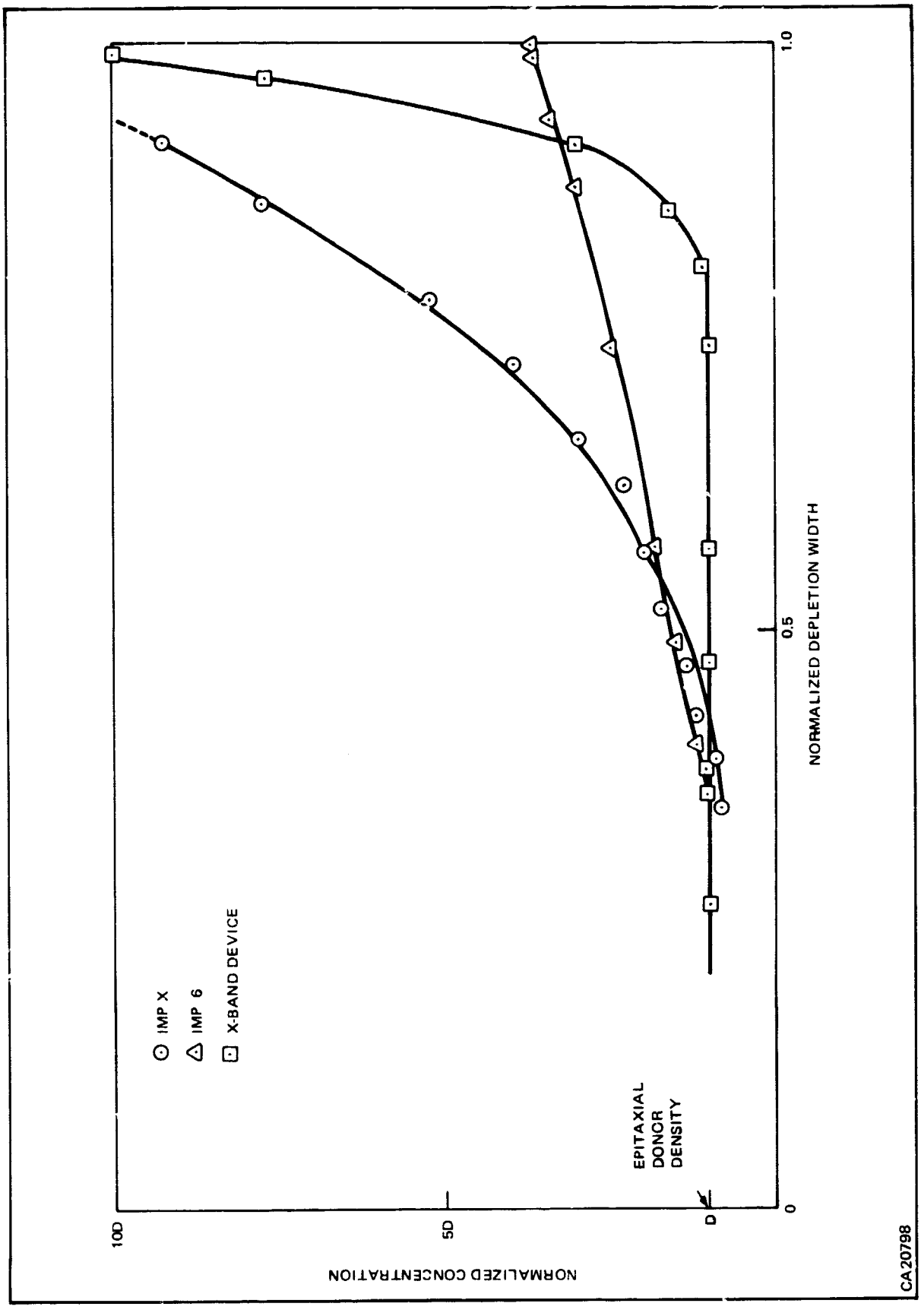

Figure 49. Donor Density versus Depletion Width

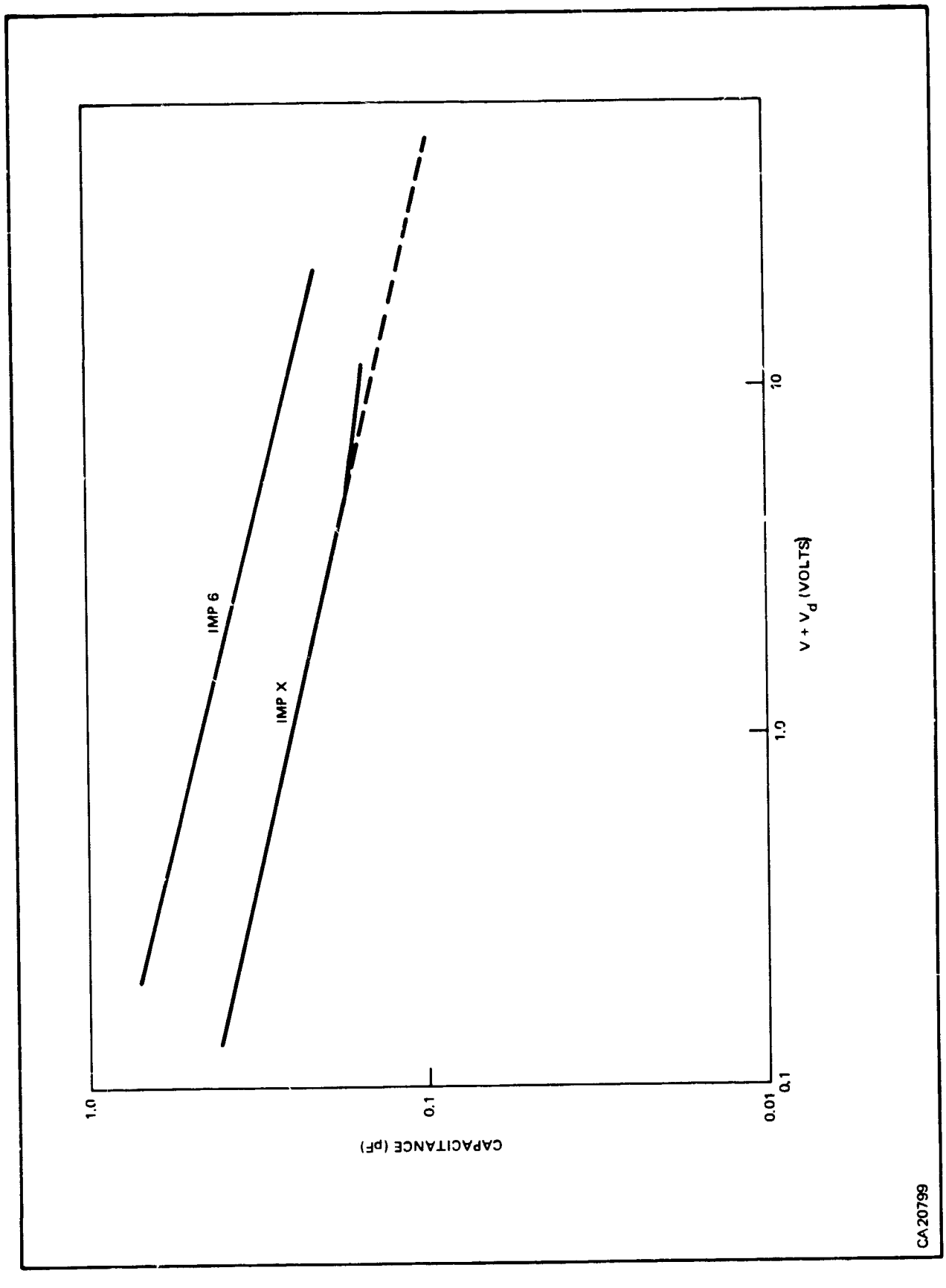

Figure 50. Diode Capacitance versus Voltage

Figure 49 shows the normalized density versus the normalized depletion width for the two devices. For comparison, an X-band avalanche diode has been included, which has the shape required for good operation. It is seen that the IMP 6 devices do not deplete, corresponding to Figure 48(b). IMP 4 devices are also undepleted at breakdown. This is also indicated by the high donor density in Table IV. Devices IMP X do deplete, but do not have very abrupt junctions. This indicates that the efficiency will be higher, as is found, but not as high as desired (3 to 5%).

Figure 50 shows the capacitance versus voltage curves for the IMP X and IMP 6 devices. Before depletion the slope

$$\left(\frac{\log C}{\log (V + V_d)} \right)$$

is a constant, given by the relation

$$C \alpha \frac{1}{(V + V_d)^n}$$

where C is the diode capacitance and V_d is the forward breakdown voltage. When depleted, this slope should reduce, as found for device IMP X. However, device IMP 6 does not show this phenomenon, verifying that IMP X devices are depleting while IMP 6 are not.

In conclusion, it would appear that the requirements for a 60-GHz device are:

a) Depletion as near to breakdown as possible

b) Very abrupt junctions

c) Donor density ~ $6 \times 10^{16} cm^{-3}$

d) Depletion width ~ 0.6 μm

e) Breakdown voltage 16 V.

Experiments have also been performed to fabricate double epitaxial diodes to compare with the conventional diffused single epitaxial diodes. Double epitaxial diodes fabricated at Texas Instruments for X-band use have much more abrupt junctions than the diffused diodes, which result in higher efficiencies. The results from double epitaxial slices showed that the N-layer was too thick and the breakdown voltage was about 35 V. The results also indicated that the carrier concentration was somewhat lower than was specified.

3. Mounting and Testing

To reduce the capacitance of the diode–which is necessary to increase its impedance at 60 GHz–it is mesa-etched to reduce the diameter. Diameters of the order of 1 mil are suitable; however, the thermal impedance has to be very low to prevent the very small diodes from burning out, hence, good bonding of the diodes to the gold-plated slugs is imperative.

There are three methods of preparing the 1/8-inch copper studs prior to bonding the diodes:

1) Plate gold to 200 μ-inch and burnish the center to a mirror finish and bond the diode to this.

2) Polish the Cu clug to a mirror finish, plate 200 μ-inch of gold onto this, and polish with 0.3 μ alumina powder to a mirror finish.

3) Polish the Cu slugs to a mirror finish, plate gold, repolish, and then evaporate more gold onto the surface, which remains as a mirror finish.

It was found initially that processes 2) and 3) give increased yields, as the burnishing process 1) hardens the gold, and contact is made to small-area projections rather than over the whole diode contact. In process 2) and 3), the gold is softer and better thermal contact is made. However, if process 1) could be improved to give contact over the whole diode contact, the thermal conductivity would be better than with the soft gold.

Initially the diodes were tested under pulsed conditions. The diodes were bonded and etched to between 2.5- and 3-mils diameter. When these were tested under pulsed conditions, output was observed. The 2.5-mil diameter diodes operated at current levels in excess of 150 mA at 20 V, and the 3-mil diameter diodes in excess of 250 mA at 20 V. The pulse width was between 2 and 10 μs with a 1 kHz repetition rate. Peak output power was in the order of 20 mW.

When operated under CW conditions, the 2.5-mil diameter diodes burned out at 100 mA (20 V – 2 W) and the 3-mil diameter diodes at 130 mA (20 V – 2.6 W) with no output. The diodes thus burn out under CW conditions before the current reaches the desired level. At this time, several improvements were made to the fabrication process including the method of etching the diodes apart. Figure 51(a) shows the shape of the diodes after they were etched apart, and Figure 51(b) shows the shape of the diodes after they were eteched to the required diameter. Serious problems with undercutting the top contact were experienced but these were eventually minimized. Some difficulty was also experienced in etching the diode to the correct diameter due to the reentrant, rather than cylindrical, shape of the diode when etched.

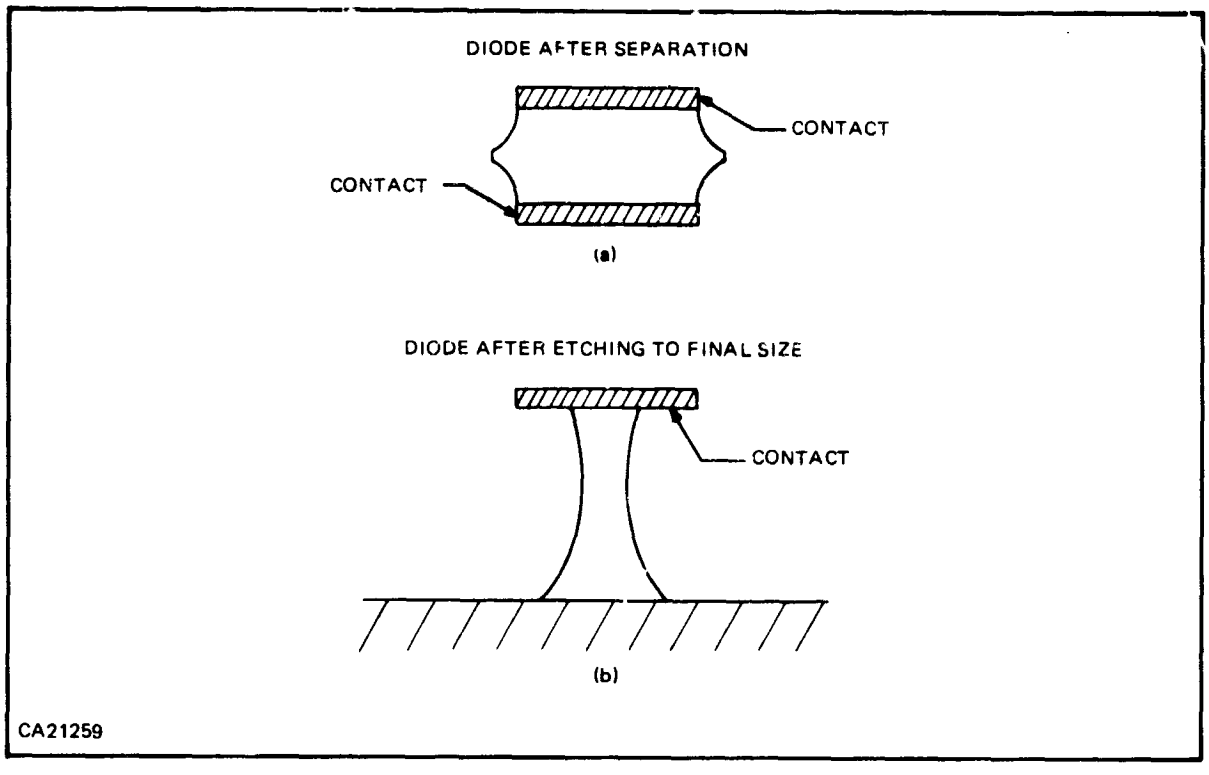

Figure 51. – (a) Diode After Separation
(b) Diode After Etching to Final Size

The diameter of the top contact of the diode is seen, from Figure 51(b), to be much larger than the diode diameter when etched. Originally, difficulty was experienced due to the sagging of this contact, but this was overcome by introducing a low-viscosity epoxy around the diode and baking the unit overnight at 100°C to harden it.

Additional IMP 4 diodes were then processed using the new fabrication process, mounting the diodes on evaporated gold (process 3). Output powers of 5 mW at 55 GHz and 20 mW at 50 GHz were achieved. Also, some IMP 6 diodes were similarly fabricated. The yield of operable devices was approximately 50%. The diodes were found to give approximately 5 mW of output power from 59 to 65 GHz (different devices). Therefore, it appears that using the doping levels and depletion layer widths available, the breakdown voltage of our devices–for a given frequency–is lower than that published by Bell.

The output frequency when pulsed is greater than when operating CW at the same current level. This is due to the heating effect since, when operating under CW conditions, the lattice temperature in the device is higher, lowering carrier mobility and velocity. This, in turn, increases the transit-time, thus reducing the frequency.

Devices prepared from a second slice have been processed. These also give output powers of approximately 5 mW, but the frequency is somewhat higher, > 65 GHz, due to the slightly lower breakdown voltage (10 to 12 V). Difficulty was experienced in achieving a frequency of 60.8 GHz with several of these devices. This second batch of devices were processed by bonding the diode to burnished slugs. Contrary to previous results, the yield was high, showing that the bonding has improved. These devices should have better thermal conductivity than those bonded to evaporated gold, but the difficulty of bonding is greater.

Some 15 V breakdown devices were also mounted (IMP X). Only six of these devices were available, because the yield on this slice was very poor. However, the best results obtained to date were achieved from these diodes (20 mW at 57 GHz with 1.0% efficiency).

A sufficient number of IMP 6 devices have been fabricated to make receiver measurements.

Because of the recent interest in using the high thermal conductivity of diamond to improve the power handling capability of semiconductor devices, work was initiated to evaluate this technique. Two rectangular, type IIa, diamonds (1.5 X 1.5 X 1 mm) were obtained. One diamond was metallized with gold tantalum and the other with molybdenum gold. These were then soldered into holes in the top of 1/8-inch copper slugs. Diodes with 13 V breakdown were bonded onto the diamonds. Because of the difficulty in keeping the top diamond surface horizontal in the slug, the bonding process was more difficult and one diode had very poor thermal contact. The other diode had a thermal equivalent resistance of 25 ohms. However, thermal resistances of this order have been observed previously and further testing is necessary to ascertain whether the result was due to a good metal bond or the diamond heatsink.

Because of the gold peeling from the diamond when removing burned devices, the complete process must be repeated for each diode, i.e., removing the diamond for sputtering, etc. Therefore, a new method of preparing the diamonds has been developed to resurface them in situ. To date no results have been obtained using this new process.

4. Frequency Stability

To stabilize the frequency of the oscillator, the diode is mounted inside a radial air cavity as shown in Figure 45. The unloaded Q of this cavity (Q_0) is given approximately by the expression $Q_0 \cong h/\delta$ where h is the separation of the cavity disks and δ is the skin depth. At 60 GHz this becomes, for a 2-mil high device, $Q_0 = 200$. The loaded Q (Q_L) depends greatly on the coupling of the diode to the cavity and the coupling of the output to the cavity, i.e.,

$$Q_L = \frac{Q_0}{1 + \beta_1 + \beta_2}$$

where β_1 and β_2 are the coupling coefficients to the diode and load. The loaded Q of the cavity is therefore quite low, probably below 60. To verify this, several different circular cavities were constructed, from 100 mils (70 GHz) to 125 mils (55 GHz) in diameter. Using these cavities and the

17 V devices, an attempt was made to correlate the frequency of the output to the disk diameter. However, the frequency of the output varied only slightly with the disk diameter indicating a behavior pattern similar to that of a tuning capacitor rather than a cavity.

The frequency stability of an IMP 6 device has been measured using a spectrum analyzer, and was found to be

65 GHz ± 15 MHz (2.5 parts in 10^4) over a period of 1 min

65 GHz ± 60 MHz (1 part in 10^3) over a period of 1 hour.

This result, while encouraging, is not sufficiently stable for most systems.

The Q of the present cavity could be improved by two methods: 1) increasing the height of the device, which increases the series resistance and is electrically and thermally disadvantageous, or 2) reducing the coupling to the load by reducing the angle of the cavity as shown in Figure 52. The latter modification would reduce the output power, hence diodes giving greater than 5 mW at 60 GHz would be required.

Because of the small size of coaxial and reentrant cavities at 60 GHz, it is quite difficult to design an alternative cavity using either of these approaches. The present cavity is formed mainly by

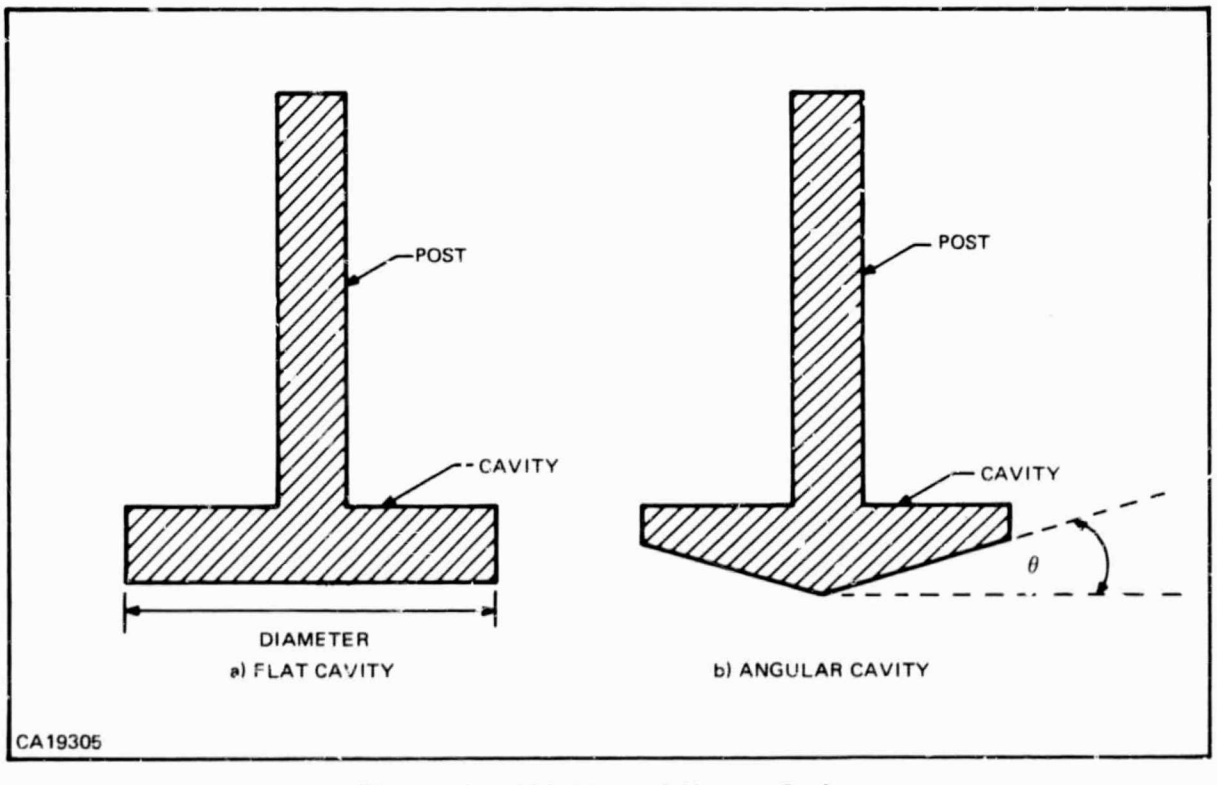

Figure 52. Side View of Circular Cavity

the short behind the diode and the tuner in front of it. A high-Q resonant filter on the output of the oscillator would improve the stability, but preliminary investigations indicate that a very high Q will be necessary.

SECTION V

MILLIMETER-WAVE RECEIVER

A. MILLIMETER-WAVE MIXER

It was decided that the best commercial mixer available was the ADTEC M-98. The specifications are:

L.O. frequency	60 GHz
Signal frequency	59.950 GHz
L.O. Power	2.5 mW
R.F. VSWR	1.55 : 1
Transducer loss	9.0 dB

The conversion loss (C_L) is given by the transducer loss less the loss due to the VSWR at the RF and IF ports. The conversion loss was estimated to be 8.6 (IF and RF VSWR = 1.55). Using a noise temperature ratio (N_{TR}) of 2 and an IF preamplifier noise figure (IF_{NF}) of 1.5 dB, the overall noise figure is given by the relation:

$$NF = C_L (N_{TR} + IF_{NF} - 1) = 12.5 \text{ dB}$$

indicating a double-sideband noise figure of 9.5 dB. Any contribution to the noise due to the L.O. will add to this figure. It should be noted that the N_{TR} is approximate and could be less than 2 for the Schottky diode used. The requirement of the contract is a double-sideband noise figure of less than 14 dB, therefore the mixer should be adequate.

B. RECEIVER MEASUREMENTS

The receiver was set up as shown in Figure 53. Because of the variation of output impedance of the single-ended mixer with local oscillator and bias levels it was extremely difficult to make noise figure measurements without using the automatic noise figure system. Difficulty was initially found with the preamplifiers which tended to oscillate and give erroneous results. This was overcome by adjusting both the bias circuit and the post amplifier gain in the receiver. Critical adjustment of the local oscillator and bias current was made and a double-sideband noise figure of 13 dB was achieved as required by the contract. This did not include the 6 dB coupler attenuation between noise source and mixer.

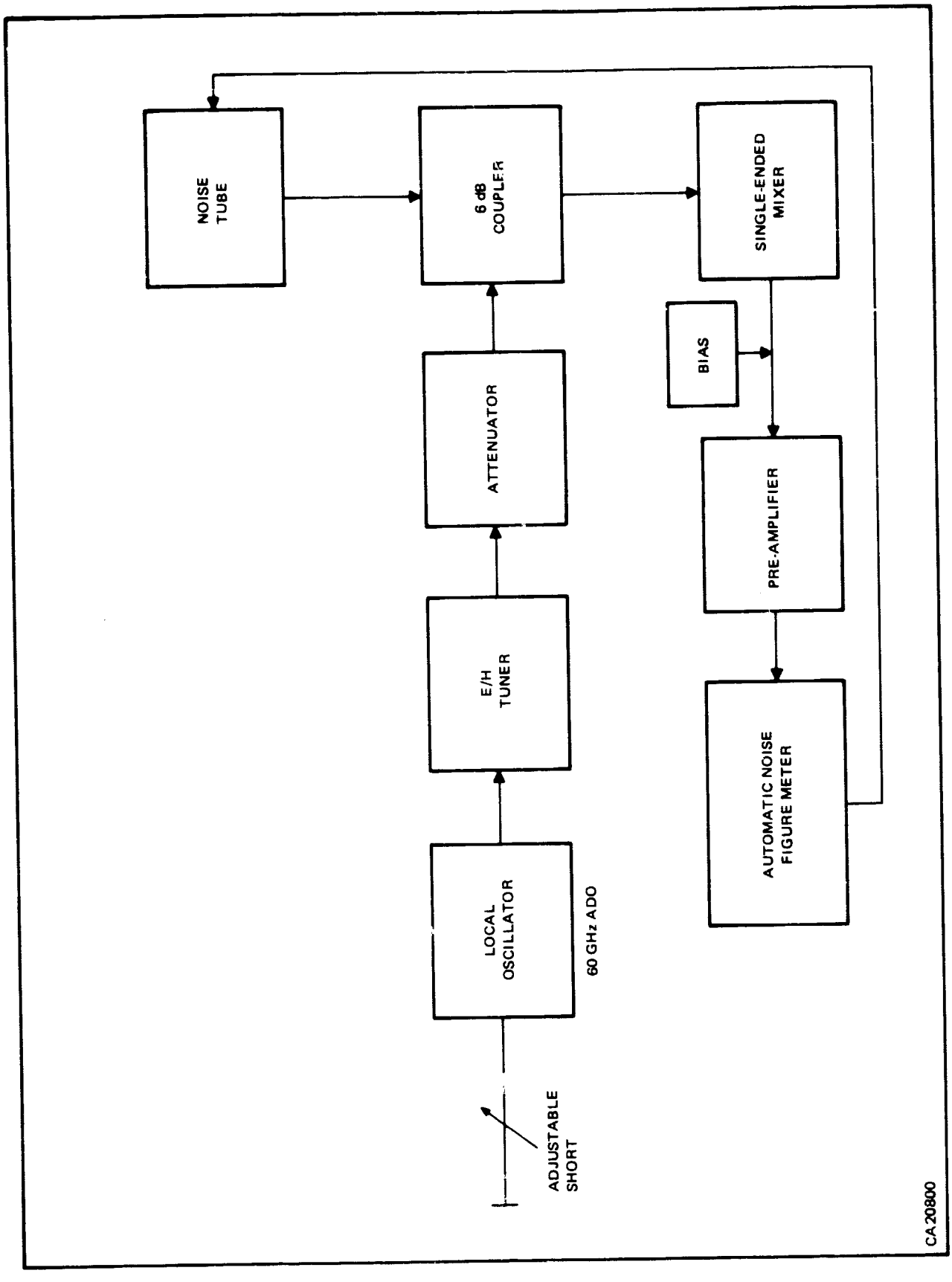

Figure 53. Block Diagram of Receiver

The noise figure of the IF amplifier used for these measurements was 2.8 dB rather than 1.5 dB, indicating a theoretical double-sideband noise figure for the mixer/I.F. of 10.3 dB rather than 9.5 dB. This noise figure indicates that the noise contribution due to the local oscillator is very approximately 13 – 10.3 = 2.7 dB.

To set up a more practical receiver using a single-ended mixer with a 6-dB coupler, a local oscillator with greater power is required (> 10 mW). The coupler would then add 1.25 dB to the overall noise figure (using a 10-dB coupler, necessitating an L.O. with > 25 mW, the contribution is only 0.5 dB). The optimum system would be to use a balanced mixer where the power requirement would be > 5 mW with, theoretically, no noise contribution due to the coupler.

SECTION VI

IF PREAMPLIFIER

A. GENERAL

The performance goals for the IF preamplifier developed under this phase of the contract were as follows:

- Power Gain . . . . . 20 dB minimum (over passband)
- Nominal Passband . . . . . .10 MHz to 110 MHz
- Passband Ripple . . . . . ± 1 dB
- Noise Figure . . . 1.5 dB maximum at 60 MHz (as low as possible over passband)

Amplifiers were designed and built with performances meeting or exceeding all of the above goals. However, as discussed below, it was found advantageous to make the nominal passband $\approx$ 20 MHz to $>$ 120 MHz in the final design.

B. AMPLIFIER DESIGN

The initial step in design was a comprehensive analytical evaluation of several circuit configurations in terms of optimum overall wideband performance. Results of this evaluation revealed that the primary conflict among the goals was that between passband and maintenance of low noise figure over the passband. This conflict stems from:

- The difficulty of realizing a source admittance that is optimum with respect to noise figure over a wide bandwidth.
- The difference between this source admittance and that required for a flat gain response.

Such difficulties are common in wideband amplifier design, but they were magnified here by the very low noise figure requirement. An overall noise figure of less than 1.5 dB dictated the use of an input-stage transistor with very low base resistance ($\sim$ 5 ohms) and high dc current gain ($>$ 50) at relatively low bias currents ($\approx$ 2 mA). The low base resistance requirement demanded the use of a device with a relatively large geometry. The inherently larger capacitances of such a device result in a relatively low cutoff frequency (f_T) at the low bias current required for low noise operation. Consequently, there is an increase in uncorrelated collector noise which, in turn, requires a large imaginary (inductive) component for the optimum source admittance at high frequencies.

The device chosen for the first stage of this amplifier has a base resistance of 4-6 ohms and an f_T of 300 MHz at 2 mA. Its optimum noise figure at 60 MHz is approximately 1 dB with an optimum source susceptance of approximately −10 mmho, corresponding to an inductance of about 260 nH at 60 MHz. The optimum source conductance is also approximately 10 mmho, a value quite close to the (estimated) IF admittance of the mixer with which the amplifier is designed to be used. The noise figure of the transistor with a purely resistive source admittance of 10 mmho is about 1.5 dB at 60 MHz. This leaves no margin for the further degradation that necessarily will accrue from bias networks and from a small second-stage contribution to the overall noise figure. Consequently, some amount of inductive susceptance must be presented to the input stage to insure meeting the noise figure requirement. For narrow-band operation, this poses no particular problem. However, over the wide band of interest here, the optimum source susceptance varies directly with frequency (corresponding to an inversely proportional variation of equivalent shunt inductance with frequency). Attempts to synthesize a simple L-C network providing such a variation in frequency were only partially successful. Moreover, such a variation was found to be in conflict with gain-flatness goals.

Some gain compensation can be provided by using feedback. However, resistive feedback networks degrade the noise figure if the loop includes the first stage. Thus feedback had to be incorporated into succeeding stages, where it tends to be less effective in compensating for gain fall-off in the input stage. After thorough investigation, the basic configuration chosen was a two-stage, common-emitter amplifier with local series feedback in the second stage only. The design accommodates a choice between two input matching networks that optimize performance over different portions of a nominal 10 MHz to 130 MHz frequency spectrum. Schematics of the basic amplifier and the two matching networks are shown in Figure 54.

Computer analysis showed that the simple shunt-L network assured meeting the 60 MHz noise figure specification with good overall performance if the passband was made ≈ 20 MHz to ≈ 120 MHz. The shunt-C, series-L input matching network was found to provide better overall performance from 10 MHz to 110 MHz but the predicted noise figure at 60 MHz appeared to be marginal insofar as meeting the 1.5 dB specification.

For initial evaluation of the design, circuits were breadboarded using conventional (discrete) components and canned transistors. Calculated and measured (breadboard circuit) performance data are shown in Figures 55 and 56. These data show that, with shunt-L input matching (see Figure 55), a transducer gain of about 23 dB ± 1 dB was realized over a passband from approximately 25 MHz to 130 MHz for a purely resistive source impedance of 100 ohms (10 mmho). The noise figure for this configuration was about 1.2 dB (for a 100 ohm source) at 60 MHz and increased to approximately 3 dB at each band edge.

For shunt-C, series-L input matching (see Figure 56) about the same gain (≈ 23 dB ± 1 dB) was obtained over a passband from 10 MHz to 110 MHz. However, noise figure at 60 MHz was 1.5 dB (the specification limit), decreasing to approximately 1 dB at the lower band edge and increasing to approximately 2.5 dB at the upper band edge.

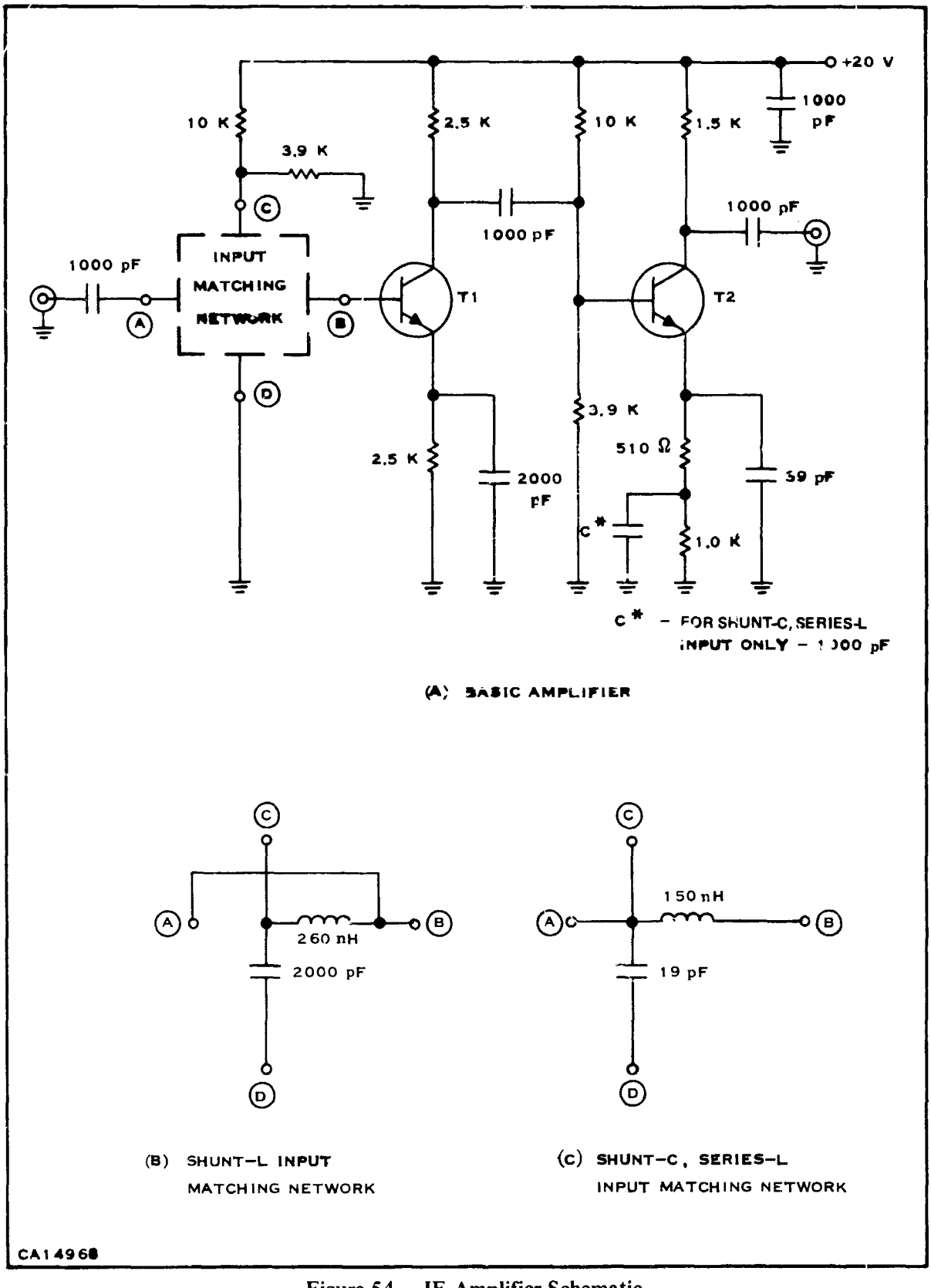

Figure 54. IF Amplifier Schematic

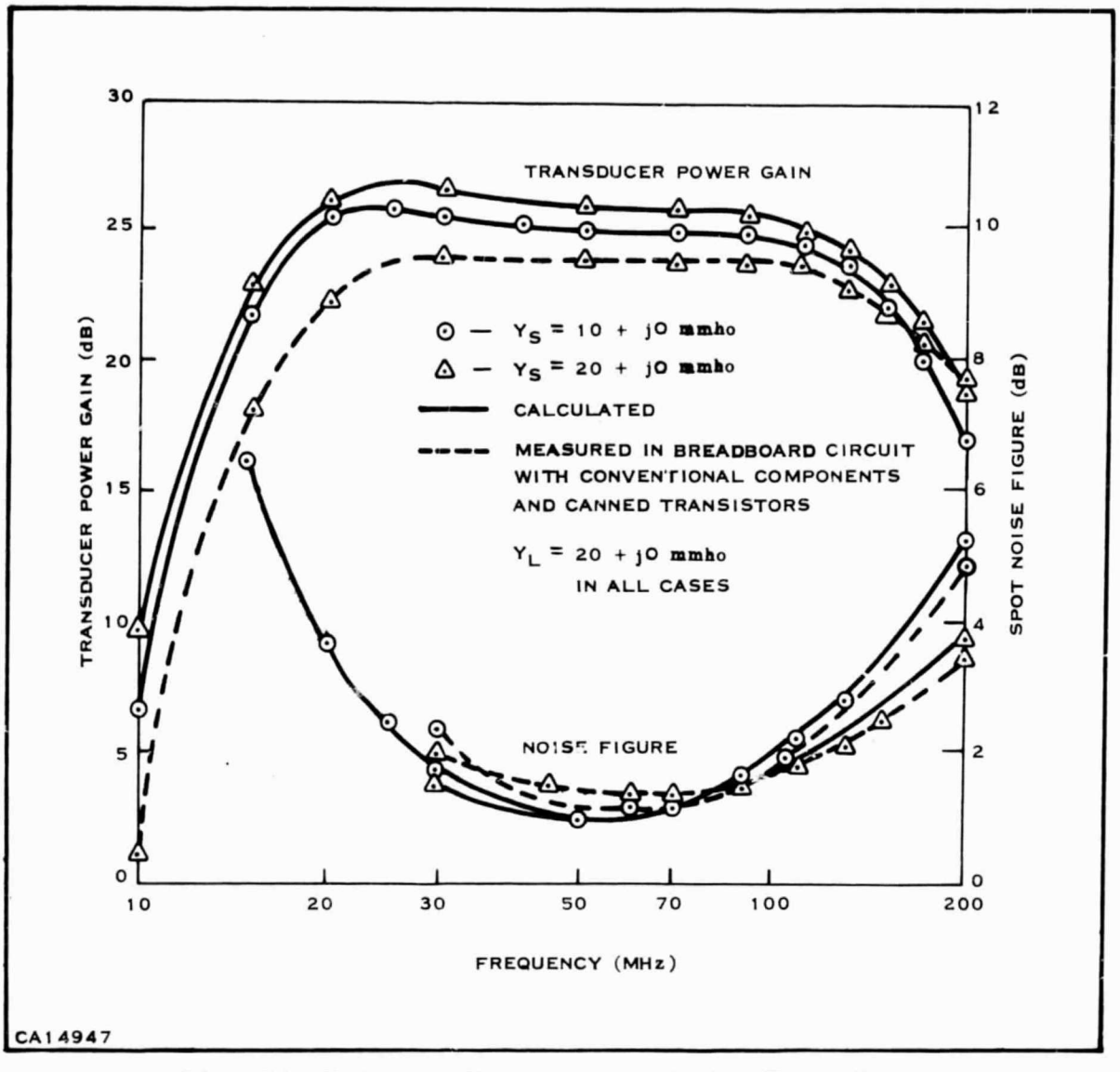

Figure 55. Performance Data-Breadboard Version, Shunt-L Input

C. HYBRID FABRICATION AND PERFORMANCE

The agreement between breadboard and calculated performance verified the design to be satisfactory and ready for fabrication in hybrid circuit form on ceramic substrate. The layout (see Figure 57) was designed such that the desired bandpass option could be selected in the final fabrication steps through selective interconnection at the input and in the RC feedback network. In both cases thin-film resistors, chip transistors and capacitors, and a miniature inductor were used. Four shunt-L versions and one shunt-C, series-L version of the amplifier were built. In all cases, circuit performance met or exceeded contract requirements. A summary of the performance data (in a 20-mmho system except as noted for noise figure) is given in Table V. A plot of performance data against frequency for one of the shunt-L hybrid circuits is shown in Figure 58.

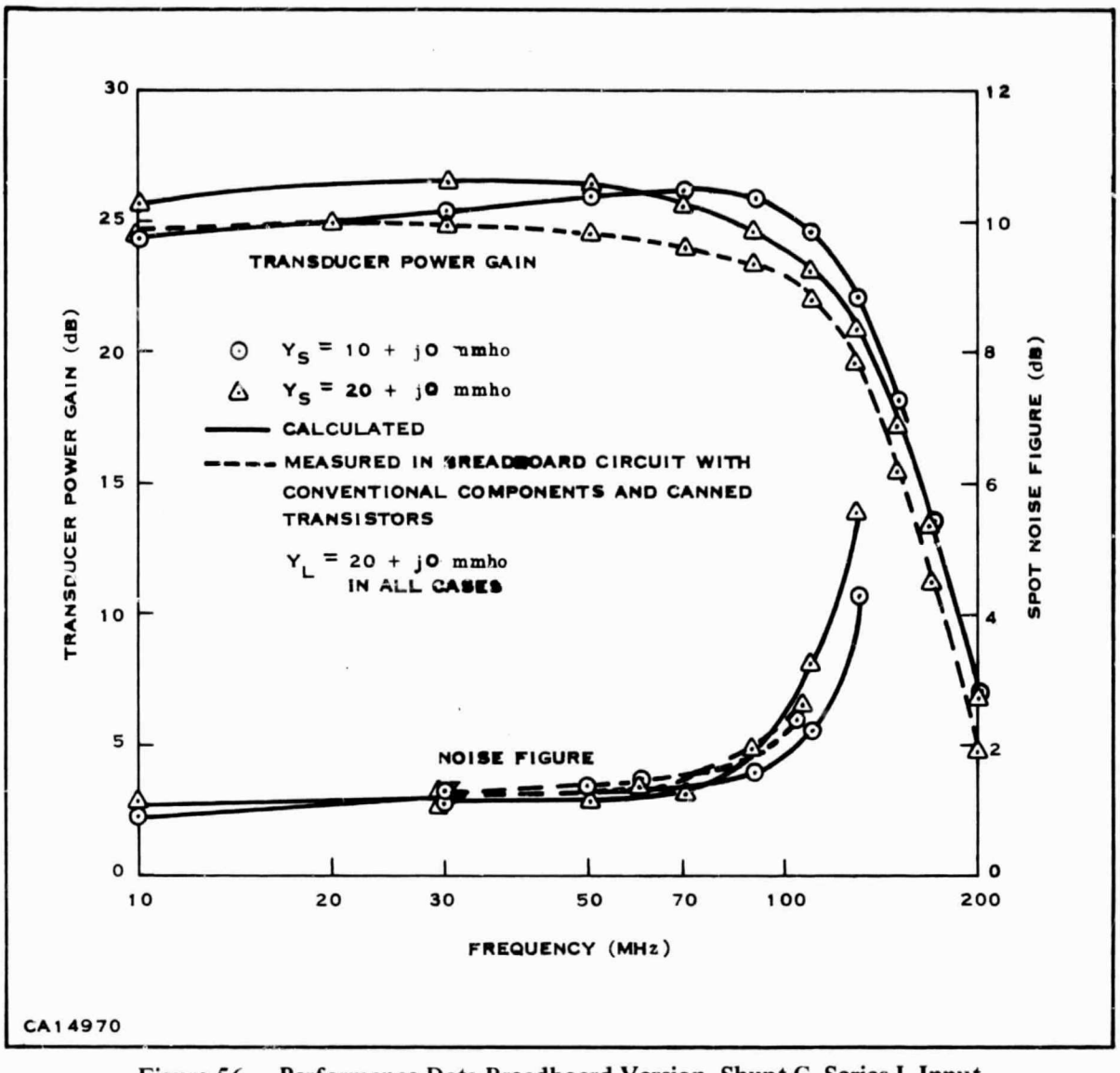

Figure 56. Performance Data-Breadboard Version, Shunt-C, Series-L Input

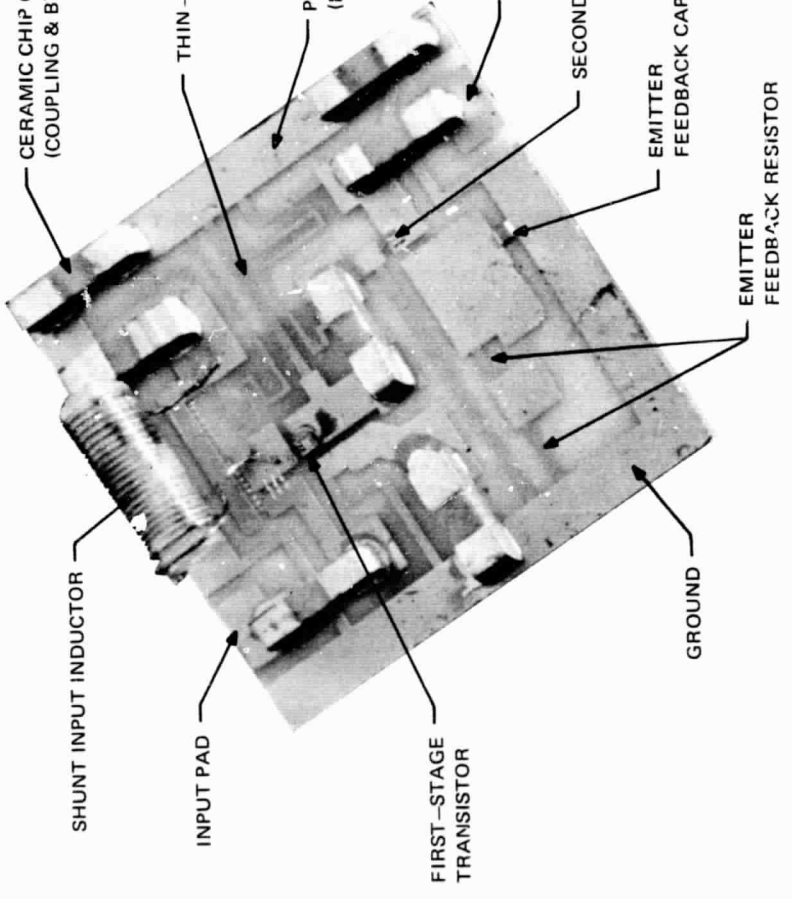

Figure 57. Physical Layout of Hybrid IF Amplifier

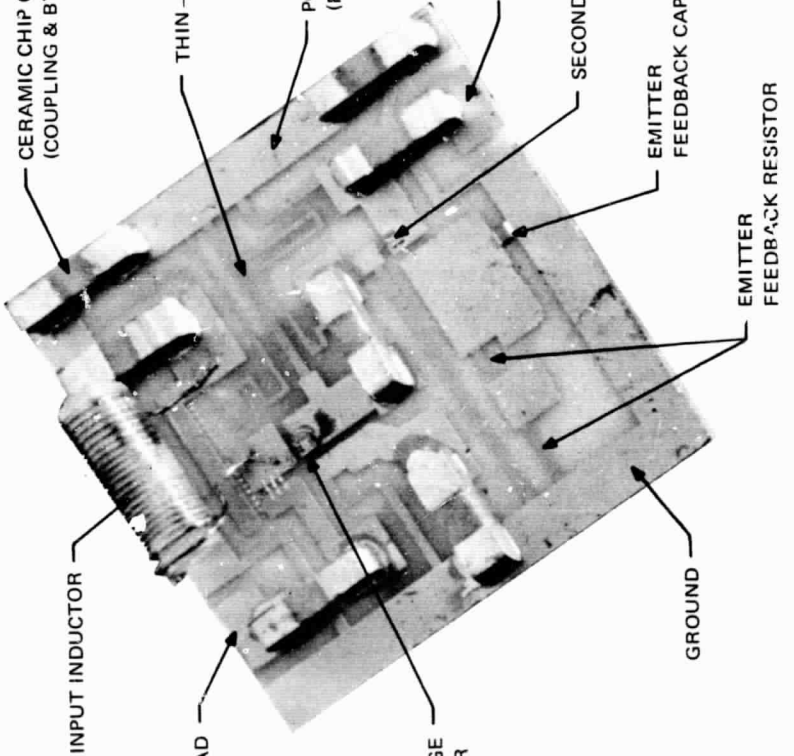

Figure 57. Physical Layout of Hybrid IF Amplifier

Table V. Hybrid Version Performance Summary

Characteristics	Shunt-L	Series-L
Midband Gain	24–28 dB	26 dB
± 1 dB Passband	≈ 20 to 120–160 MHz	10–110 MHz
3 dB Bandwidth	140–180 MHz	≈ 110 MHz
Noise Figure		
60 MHz, Y_S = 20 mmho	1.3–1.4 dB	1.4 dB
60 MHz, Y_S = 10 mmho	1.1–1.3 dB	1.5 dB

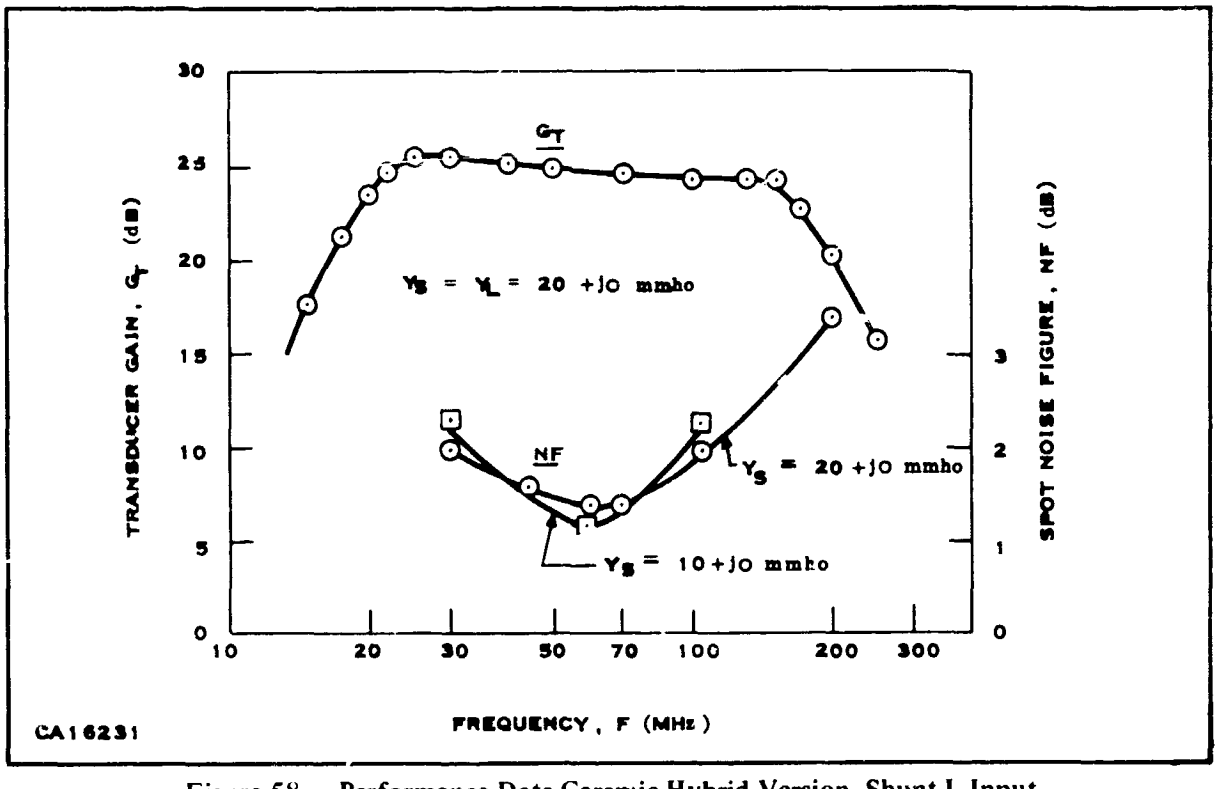

Figure 58. Performance Data-Ceramic Hybrid Version, Shunt-L Input

SECTION VII

CONCLUSIONS

The semi-insulating GaAs manufactured at TI has been found to be suitable for the fabrication of active devices at 60 GHz. The problems, and associated solutions, found in the manufacture and subsequent processing of semi-insulating GaAs are described in Reports No. 1-5 under Contract No. AF33(615)-5102.

The dielectric constant of this semi-insulating GaAs has been measured to be 13.2 ± 0.2, and is invariant with frequency over the range of interest.

Loss measurements on the microstrip circuits in both E-band (60 GHz to 90 GHz) and R-band (26 GHz to 40 GHz) were carried out. The results are very encouraging, about 0.3 dB/λg in E-band and 0.2 dB/λg in R-band. However, they still are slightly higher than the calculated conductor and dielectric loss. Theoretical calculation showed that this extra loss does not come from the thin (< 200 Å) molybdenum layer under the gold. This small discrepancy probably came from either radiation loss or uncertainty in measurements, or both.

Several transitions from the microstripline to waveguide have been investigated. The single-ridged waveguide transition gives good results up to R-band, but is not easy to use at 60 GHz owing to the destruction of the very thin substrates used at this frequency. Antenna coaxial and antenna feedthrough transitions have been found to be the most suitable, having insertion losses less than 1 dB/transition up to 90 GHz, but the results are not easily reproduced.

Several passive circuit elements such as quarter-wave stubs and circular cavities have been constructed and evaluated. The results show that the circuits perform as the theory indicates at frequencies up to 100 GHz.

Planar Gunn oscillators have been fabricated for operation at 60 GHz in the high-frequency (L.S.A.) mode. To date no output has been achieved from these devices at this frequency. Similar Gunn oscillators have been fabricated for operation at 30 GHz in the transit-time mode. These planar Gunn oscillators were mounted in ceramic microstrip circuits for evaluation. The power obtained was 1.5 mW at 28 GHz. At the present time reproducibility of such devices is poor because of variations in the thickness and concentration of the N^- layer.

The application of lower-frequency Gunn diodes in the transit-time mode (6 to 15 GHz) for microstripline oscillators has been investigated. J-band Gunn oscillators were integrated into both disc and full-wavelength microstrip cavities to give higher efficiencies than those obtained from a waveguide configuration. Also 25 mW CW has been achieved at 10 GHz from a stripline circuit using a Gunn diode.

Planar Schottky barrier diodes have been successfully integrated into single-ended mixer circuits to give a minimum detectable signal of −54 dBm/Hz at 87 GHz, with a conversion efficiency 5 dB better than a waveguide counterpart. Although similar Schottky barrier diodes have been integrated into balanced mixer circuits, the results have not been good because of the difficulty of aligning both the diodes in fabrication. This causes imbalance and subsequent loss of sensitivity. To date the minimum detectable signal was measured to be −125.5 dBm/Hz at 71 GHz.

Results of the single-ended and balanced mixers confirm three major assumptions:

- The surface-oriented Schottky barrier diodes can meet the fast response-time requirements in the millimeter-wave region.
- Microstriplines are usable in the millimeter-wave region.
- The antenna-feedthrough waveguide-to-microstripline transition is acceptable.

Measurements on the Schottky barrier diodes have been made at X-band, when a noise figure of 6.2 dB was obtained, for a device of area 0.2 X 0.6 mil having a series resistance of 20 ohms, cutoff frequency of 140 GHz, and zero-bias capacitance of 0.056 pF.

Manufacture of a complete, operable monolithic receiver has not been successful owing to spurious growths on the surface of the substrate. However, some devices in the receiver were probed and found to be operable.

Owing to the estimated time needed to develop a monolithic receiver at this stage, it was mutually decided to investigate the fabrication of the receiver using hybrid techniques.

After considering several substrates, quartz was found to be the most suitable, because of its low dielectric constant (3.75) and thermal expansion, and its good surface finish. Disadvantages, however, are low thermal conduction and fragility, since it has to be lapped to 4 mils for operation at 60 GHz. A detailed theoretical study of the electrical characteristics of quartz has beer carried out, and experimental results confirm this theory.

A balanced mixer based on a 3 dB hybrid coupler has been theoretically analyzed and a practical circuit designed and fabricated. The diode used in this circuit had a cutoff frequency of 240 GHz, zero-bias capacitance of 0.066 pF, and series resistance of less than 10 ohms.

The local-oscillator power necessary for the balanced mixer is expected to be approximately 5 mW at 60 GHz. A stripline quadrupler from 15 to 60 GHz was designed on quartz substrate. The requirements for the diode are a cutoff frequency of 600 GHz with a zero-bias capacitance of 0.07 pF. The quadrupler is made up of a low-pass input and band-pass output filter, a series connected diode, and correct termination for the second harmonic (30 GHz). The best conversion loss measured was approximately 20 dB, but the overall circuit was not ideal since the devices were 15 mil squares, with a 3 X 3 array of various-area Schottky barrier diodes on them making lengthy connecting wires necessary. The use of beam-lead devices, which should shortly be available at TI would greatly improve the performance of both the balanced mixer and quadrupler.

To facilitate the design of stripline oscillators incorporating Gunn diodes, the impedance required to be presented to the diode to achieve maximum output was measured. The results showed that the real part of the impedance was approximately constant with frequency for a given slice, but the imaginary part varied considerably, as expected. Diodes from different slices had different real parts. Therefore, at any one frequency, a fixed-tuned circuit could be designed for diodes of a given slice, with one degree of tuning for a given frequency range. However, two degrees of tuning would be necessary for a circuit to operate with diodes from different slices. Improved control in the processing of the Gunn diodes would produce diodes with more nearly similar impedances from slice to slice.

At this point it was mutually decided by NASA-ERC and TI that the most direct method should be taken. Therefore, a waveguide approach was initiated.

Two methods of generating the local osciallator signal were available:

- Generating sufficient power at 15 GHz to be followed by a waveguide quadrupler or
- Directly, using Gunn or Impatt diodes.

A source at 15 GHz was readily available, giving 80 mW of output power using an avalanche diode, or 25 mW using a Gunn diode.

A quadrupler was constructed in waveguide and the conversion loss from 15 to 60 GHz was measured using several different varactor diodes. The conversion loss was not reduced below 25 dB due to the low cutoff frequency of the diodes, and insufficient time to perfect the waveguide circuit.

However, suitable avalanche diodes have been fabricated for the direct generation of 60 GHz and a waveguide jig has been built. Output powers of > 5 mW at 60 GHz and 20 mW at 57 GHz have been obtained.

Performance can be further improved through: 1) Improved impurity profiles in the diode which will result in higher efficiency; and 2) A cavity with a higher Q at the operating frequency.

Further development will increase the output power of the diodes, which would enable improvements to be made to the waveguide circuit to increase the frequency stability, and decrease the noise contribution of the avalanche diodes. This form of millimeter-wave local oscillator shows great promise for future systems use.

A thin-film hybrid integrated circuit amplifier was designed and fabricated with 20 dB gain, passband extending from 10 to 110 MHz and a noise figure < 1.5 dB at 60 MHz. This represents a substantial advanced in the performance of such amplifiers.

SECTION VIII

REFERENCES

1. D. T. Young and J. C. Irvin, "Millimeter Frequency Conversion Using Au on N-Type GaAs Schottky Barrier Epitaxial Diode," *Proc. IEEE*, Vol. 53 (December 1965), pp. 2130-2131.

2. J. A. Copeland, "LSA Oscillator-Diode Theory," *J. App. Phys.*, Vol. 38 (July 1967), pp. 3096-3101.

3. J. A. Copeland, "CW Operation of L.S.A. Oscillator Diodes - 44 to 88 GHz," *Bell. Syst. Tech. Journal* (January 1967), pp. 284-287.

4. T. Misawa, "Microwave Silicon Avalanche Diode with Nearly Abrupt Junctions," *IEEE Trans.* Vol. ED-14, No. 9 (September 1967), p. 580.

5. R. D. Larrabee and W. A. Hicinbothem, "Resonance Behavior of the Dielectric Constant of GaAs at Microwve Frequencies," *Appl. Phys. Letters*, Vol. 10 (June 1967), p. 334.

6. Stan Jones and Shing Mao, "The Dielectric Constant of GaAs at Microwave and Millimeter Wave Frequencies," *Appl. Phys. Letters*, Vol. 11 (December 1967), p. 351.

7. K. S. Champlin, R. L. Erlandson, G. A. Glover, P. S. Hauge and T. Lu, "Search for REsonance Behaviour in the Microwave Dielectric Constant of GaAs," *Applied Phys. Letters*, Vol. 11 (December 1967), pp. 348-349.

8. N. Braslau, "On the Dielectric Constant of GaAs at Microwave Frequencies," *App. Phys. Letters*, Vol. 11 (December 1967) pp. 350-353.

9. C. B. Rogers, G. H. B. Thompson, and G. R. Antell, "Dielectric Constant and Loss Tangent of Semi-Insulating GaAs at Microwave Frequencies," *Appl. Phys. Letters*, Vol. 11 (December 1967), pp. 353-354.

10. K. G. Hambleton, C. Hilsum and B. R. Holeman, "Determination of the Effective Ionic Charge of Gallium Arsenide from Direct Measurements of the Dielectric Constant," *Proc. Phys. Soc.* 77 (1961), p. 1147.

11. Max Sucher and Jerome Fox (editors), *Handbook of Microwave Measurements;* Wiley (1963), p. 530.

12. T. E. Walsh, "Gallium Arsenide Electro-Optic Modulators," *RCA Review*, Vol. XXVII, No. 3. (September 1966).

13. K. S. Champlin, private communication.

14. J. D. Welch and H. T. Pratt, "Losses in Microstrip Transmission Systems for Integrated Microwave Circuits," *1966 NEREM Record.*

15. H. A. Wheeler, "Transmission-Line Properties of Parallel Strip Separated by a Dielectric Sheet," *IEEE Trans. on MTT* (March 1965), pp. 172-185.

16. R. A. Pucel, D. J. Masse, and C. P. Hartwig, "Losses in Microstrip," *IEEE Trans. on MTT*, Vol. 16, No. 6, (June 1968), pp. 342-350.

17. W. W. Mumford, "The Optimum Piston Position for Coaxial to Waveguide Tranducers," IRE National Convention, New York (March 1952).

18. E. L. Ginzton, *Microwave Measurements*, McGraw-Hill Book Co., New York (1957), p. 404.

19. W. S. Jones, "A Survey of Some Conditions Limiting the Application of Hybrid Microstripline Techniques at Millimeter-Wave Frequencies,", to be published.

20. C. B. Burckhardt, "Analysis of Varactor Frequency Multipliers for Arbitrary Capacitance Variation and Drive Level," *B.S.T.J.* Vol. 44 (April 1965), pp. 675-692.

21. Stan Jones, "Frequency-Stable, Microstripline X-Band Gunn Oscillator" (to be published).

22. T. P. Lee and C. W. Burrus, "Millimeter Wave Quadrupler and an Up-Converter Using Planar-Diffused Gallium Arsendie Varactor Diodes," *IEEE Trans. MTT*, Vol. MTT-16, No. 5, May 1968.

23. T. P. Lee, R. D. Standley and T. Misawa, "A 50 GHz Silicon Impatt-Diode Oscillator and Amplifier," presented at 1968 International Solid-State Circuit Conference, Philadelphia, Pa., February 14-16, 1968.